Pseudorotation in Jahn-Teller Systems

Lubna. M. Sindi, M.Sc.

Thesis submitted to The University of Nottingham
for the degree of Doctor of Philosophy

October 2008

Dedicated to ...

my lovable parents, my wonderful husband, my brothers and sisters and my sweet daughters.... with love and gratitude.

Abstract

The molecular shape of any nonlinear molecule can be strongly influenced by the coupling between electrons and vibrations (vibronic coupling) via the Jahn-Teller (JT) interaction within the molecule. This influence appears as a distortion of the symmetrical shape of the original molecule. In such molecules, the adiabatic potential energy surface (APES) possesses either a trough of minimum-energy points or several isoenergetic minima ('wells') depending on the nature of the interactions present.

In the case when coupling is infinite, the wells are very deep and the system will be locked into one of these distorted states. The vibronic states associated with these wells are good eigenstates of the system in this limiting static case. However, real molecules have finite coupling, so the system can migrate from one well to another in a process that is often referred to as the dynamic JT effect. If the wells are deep, then the motion must involve quantum mechanical tunnelling. Generally, the motion between wells gives the illusion that the molecule has rotated and this type of motion is referred to as pseudorotation. The eigenstates of the general system can then be approximated by symmetry-adapted states (SAS) which are a linear combination of the states associated with the wells.

In this thesis, we focus on studying the dynamical nature of the JT effect through investigating the pseudorotation mechanism in different systems using a simple method employing the time-evolution operator. This allows us to obtain analytical expressions for the probabilities that a system that starts off localised in one initial well, may become localised in another well at some later time. These expressions are plotted versus time to show the pseudorotation regime and a comparison between different cases of pseudorotation in different molecules is made.

Determination of the rates of pseudorotation leads to a better knowledge of the strength and nature of the vibronic coupling in the system and is a quantity

that is, in principle, experimentally measurable. Also, more information about the tunnelling splitting between the SASs can be gained from this study.

Acknowledgements

I would like to express my gratitude to my supervisors, Dr. Janette Dunn and Prof. Colin Bates whose expertise, understanding, and patience added considerably to my graduate experience. I appreciate their vast knowledge and skill in many areas of my project and believe that without their motivation and encouragement I would not have completed my research and been able to cope with the pressures of the research environment.

A very special thanks goes out to Dr. Ian Hands, who took time out from his busy schedule to provide me with direction and technical support at all levels of the research project and became more of a mentor and friend than a colleague.

I would also like to thank the other members of my group: Dr. Wajood Diery and Dr. Elie Moujaes for discussions that enriched my research experience and helped me along the way.

It is beyond words to express my ever thankful gratitude to: My parents, to whom I doubt that I will ever be able to convey my appreciation fully, but I owe to them my eternal gratitude; My husband, who has truly made a difference in my life, and prepared a wonderful atmosphere for study during the period of this research. He has supported me, and contributed significantly to the completion of this thesis; My sweet little daughters, who made my stay in Nottingham fun and enjoyable.

I also wish to thank Asha Yassin, who was there at all times helping and supporting me.

Last, but not least, I would like to thank Prof. K. A. Siddiqui and Dr. M. S. Al Ahmadi for their continual encouragement and support.

Contents

1 Introduction **1**

2 Background theory **5**

2.1 The adiabatic approximation 8

2.2 The vibronic Hamiltonian 10

2.2.1 Basis wave functions 11

2.2.2 The adiabatic potential energy surface (APES) 14

2.3 Computational methods 15

2.3.1 The unitary shift transformation 15

2.3.2 The method of Öpik and Pryce 17

2.3.3 Projection operators 18

2.4 The icosahedral point group 20

2.4.1 Irreducible representations (irreps) 22

2.4.2 Electronic structure of C_{60} 22

2.5 Vibronic coupling in C_{60} 25

3 A discussion of pseudorotation in JT systems **27**

3.1 The time-evolution operator 30

3.2 Time-evolution in JT systems 31

3.3 Application to C_{60}^{-} 34

3.4 Experimental Techniques 37

4 $T \otimes (e \oplus t_2)$ JT system in cubic symmetry 39

4.1 The transformed Hamiltonian for $T \otimes (e \oplus t_2)$ 40

4.1.1 The $T \otimes e$ JT system 41

4.1.2 The $T \otimes t_2$ JT System 42

4.1.3 The $T \otimes (e + t_2)$ JT System 48

4.2 Summary 52

5 The Quadratic $p^2 \otimes h$ JT Interaction: A model for C_{60}^{2-} 55

5.1 The JT Effect in C_{60}^{2-} 57

5.1.1 Electronic basis states and the linear interaction Hamiltonian 59

5.1.2 The quadratic interaction Hamiltonians for C_{60}^{2-} 64

5.2 The unitary shift transformation and energy minimisation 65

5.2.1 The adiabatic potential energy surface (APES) 66

5.2.2 Well positions and electronic states 70

5.2.3 Symmetry-adapted states 71

5.2.4 Energies of the SASs 75

5.3 Pseudorotation in C_{60}^{2-} anion without Coulomb interaction 79

5.3.1 D_{5d} Symmetry 79

5.3.2 D_{3d} Symmetry 81

5.4 Summary and Discussion 85

6 A further investigation of the C_{60}^{2-} anion with e-e repulsion included 87

6.1 A general review of the system 87

6.2 D_{5d} minima 88

6.3 D_{3d} minima 91

6.4 Symmetry-adapted states 93

6.4.1 Energies of the SASs from D_{5d} minima 93

6.4.2 Energies of the SASs from D_{3d} minima 94

6.5 Discussion 95

7 The $H \otimes h$ JT system: A model for C_{60}^{+} 99

7.1 Pseudorotation in the $H \otimes h$ JT system 100

7.1.1 The D_{5d} minima 101

7.1.2 The D_{3d} minima 104

7.2 Discussion 109

8 The $(h^{+})^{2} \otimes h$ JT system: A model for C_{60}^{2+} 111

8.1 The $(h^{+})^{2} \otimes h$ JT system 112

8.2 Pseudorotation in D_{2h} 113

8.3 Summary 120

9 Conclusions 122

A The SASs arising from the D_{2h} wells in the C_{60}^{2+} cation 126

Bibliography 128

Chapter 1

Introduction

The Jahn-Teller (JT) effect is of fundamental importance in many areas of physics and chemistry and continues to be of great interest to researchers around the world. This interest extends to both experimental and theoretical aspects of the theory. The main target of the work presented in this thesis is a study of the dynamical JT effects in different ions derived from the icosahedral molecule C_{60}. This molecule has a simple but beautiful structure, as shown in Fig. 1.1, which endows it with a symmetry that is not often found in Nature. This high symmetry makes it highly susceptible to effects derived from electron-vibration interaction as exemplified by the JT effect. This symmetry will be discussed in some detail in this thesis.

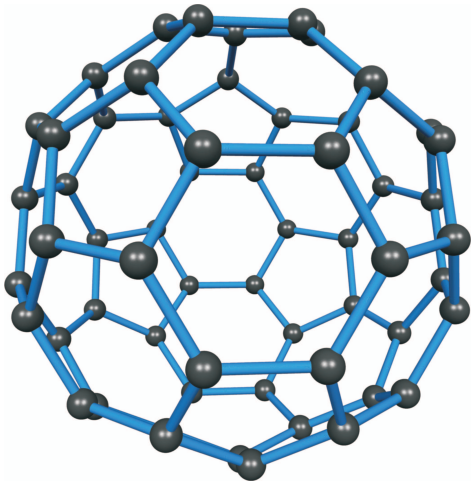

Figure 1.1: The fullerene C_{60} molecule.

One of the characteristic features of the JT effect is that the electron-vibration interaction lowers the symmetry of the molecule involved. If the interaction is very strong, we can therefore expect the icosahedral cage to become permanently

distorted. This is the situation usually described as a *static* JT interaction. If the interaction is more moderate, then the effect is referred to as being *dynamic*. The reason for this motion is easy to understand. The high symmetry of the molecule means that there will be several equivalent ways in which the molecule could distort in order to lower the total energy. Obviously, a certain amount of energy is required in order for the system to change from one preferred configuration to another. In real molecules, these barriers are finite and so conversion between the different distorted forms is permissible. In fact, the nuclear motion which results from this dynamic picture is unique. In this thesis, we shall generally refer to this motion as *pseudorotation*. A more detailed description of pseudorotation is given in Chapter 3.

The uniqueness of pseudorotation means that if such motion is observed, then we have a clear indication that the system under observation is susceptible to a dynamic JT effect. In fact, the rate at which pseudorotation occurs must, in some way, be related to the strength of the electron-vibration coupling within the observed system. One of the aims of this thesis is to determine exactly how the pseudorotation depends on the underlying coupling. A number of systems will be studied, mostly related to C_{60} because of its current high interest.

To date, there have been no direct observations of pseudorotation in any system derived from C_{60}. However, modern experimental techniques are capable of operation on a femtosecond timescale or faster. On these timescales, the movement of the nuclei associated with pseudorotation is frozen. Therefore, by making use of appropriate ultrafast techniques we can hope that pseudorotation in the fullerenes will soon be observed. The purpose of this work is to put in place the relevant theory so that observation of pseudorotation in these systems can be used to infer the strength of the coupling present. An idea of how fast these rates will be can be gained from similar experiments performed on the neutral C_{60}. Using picosecond lasers, Rubtsov *et al.* [1] used a transient grating technique to determine the rotational reorientation rates of C_{60} in several solvents. The rotation times ranged from 3.5 ± 1.5 ps (in decalin) to 13 ± 2 ps (in *o*-xylene). Intuitively, we would expect pseudorotation to be faster than these rates and, therefore, measurable provided experiments on a femtosecond timescale are used. Suggestions for the types of experiments that could yield the relevant pseudorotation rates have been proposed [2]. It is hoped that such experiments will soon provide the data required. Using

the theory and results developed here, we therefore hope to be able to interpret the observed rates in order to derive an improved estimate of the strength and nature of the electron-vibration coupling in some very important ions.

In Chapter 2 we present a useful discussion of some of the theoretical tools used throughout the thesis. A brief resumé of the theory of the JT effect is presented and the general form of the interaction Hamiltonian is derived. The methods that will be used to solve such Hamiltonians are discussed. In particular, details are provided of the *unitary shift transformation* which is used to help isolate the lowest manifold of the adiabatic potential energy surface (APES). This procedure, which is based on a second-quantisation technique as developed by Bates *et al.* [3], produces a displacement in the nuclear coordinates. Minimisation of the energy with respect to the displacement is achieved using the method of Öpik and Pryce [4]. This allows minima and other extremal points on the APES to be found. Projection operator techniques are also discussed and later used to find the eigenstates for the dynamical motion of our systems. As most of the work contained within this thesis relates to icosahedral systems, a discussion of this symmetry is also provided.

The technique which will be used to study the dynamical behaviour for different JT systems is introduced in detail in Chapter 3. The method employs the time-evolution operator to investigate pseudorotation between the available minima produced by the JT effect. It allows us to derive analytical expressions for the rate of pseudorotation as a function of the vibronic coupling parameters. As an illustration of the method, a discussion is given of the application of the technique to the $T \otimes h$ JT problem which is relevant to the C_{60}^{-} anion.

As the icosahedral systems tend to be quite complex and not easy to visualise, a treatment of the more familiar, and less complicated, $T \otimes (e \oplus t_2)$ JT problem is given in Chapter 4. The problem of pseudorotation in this cubic symmetry is discussed as an introduction to the general behaviour to be expected in the study of the more advanced systems. This problem has been studied over a very long period of time [5, 6], and the low dimensionality of it facilitates interpretation of the results using simple graphical methods.

Some work has already been published on pseudorotation in the C_{60}^{-} anion [2]. A natural extension of this work is to consider the case of the doubly-charged C_{60}^{2-} dianion. Therefore, in Chapter 5, a $p^2 \otimes h$ JT Hamiltonian is developed to model

this ion which includes second order electron-vibration interactions. This is the first time that this system has been considered at this level of sophistication and we use the results to discuss the pseudorotation to be expected in this ion. For this system, the complication that arises due to the presence of two electrons will be avoided by ignoring the term splitting through the study that appears from the electron repulsion. Overall, at this level of approximation, it is found that the APES contains minima of either D_{5d} or D_{3d} symmetry. The expressions for the energies are derived for these minima and the linear combinations of the states are formulated for the ion at intermediate coupling strengths. Pseudorotation is then considered.

A further investigation of the system when the repulsion between the two electrons is included will be presented in Chapter 6. This is done by including the Hamiltonian that represents the splitting between the resultant electronic terms ^1H_g and ^1A_g. The strength of the Coulomb interaction is not well known and so a new variable has to be included in the theory in order to obtain an analytical expressions of the energies for the different states.

In Chapters 7 and 8, our attention moves to the cations of C_{60}. These are important because it is calculated that the vibronic coupling in these ions is larger than in the anions [7]. Thus, it may be easier to detect pseudorotation in these systems compared to their negatively doped counterparts, although they are difficult to obtain experimentally. Both C_{60}^+ and C_{60}^{2+} are investigated. Each cation shows different tunnelling behaviour depending on the distorted symmetry involved. C_{60}^+ distorts to either pentagonal, D_{5d}, or trigonal, D_{3d}, symmetry, while the C_{60}^{2+} distorts to either D_{3d}, D_{5d}, D_{2h} or C_{2h} symmetries. A study of the pseudorotation between these more exotically distorted minima is then carried out for the case where C_{60}^{2+} undergoes distortion to D_{2h} symmetry.

Finally, in Chapter 9, general conclusions are drawn and a summary of the main results of the thesis are given.

Chapter 2

Background theory

The JT effect was explained for the first time in the spring of 1936 by H. Jahn and E. Teller at the Washington meeting of the American Physical Society. The background to this theoretical announcement started two years earlier following a discussion between Teller and Landau concerning the degenerate electronic states in linear molecules such as CO_2. The Landau hypothesis was that a molecule with orbitally degenerate electronic states would be unstable with respect to symmetry-lowering distortions of its nuclear configuration. Relying on a PhD thesis of Teller's student (R. Renner) which dealt with linear triatomic molecules, Teller was able to convince Landau that linear molecules were an exception to this general supposition. In the following year, Teller met Jahn in London and together they demonstrated that linear molecules were the only exception to this theory for the case of orbital degeneracy. The other exception is Kramer's degeneracy for spin doublets, which cannot be removed through any nuclear displacement but will split under an external magnetic field. They finally formulated their theorem which formally states: "for any non-linear molecular system in a degenerate electronic state a distortion will occur so as to lower the symmetry and remove the degeneracy and lower the energy" [8]. One of the most important consequences of this is that the perfect geometry of the molecule can no longer exist, since the distorted molecule is the energetically preferred structure.

Later, in 1939, a paper was written by J. Van Vleck devoted to the JT effect [9]. It presented the interaction between a 2-fold degenerate electronic term E and 2-fold degenerate e vibrations. This so-called $E \otimes e$ interaction was explored for the first time and it showed that the adiabatic potential energy surface (APES) has the form of a Mexican hat. In this paper, Van Vleck wrote that "*it is a great*

merit of the JT effect that it disappears when not needed." This announcement showed the poor understanding at that time of the observable effects that arise as a consequence of the JT interaction. The misunderstanding of the JT effect lasted for almost two decades and this was confirmed in 1960 when Low stated in his book "*it is a property of the JT effect that whenever one tries to find it, it eludes measurements*" [10].

In 1950, Abragam and Pryce were the first to reveal the dynamical nature of the JT distortions by analysing the temperature dependence of the electronic spin resonance (ESR) spectra of Cu^{2+} compounds [11].

Seven years later, Öpik and Pryce developed a method to find the number and kind of the minimum points or wells of the APES for the $T\otimes(e+t_2)$ interaction [4].

From 1957-1958, Moffit and Thorson [12] and Longuet-Higgins *et al.* [13] showed that the wave functions of a molecule exhibiting a JT interaction should be vibronic in nature (i.e.contain both electronic and vibrational parts that can not be separated). In the same period, Liehr and Ballhausen were the first to include the quadratic terms of vibronic interactions in the $E \otimes e$ interaction [14]. They explored the nature of the warping of the $E\otimes e$ APES (i.e.warping of the Mexican hat). They found three equivalent minima along the bottom of the trough which correspond to the three directions of tetragonal distortions of the system. Since that time, a considerable number of publications have explored many different kinds of JT systems.

In 1961-1963, Bersuker was the first person to consider the splitting of the lowest vibronic energy levels due to the tunnelling of the system between the isoenergetic distorted configurations [15]. Subsequently, in 1964, O'Brien treated the $E \otimes e$ JT problem numerically with the linear and quadratic coupling included and calculated the corresponding energy levels [16]. One year later, a major advance in this field was achieved by Ham, when he introduced the concept of the vibronic reduction factor which allows physical properties of electronic origin to be calculated without fully solving the vibronic coupling problem [17]. In 1972, Englman published the first book which presents a full understanding of the basics of the JT theory as a whole [18].

However, during these years virtually all of the research work on the JT effect was directed towards cubic molecules and crystals. At that time, there was little

interest in icosahedral systems as only a few examples were known to exist. In 1978, Khlopin *et al.* were the first to study in detail the JT effect in these systems and they found solutions to various icosahedral problems [19]. Another important work on icosahedral systems at that time was by Pooler in 1980 who discussed the underlying group theory and possible symmetries of the Hamiltonian [20].

In 1985, the interest in icosahedral systems significantly increased due to the discovery of the Buckminsterfullerene C_{60} molecule by Kroto *et al.* [21]. Since then, many publications concerning JT effects in this molecule have been written. In fact, the high degeneracy of the electronic and vibrational states of this molecule makes it a rich area for JT studies as the latter requires the presence of electronic degeneracy.

In 1987, Bates and Dunn developed a new technique for studying strongly coupled JT systems which involves making unitary shift transformations [3]. They applied this method to study the $T \otimes (e + t_2)$ JT system and the results obtained showed a good agreement with those previously obtained by other authors, with one extra advantage that the states produced were automatically vibronic in nature. In 1995, the same method was applied by Dunn and Bates [22] to investigate the more complicated $T_{1u} \otimes h_g$ JT system in the fullerene C_{60}^{-}. This was the first time that vibronic states and their energies were written down in an explicit algebraic form for systems of icosahedral symmetry. This method has been used almost without exception in this thesis to study several JT interaction Hamiltonians of interest and will be discussed in more detail in Section 2.3.1.

Any molecular system subject to the JT effect can be described by a general form of Hamiltonian. This Hamiltonian usually has a complicated form and cannot be solved directly. Therefore, several approximations are used in order to simplify this Hamiltonian. Important examples include the adiabatic and harmonic approximations and these are introduced in Section 2.1. Applying these approximations leads to a less complicated form of Hamiltonian known as the vibronic (interaction) Hamiltonian from which the JT effect can be studied. This vibronic Hamiltonian can be solved using the unitary shift transformation. New positions of the nuclear displacements are produced as a result of this transformation. In order to locate these positions in the nuclear frame and to find the corresponding states, a very useful method first used by Öpik and Pryce will be used. This method is discussed fully in Section 2.3.2. Projection operator tech-

niques and the concept of symmetry-adapted states (SASs) for the system will be introduced together with a discussion of their usefulness and application in Section 2.3.3.

2.1 The adiabatic approximation

For an isolated molecule, the vibrational motion of the atoms can be resolved into fundamental vibrational motions for the entire molecule, called normal modes of vibration. The normal coordinate Q represents the progress of the normal mode so that it can be followed. The Hamiltonian for such a molecule is of the form

$$\hat{\mathcal{H}}(r,Q) = \hat{T}_{el}(r) + \hat{T}_N(Q) + \hat{U}(r,Q), \tag{2.1.1}$$

where

$$\hat{U}(r,Q) = \hat{V}_{el}(r,Q_0) + \hat{V}_N(Q) + \hat{V}(r,Q), \tag{2.1.2}$$

and where r and Q represent the electronic and the normal coordinates respectively. The term $\hat{T}_{el}(r)$ represents the kinetic energy of the electrons, $\hat{T}_N(Q)$ is the kinetic energy of the nuclei, while $\hat{U}(r,Q)$ includes the electronic $\hat{V}_{el}(r,Q_0)$ and nuclear $\hat{V}_N(Q)$ potential energies. $\hat{V}(r,Q)$ represents the electron-nuclei interaction. This is the term which concerns us most in this thesis. The corresponding Schrödinger equation to the above Hamiltonian is very difficult to solve due to the complexity of its terms. Therefore, it is necessary to introduce some approximations to solve it. One of these approximations is known as the adiabatic approximation due to Born and Huang [23]. Under this approximation, the nuclear motion is assumed to be slow compared to the electronic motion, because the nuclei are much heavier than the electrons and can therefore be expected to move slowly. This assumption allows the electronic Schrödinger equation to be solved first for the case of static nuclei, whilst regarding the nuclear kinetic energy $\hat{T}_N(Q)$ as a small perturbation. The total Hamiltonian in Eq. (2.1.1) can therefore written as

$$\mathcal{H}(r,Q) = [\hat{T}_{el}(r) + \hat{V}_{el}(r,Q_0)] + \{\hat{V}_N(Q) + \hat{V}(r,Q)\}. \tag{2.1.3}$$

The terms in the square brackets [ ] describe the electronic motion of the static nuclei, while the curly brackets {} describe the coupling between the electronic motion and the nuclear vibrations. It should be noted here that the coordinates

Q_0 represents the undistorted high symmetry configuration of the molecule or ion, while Q represents the coordinates of the distorted configuration. Thus the electronic Schrödinger equation can be written as

$$[\hat{T}_{el}(r) + \hat{V}_{el}(r, Q_0)]u_{\Gamma_i}(r, Q_0) = E_{0\Gamma}(Q_0)u_{\Gamma_i}(r, Q_0), \tag{2.1.4}$$

where $u_{\Gamma_i}(r, Q_0)$ are the electronic eigenvectors which provide an electronic basis for a matrix representation of the Hamiltonian (2.1.3), $E_{0\Gamma}$ are the corresponding eigenvalues and Γ_i indexes the set of wave functions. Here, Γ identifies an electronic irrep and i the component of the irrep.

From perturbation theory, corrections to the electronic energies $E_{0\Gamma}(Q_0)$ can be made, if the distortion in the nuclear framework and the coupling between the normal modes and the electrons is dealt with as a perturbation. Therefore, the vibronic coupling can be studied by solving the energy perturbation equation

$$\{\hat{V}_N(Q) + \hat{V}(r, Q)\}u_{\Gamma_i}(r, Q) = E_{\Gamma_i}(Q)u_{\Gamma_i}(r, Q). \tag{2.1.5}$$

This equation enables us to determine the energy corrections due to the nuclear distortions and the vibronic coupling. The vibronic interaction removes the electronic degeneracy and therefore it is convenient to write the $u_{\Gamma_i}(r, Q)$ in the form of the expansion

$$u_{\Gamma_i}(r, Q) = \sum_i c_i(Q)u_{\Gamma_i}(r, Q_0). \tag{2.1.6}$$

The states $u_{\Gamma_i}(r, Q)$ are called static JT eigenvectors or adiabatic eigenvectors. The energy eigenvalues $E_{\Gamma_i}(Q)$ are the APESs which contain several stationary points such as maxima, minima and saddle points. It is assumed that these APESs are well separated and mixing between them can be ignored when the vibronic coupling is considered [23, 5]. In this case the vibronic states may be approximated to a simple product of states

$$\Psi_{\Gamma_i}(r, Q) = \psi_{\Gamma_i}(Q)u_{\Gamma_i}(r, Q), \tag{2.1.7}$$

where $\psi_{\Gamma_i}(Q)$ describes the nuclear motion of the molecule and the electronic state $u_{\Gamma_i}(r, Q)$ of the molecule is the associated states with the APES defined by $E_{\Gamma_i}(Q)$. The approximation which led to this equation is called the adiabatic Born-Oppenheimer approximation [24].

2.2 The vibronic Hamiltonian

A further approximation called the harmonic approximation can now be made to simplify the above Hamiltonian in Eq. (2.1.5) in order to find a simple form for the vibronic Hamiltonian. This can be done by assuming that the amplitudes of the nuclear vibrations are small compared with the inter-nuclear separation. This allows the potential $\hat{V}(r,Q)$ in Eq. (2.1.5) to be expanded as a Taylor series about the equilibrium configuration Q_0 in the form:

$$\begin{aligned}\hat{V}(r,Q) &= \hat{V}(r,Q_0)+\sum_i\left[\left(\frac{\partial\hat{V}(r,Q)}{\partial Q_i}\right)_{Q_0}(Q_i-Q_{0i})\right] \\ &+ \frac{1}{2}\sum_{ij}\left[\left(\frac{\partial^2\hat{V}(r,Q)}{\partial Q_i\partial Q_j}\right)_{Q_0}(Q_i-Q_{0i})(Q_j-Q_{0j})\right]+\ldots\end{aligned} \tag{2.2.1}$$

Here, $\hat{V}(r,Q_0)$ represents the electrostatic potential energy experienced by the active electron with the nuclei fixed at $Q=Q_0$ and the sums over i and j are over all the nuclei in the molecule. It is too complicated to deal with the expansion in the above equation for real molecules because the sums over the many nuclei become large. Therefore, it is necessary to use a coordinates system that represent the whole movement of the framework of the nuclei in the molecule which transform according to the irrep of the point group of the problem. These coordinates are called the collective symmetrized coordinates Q_{Γ_γ} which will replace the coordinate system used above. Thus, each of the Q_{Γ_γ} represents a net displacement of all the nuclei, and transform as the component γ of the irrep Γ of the molecule's point group.

In terms of these coordinates, Eq. (2.2.1) can be rewritten as

$$\begin{aligned}\hat{V}(r,Q) &= \hat{V}(r,Q_0)+\sum_{\Gamma\gamma}\left[\left(\frac{\partial\hat{V}(r,Q)}{\partial Q_{\Gamma\gamma}}\right)_{Q_0}Q_{\Gamma\gamma}\right] \\ &+ \frac{1}{2}\sum_{\Gamma_i\gamma_i}\sum_{\Gamma_j\gamma_j}\left[\left(\frac{\partial^2\hat{V}(r,Q)}{\partial Q_{\Gamma_i\gamma_i}\partial Q_{\Gamma_j\gamma_j}}\right)_{Q_0}Q_{\Gamma_i\gamma_i}Q_{\Gamma_j\gamma_j}\right]+\ldots\end{aligned} \tag{2.2.2}$$

or

$$\hat{V}(r,Q)=\hat{V}(r,Q_0)+\sum_{\Gamma\gamma}\hat{V}_{\Gamma\gamma}(r,Q)Q_{\Gamma\gamma}+\frac{1}{2}\sum_{\Gamma_i\gamma_i}\sum_{\Gamma_j\gamma_j}\hat{W}_{\Gamma_i\gamma_i,\Gamma_j\gamma_j}(r,Q)Q_{\Gamma_i\gamma_i}Q_{\Gamma_j\gamma_j}. \tag{2.2.3}$$

$\hat{V}_{\Gamma\gamma}(r,Q)$ and $\hat{W}_{\Gamma_i\gamma_i,\Gamma_j\gamma_j}(r,Q)$ are called the linear and quadratic coupling constants respectively.

This equation can be further simplified by expressing the terms $\hat{W}_{\Gamma_i\gamma_i,\Gamma_j\gamma_j}(r,Q)$ and $Q_{\Gamma_i\gamma_i}Q_{\Gamma_j\gamma_j}$ in tensor forms

$$\{\hat{W}(\Gamma_i\otimes\Gamma_j)\}_{\Gamma\gamma}=\sum_{\gamma_i}\sum_{\gamma_j}\left[\hat{W}_{\Gamma_i\gamma_i,\Gamma_j\gamma_j}(r,Q)\langle\Gamma_i\gamma_i\ \Gamma_j\gamma_j|\Gamma\gamma\rangle\right] \tag{2.2.4}$$

and

$$\{Q(\Gamma_i\otimes\Gamma_j)\}_{\Gamma\gamma}=\sum_{\gamma_i}\sum_{\gamma_j}\left[Q_{\Gamma_i\gamma_i}Q_{\Gamma_j\gamma_j}\langle\Gamma_i\gamma_i\ \Gamma_j\gamma_j|\Gamma\gamma\rangle\right]. \tag{2.2.5}$$

Therefore, the vibronic potential Eq. (2.2.3) can be rewritten in the form

$$\begin{aligned}\hat{V}(r,Q) &= \hat{V}(r,Q_0)+\sum_{\Gamma\gamma}\hat{V}_{\Gamma\gamma}(r,Q)Q_{\Gamma\gamma} \\ &+ \frac{1}{2}\sum_{\Gamma\gamma}\sum_{\Gamma_i\Gamma_j}\{\hat{W}(\Gamma_i\otimes\Gamma_j)\}_{\Gamma\gamma}\{Q(\Gamma_i\otimes\Gamma_j)\}_{\Gamma\gamma}.\end{aligned} \tag{2.2.6}$$

The first term in this equation is the potential energy of the electron as mentioned before in Eq. (2.1.2). Substituting the above potential into Eq. (2.1.2) and then into the Hamiltonian Eq. (2.1.1) gives

$$\hat{\mathcal{H}}(r,Q)=\hat{\mathcal{H}}_e(r,Q_0)+\hat{\mathcal{H}}_v(r,Q), \tag{2.2.7}$$

where the electronic Hamiltonian is given by

$$\hat{\mathcal{H}}_e(r,Q_0)=\hat{T}_{el}(r)+\hat{V}(r,Q_0), \tag{2.2.8}$$

and the vibronic Hamiltonian as

$$\begin{aligned}\hat{\mathcal{H}}_v(r,Q) &= \sum_{\Gamma\gamma}\hat{V}_{\Gamma\gamma}(r,Q)Q_{\Gamma\gamma} \\ &+ \frac{1}{2}\sum_{\Gamma\gamma}\sum_{\Gamma_i\Gamma_j}\{\hat{W}(\Gamma_i\otimes\Gamma_j)\}_{\Gamma\gamma}\{Q(\Gamma_i\otimes\Gamma_j)\}_{\Gamma\gamma}.\end{aligned} \tag{2.2.9}$$

2.2.1 Basis wave functions

In order to study the JT interaction, we shall use the matrix representation form of the JT Hamiltonian. As shown above, several assumptions have been made to simplify the molecular Hamiltonian in order to derive a general form of the vibronic Hamiltonian from which the JT effect can be studied. Now, the vibronic

Hamiltonian in Eq.(2.2.9) can be expressed as a matrix representation by placing it between the electronic states $u_{\Gamma_i}(r, Q_0)$ which form the basis for the matrix. This is written as

$$\begin{aligned}\langle u_{\Gamma_i}|\hat{\mathcal{H}}_v|u_{\Gamma_j}\rangle &= \sum_{\Gamma\gamma}\langle u_{\Gamma_i}|\hat{V}_{\Gamma\gamma}(r,Q)|u_{\Gamma_j}\rangle Q_{\Gamma\gamma} \\ &+ \frac{1}{2}\sum_{\Gamma\gamma}\sum_{\Gamma_i\Gamma_j}\langle u_{\Gamma_i}|\hat{W}(\Gamma_i\otimes\Gamma_j)_{\Gamma\gamma}|u_{\Gamma_j}\rangle Q(\Gamma_i\otimes\Gamma_j)_{\Gamma\gamma}.\end{aligned} \tag{2.2.10}$$

This matrix element can be simplified further if we exclude the term for the totally symmetric A mode. The A term which is linear in $Q_{\Gamma\gamma}$ causes an energy shift to all the electronic levels and can therefore be ignored by redefining the zero of energy. The other term which is quadratic in $Q_{\Gamma\gamma}$ is equal to the elastic energy of the nuclei $\frac{1}{2}\sum_{\Gamma\gamma}\mu\omega_\Gamma^2 Q_{\Gamma\gamma}^2$, where μ and ω are the reduced mass of the nuclei and the frequency of vibrations respectively. The elastic energy can be added to the kinetic energy of the nuclei $\frac{1}{2}\sum_{\Gamma\gamma}\frac{1}{\mu}P_{\Gamma\gamma}^2$ to form the Hamiltonian for a set of simple Harmonic oscillators

$$\mathcal{H}_{SHO} = \frac{1}{2}\sum_{\Gamma\gamma}\left(\frac{1}{\mu}P_{\Gamma\gamma}^2 + \mu\omega_\Gamma^2 Q_{\Gamma\gamma}^2\right), \tag{2.2.11}$$

where $P_{\Gamma\gamma}$ is the linear momentum of the nuclei.

The Wigner-Eckart theorem [25] can be applied to Eq. (2.2.10) so that the matrix elements on the right can be written as

$$\begin{aligned}\langle u_{\Gamma_i}|\hat{V}_{\Gamma\gamma}(r,Q)|u_{\Gamma_j}\rangle &= \langle u_\Gamma||\hat{V}_\Gamma(r)||u_\Gamma\rangle\ \langle\Gamma\gamma u_{\Gamma_i}|u_{\Gamma_j}\rangle \\ \langle u_{\Gamma_i}|\hat{W}(\Gamma_i\otimes\Gamma_j)_{\Gamma\gamma}|u_{\Gamma_j}\rangle &= \langle u_\Gamma||\hat{W}(\Gamma_i\otimes\Gamma_j)_\Gamma||u_\Gamma\rangle\ \langle\Gamma\gamma u_{\Gamma_i}|u_{\Gamma_j}\rangle.\end{aligned} \tag{2.2.12}$$

The $\langle u_\Gamma||\hat{V}_\Gamma(r)||u_\Gamma\rangle$ and $\langle u_\Gamma||\hat{W}(\Gamma_i\otimes\Gamma_j)_\Gamma\rangle$ are called the reduced matrix elements or respectively the linear and quadratic vibronic coupling coefficients. They measure the strength of the electron-phonon coupling in both the linear and quadratic interaction and for simplicity they will be denoted by $V_{\Gamma\gamma}$ and $W_\Gamma^{\Gamma_i\Gamma_j}$.

Now, the interaction Hamiltonian Eq. (2.2.10) can be rewritten in matrix form as

$$\begin{aligned}\langle u_{\Gamma_i}|\hat{\mathcal{H}}_v|u_{\Gamma_j}\rangle &= \frac{1}{2}\sum_{\Gamma\gamma}\left(\frac{1}{\mu}P_{\Gamma\gamma}^2 + \mu\omega_\Gamma^2 Q_{\Gamma\gamma}^2\right) I \\ &+ \sum_{\Gamma\gamma\neq A} V_{\Gamma\gamma}Q_{\Gamma\gamma}\langle\Gamma\gamma u_{\Gamma_i}|u_{\Gamma_j}\rangle \\ &+ \frac{1}{2}\sum_{\Gamma\gamma\neq A}\sum_{\Gamma_i\Gamma_j} W_\Gamma^{\Gamma_i\Gamma_j}Q(\Gamma_i\otimes\Gamma_j)_{\Gamma\gamma}\langle\Gamma\gamma u_{\Gamma_i}|u_{\Gamma_j}\rangle.\end{aligned} \tag{2.2.13}$$

where I is the identity matrix. This is called the vibronic Hamiltonian in which the first term describes a set of simple harmonic oscillators. The second term represents the linear coupling between the electrons and phonons whilst the third term represents the quadratic coupling. The $\langle \Gamma\gamma u_{\Gamma_j}|u_{\Gamma_i}\rangle$ terms are called the Clebsch-Gordon (CG) coefficients [26, 27]. These coefficients can be arranged into square matrices of dimension $[\Gamma \times \Gamma]$.

The terms in the above Hamiltonian can be defined as

$$\begin{aligned} \mathcal{H}_{vib} &= \frac{1}{2}\sum_{\Gamma\gamma}\left(\frac{1}{\mu}P^2_{\Gamma\gamma} + \mu\omega^2_{\Gamma}Q^2_{\Gamma\gamma}\right) I, \\ \mathcal{H}_{int} &= \sum_{\Gamma\gamma\neq A} V_{\Gamma\gamma}Q_{\Gamma\gamma}\langle \Gamma\gamma u_{\Gamma_i}|u_{\Gamma_j}\rangle, \\ \mathcal{H}_{quad} &= \frac{1}{2}\sum_{\Gamma\gamma\neq A}\sum_{\Gamma_i\Gamma_j} W^{\Gamma_i\Gamma_j}_{\Gamma} Q(\Gamma_i \otimes \Gamma_j)_{\Gamma\gamma}\langle \Gamma\gamma u_{\Gamma_i}|u_{\Gamma_j}\rangle. \end{aligned} \tag{2.2.14}$$

Thus, a general form of the total vibronic Hamiltonian may be expressed as

$$\mathcal{H}_{tot} = \mathcal{H}_{vib} + \mathcal{H}_{int} + \mathcal{H}_{quad} \tag{2.2.15}$$

The above form of the Hamiltonian is the one which can apply to any JT system. The linear interaction Hamiltonian for the $T_{1u} \otimes h_g$ JT system will be taken here as an example of how to construct such a Hamiltonian. Let us start with the second term in Eq. 2.2.14, this term can be expanded as

$$\mathcal{H}_{int} = V_1 Q_\theta \begin{bmatrix} \langle T_{1x}h_\theta|T_{1x}\rangle & \langle T_{1x}h_\theta|T_{1y}\rangle & \langle T_{1x}h_\theta|T_{1z}\rangle \\ \langle T_{1y}h_\theta|T_{1x}\rangle & \langle T_{1y}h_\theta|T_{1y}\rangle & \langle T_{1y}h_\theta|T_{1z}\rangle \\ \langle T_{1z}h_\theta|T_{1x}\rangle & \langle T_{1z}h_\theta|T_{1y}\rangle & \langle T_{1z}h_\theta|T_{1z}\rangle \end{bmatrix} + \ldots, \tag{2.2.16}$$

where $T_{1\alpha}$ represents the α component of the T electronic states which forms the bases for the matrix representation, h_θ is the θ component of the h vibrational mode and $\langle T_{1x}h_\theta|T_{1x}\rangle$ is a CG coefficient which are given in Ref. [27]. The ellipsis represents equivalent terms for the other components of $\{h_\theta, h_\epsilon, h_4, h_5, h_6\}$. Constructing the interaction Hamiltonian is straightforward now but care should be taken when using the tables in Ref. [27] to obtain CG coefficients. Substituting the CG coefficients, this Hamiltonian becomes

$$\mathcal{H}_{int} = \frac{1}{2}\sqrt{\frac{3}{5}} V_1 Q_\theta \begin{bmatrix} \phi^{-1} & 0 & 0 \\ 0 & -\phi & 0 \\ 0 & 0 & 1 \end{bmatrix} + \ldots, \tag{2.2.17}$$

where $\phi = \frac{1}{2}(\sqrt{5}+1)$ is the golden mean.

Summing all the components, the linear interaction Hamiltonian for this system has the form [22],

$$\mathcal{H}_{int} = \frac{\sqrt{3}}{2\sqrt{5}} V_1 \begin{bmatrix} \phi^{-1}Q_\theta + \frac{\phi^2 Q_\epsilon}{\sqrt{3}} & \sqrt{2}Q_6 & \sqrt{2}Q_5 \\ \sqrt{2}Q_6 & -\phi Q_\theta - \frac{\phi^{-2}Q_\epsilon}{\sqrt{3}} & \sqrt{2}Q_6 \\ \sqrt{2}Q_5 & \sqrt{2}Q_4 & Q_\theta - \sqrt{\frac{5}{3}}Q_\epsilon \end{bmatrix}. \qquad (2.2.18)$$

Further details on the construction of such matrices can be found in Refs. [28] and [29].

2.2.2 The adiabatic potential energy surface (APES)

Assuming that the above vibronic Hamiltonian may be diagonalized, as mentioned earlier, a set of APESs will be generated. If the coupling is strong, the energy difference between the APESs will be much greater than the vibrational energy $\hbar\omega$. Therefore, it is assumed that the nuclear motion is confined to the lowest APES (LAPES). An analysis of this LAPES shows that, when only linear coupling terms are included, there will be either a continuous equal energy surface (trough) or a set of distinct minima (wells). If the quadratic coupling terms are included, then for the case when the energy surface is a trough, the surface of the trough will warp to give local minima (for example, this happens in the $E \otimes e$ system). In the case of wells, the depth of the wells and their separation from each other will be modified with no change in the behaviour of the system. The work presented in this thesis assumes the case when the LAPES shows distinct minima through linear or quadratic coupling.

Up to this point, the wave functions for each case are specified according to the strengths of the coupling. In infinite coupling where the wells are infinitely deep, the JT system is localised in one of the wells and therefore the eigenstates for the system will be the associated well states, and this what is called a *static* JT system.

For finite coupling strengths, when the height of the barriers between the wells is finite, the system will be able to tunnel from one well to another and therefore the correct eigenstates will be the symmetry-adapted states which are linear combinations of the well states. The tunnelling between wells of the system is known

as the *dynamical* JT effect.

2.3 Computational methods

This section presents some techniques that will be used to treat JT problems in the case when the APES has the form of distinct minima.

2.3.1 The unitary shift transformation

The interaction Hamiltonian (2.2.13) is still very difficult to diagonalize within the electronic basis in order to find the well positions (or minima) on the LAPES and the associated states. The difficulty arises because the vibronic Hamiltonian still includes both electronic and vibrational terms. An efficient method to deal with this problem is to use a unitary shift transformation. This method was introduced by Bates and Dunn [3] and involves applying a transformation operator to the Hamiltonian in order to displace, or shift, each of the nuclear coordinates Q_j to points $Q_j - \alpha_j \hbar$, where the α_j specify the positions of the wells on the APES. The unitary shift operator is defined as

$$U = \exp\left[\mathrm{i}\sum_j \alpha_j P_j\right], \tag{2.3.1}$$

where P_j is the momentum operator conjugate to Q_j. These are expressed in terms of creation and annihilation operators $b_j^\dagger$ and b_j, respectively, as follows

$$P_j = -\mathrm{i}\hbar\frac{\partial}{\partial Q_j} = \mathrm{i}\sqrt{\frac{\hbar\mu\omega}{2}}\left(b_j - b_j^\dagger\right) \tag{2.3.2}$$

$$Q_j = -\sqrt{\frac{\hbar}{2\mu\omega}}\left(b_j + b_j^\dagger\right) \tag{2.3.3}$$

where b_j and $b_j^\dagger$ act on the states in the following way

$$b\,|n\rangle = \sqrt{n}\,|n-1\rangle\,, \tag{2.3.4}$$

$$b^\dagger\,|n\rangle = \sqrt{n+1}\,|n+1\rangle\,. \tag{2.3.5}$$

The general form of the Schrödinger equation for the system is written as the total Hamiltonian operating on the untransformed vibronic state as

$$\begin{aligned} \mathcal{H}_{tot}|\Psi'\rangle &= E|\Psi'\rangle \\ U^\dagger\mathcal{H}_{tot}|\Psi'\rangle &= E\ U^\dagger|\Psi'\rangle \\ U^\dagger\mathcal{H}_{tot}U\ U^\dagger|\Psi'\rangle &= E\ U^\dagger|\Psi'\rangle \end{aligned} \tag{2.3.6}$$

or

$$\tilde{\mathcal{H}}|\Psi\rangle = E\ |\Psi\rangle \tag{2.3.7}$$

where a tilde indicates the transformed Hamiltonian $\tilde{\mathcal{H}} = U^\dagger\mathcal{H}_{tot}U$ and $|\Psi\rangle = U^\dagger|\Psi'\rangle$. The untransformed eigenfunctions are therefore

$$|\Psi'\rangle = U\ |\Psi\rangle. \tag{2.3.8}$$

The advantage of acting by the shift operator is that, the full vibronic Hamiltonian Eq. (2.2.15) may be split into two terms as

$$\tilde{\mathcal{H}} = U^\dagger\mathcal{H}_{tot}U = \tilde{\mathcal{H}}_1 + \tilde{\mathcal{H}}_2, \tag{2.3.9}$$

The $\tilde{\mathcal{H}}_1$ term contains only values of α_j while $\tilde{\mathcal{H}}_2$ contains all the other terms related to Q_j and P_j. As our aim is to determine the ground states of the system in strong coupling, only the $\tilde{\mathcal{H}}_1$ term needs to be considered. At this stage, we ignore the $\tilde{\mathcal{H}}_2$ terms.

The shift transformation is accomplished as follow

$$\begin{aligned} \tilde{\mathcal{H}} &= U^\dagger\mathcal{H}_{tot}U \\ &= U^\dagger[\mathcal{H}_{tot}, U] + U^\dagger U\mathcal{H}_{tot} \\ &= U^\dagger[\mathcal{H}_{vib}, U] + U^\dagger[\mathcal{H}_{int}, U] + U^\dagger[\mathcal{H}_{quad}, U] + \mathcal{H}_{tot} \end{aligned} \tag{2.3.10}$$

Simplifying this Hamiltonian can be achieved readily with the help of the following commutators

$$\begin{aligned} [Q_j, P_k] &= \mathrm{i}\hbar\delta_{jk}, \\ [Q_j, U] &= -\hbar\alpha_j U, \\ [Q_jQ_k, U] &= U\hbar\left(\hbar\alpha_j\alpha_k - \alpha_jQ_k - \alpha_kQ_j\right) \\ &= -\hbar\left(\hbar\alpha_j\alpha_k + \alpha_jQ_k + \alpha_kQ_j\right)U, \end{aligned} \tag{2.3.11}$$

which can be easily verified by direct calculation. We are only interested in finding $\tilde{\mathcal{H}}_1$ and so anything still involving phonon operators can be dropped because they

will belong to $\tilde{\mathcal{H}}_2$. For example, the first term in Eq. 2.3.10 can be written, using Eq. (2.3.11), as

$$\begin{aligned} U^\dagger[\mathcal{H}_{vib}, U] &= \frac{1}{2}U^\dagger \sum_j \left(\tfrac{1}{\mu}[P_j^2, U] + \mu\omega^2[Q_j^2, U]\right) \\ &= \frac{1}{2}\hbar\mu\omega^2 \sum_j \left(\hbar\alpha_j^2 - 2\alpha_j Q_j\right). \end{aligned} \tag{2.3.12}$$

Therefore, it will contribute $\frac{1}{2}\hbar^2\mu\omega^2\sum_j \alpha_j^2$ to $\tilde{\mathcal{H}}_1$ and $-\hbar\mu\omega^2\sum_j \alpha_j Q_j$ to $\tilde{\mathcal{H}}_2$.

Having obtained $\tilde{\mathcal{H}}_1$, the values of α_j required to minimise the energy (and their associated eigenfunctions) can be determined by using the minimisation procedure developed by Öpik and Pryce, which will be discussed in the following section.

2.3.2 The method of Öpik and Pryce

This method is concerned with identifying the positions of the stationary points on the APES. According to the approximations discussed previously, we have produced a Hamiltonian $\tilde{\mathcal{H}}_1(\alpha_j)$ that contains only values of α_j and satisfies the Schrödinger equation

$$\tilde{\mathcal{H}}_1(\alpha_j)|\Psi(r)\rangle = E|\Psi(r)\rangle, \tag{2.3.13}$$

where $\Psi(r)$ is the eigenvector (assumed normalised so that $\langle\Psi(r)|\Psi(r)\rangle = 1$) which can be described by c_i parameters that represents the direction cosines between the eigenvector $\Psi(r)$ and the main components of the electronic basis. The energy of the system is given by the expectation value of $\tilde{\mathcal{H}}_1(\alpha_j)$ within the electronic eigenvector $\Psi(r)$ as

$$E = \langle\Psi(r)|\tilde{\mathcal{H}}_1(\alpha_j)|\Psi(r)\rangle. \tag{2.3.14}$$

Following the method of Öpik and Pryce [4], we minimize this expression for the energy with respect to the values of α_j by setting

$$\begin{aligned} \frac{\partial E}{\partial \alpha_j} &= 0 \\ &= \frac{\partial}{\partial \alpha_j}\left(\langle\Psi(r)|\tilde{\mathcal{H}}_1(\alpha_j)|\Psi(r)\rangle\right) \\ &= \langle\Psi(r)|\frac{\partial\tilde{\mathcal{H}}_1(\alpha_j)}{\partial\alpha_j}|\Psi(r)\rangle, \end{aligned} \tag{2.3.15}$$

A set of equations for α_j the positions on the APES in terms of c_i may be found. These steps are analogous to those accomplished by Ceulemans and Fowler in

Ref. [30]. Substituting these αs back into Eq. (2.3.14) gives an expression which is a function of c_i only namely

$$E = \langle \Psi(r)|\tilde{\mathcal{H}}_1(c_i)|\Psi(r)\rangle. \tag{2.3.16}$$

By minimising this expression with respect to these parameters as

$$\begin{aligned} \frac{\partial E}{\partial c_i} &= 0 \\ &= \frac{\partial}{\partial c_i}\left(\langle \Psi(r)|\tilde{\mathcal{H}}_1(c_i)|\Psi(r)\rangle\right) \\ &= \langle \Psi(r)|\frac{\partial \tilde{\mathcal{H}}_1(c_i)}{\partial c_i}|\Psi(r)\rangle, \end{aligned} \tag{2.3.17}$$

the electronic coefficients can be found and therefore the transformed electronic eigenvectors $|A;0\rangle$ can be obtained. The values of the α_js can then be calculated straightforwardly by substituting the electronic coefficients into the equations obtained for the α_js.

The vibronic states which are the eigenstates for the interaction Hamiltonian $\mathcal{H}_{tot}$ before the shift transformation, can be found by multiplying the transformed electronic eigenvectors $|A;0\rangle$ by the value U_A for that state namely

$$|A';0\rangle = U_A|A;0\rangle = U_A|A\rangle|0\rangle, \tag{2.3.18}$$

where $|A\rangle$ represents the transformed orbital state and $|0\rangle$ denotes that all phonon modes are in their ground states. The states like (2.3.18) are called the untransformed states (or Glauber states [31]) and they are automatically vibronic as the shift operators U_A contain phonon operators.

2.3.3 Projection operators

In the previous section, it has been shown how the positions of the minima in the APES can be located by using the Öpik-Pryce method and therefore the form of the associated wave functions at the minima can be found. As mentioned in Section 2.2.2, if the system has infinite coupling, then the system will be localised in one of these minima and the vibronic states obtained already for the system are good eigenstates for the static JT case. However, if the coupling strength is finite, then the vibronic states associated with the wells are not appropriate eigenstates for the system as a whole and the correct eigenstates will be a linear

combination of the well states due to the tunnelling between the wells (see e.g. Refs [32] and [33]). Therefore, the projection operator technique can be used to construct the required combination which generates a set of symmetry adapted states (SASs) from a set of non-symmetrized states.

The general theory of projection operators can be found in Refs. [34]-[35]. For any point group of symmetry $\mathcal{G}$ with irreps Γ^i, the projection operators ρ^i_{ts} for each of the irreps can be defined as [36]

$$\rho^i_{ts} = \frac{d_i}{g} \sum_{R \in \mathcal{G}} D^i_{ts}(R)^* \hat{R}, \tag{2.3.19}$$

where g is the order of the group $\mathcal{G}$, d_i is the dimension of the irreps Γ^i, $\hat{R}$ is a symmetry operation of the group $\mathcal{G}$ and $D^i_{ts}(R)^*$ is the complex conjugate of the ts^{th} element of the matrix representation of the symmetry operation $\hat{R}$. The effect of the operator ρ^i_{ts} when applied to a state of undefined symmetry acting in a space of group operators produces either zero or a linear combination of the basis; for the irreps Γ^i (e.g. Γ^i for the group I are A, T_1, T_2, G and H). In another words, a complete basis set of SASs can be obtained by applying the projection operator for each irrep to an arbitrary function until we obtain all the required basis states. For example, for the $T \otimes h$ problem it was found that for the case of D_{5d} minima, on applying the projection operator with T_{1ux} irrep to $|A';0\rangle$ the state of well A, the obtained SAS has the form

$$|T_{1ux}\rangle = [\phi^{-1}(|C';0\rangle + |D';0\rangle) + (|E';0\rangle - |F';0\rangle)], \tag{2.3.20}$$

where $|T_{1ux}\rangle$ is the SAS of T_{1ux} irrep. In order to construct the projection operators for a certain point group, the matrix representations of the symmetry operations for each irrep are required. For the C_{60} molecule, some of the required matrices are given in Ref. [37].

To find the energies corresponding to the SASs, the matrix elements of the total Hamiltonian $\mathcal{H}_{tot}$ between all relevant untransformed vibronic states $|X';0\rangle$ should be evaluated first. This can be done by evaluating

$$M_{X_1X_2} = \langle X'_1;0|\mathcal{H}_{tot}|X'_2;0\rangle. \tag{2.3.21}$$

The energy of the SASs follow from these $M_{X_1X_2}$. Applying this to the above SAS, we can find that the energy of the state is

$$E_{T1u} = \frac{M_{CD} + \ldots}{\langle T_{1ux}|T_{1ux}\rangle}. \tag{2.3.22}$$

The denominator here involves matrix elements of the form $\langle C';0|\mathcal{H}_{tot}|D';0\rangle$, which can be simplified to $S\langle D'|C'\rangle_{elect}$. The term S refers to the phonon overlap $\langle 0|U_D^{\dagger}U_C|0\rangle$ which can be obtained for the different wells D and C using the formula

$$S = \exp\left[-\frac{1}{2}\sum_i \left(C_i^{(D)} - C_i^{(C)}\right)^2\right], \tag{2.3.23}$$

where

$$C_i^{(j)} = -\sqrt{\frac{\hbar\mu\omega}{2}}\alpha_i^{(j)}, \tag{2.3.24}$$

and j labels the components of the phonon states (e.g. for the h mode $j = \{\theta, \epsilon, 4, 5, 6\}$). Further information about Eq.(2.3.23) can be found in Ref. [33].

2.4 The icosahedral point group

Since our interest in this thesis is to study the dynamic JT systems in different systems involving C_{60} ions, it is very useful to start by considering the symmetry group to which our fundamental system belongs. This will facilitate identifying the electronic and vibrational states in JT systems by labelling them with the help of group theory.

The C_{60} molecule belongs to the icosahedral point group (I_h), which is the largest symmetry point group allowed in three dimensional space. The molecule itself possesses the geometry of a truncated icosahedron as shown in Fig. 2.1, with the 60 carbon atoms located at the vertices. Twelve pentagonal faces replace the twelve truncated vertices of the icosahedral and twenty hexagonal faces replacing the twenty triangles. The symmetry group I of the icosahedron consists of 60 rotation operations, which correspond to the rotation of the icosahedron by an angle $\alpha = \frac{2\pi}{n}$ about the various n-fold symmetry axes present. In all, there are fifteen 2-fold, ten 3-fold and six 5-fold axes of rotation. The 5-fold axes join two different opposing vertices. The 3-fold axes join the centres of two opposite triangles, while the 2-fold axes join the mid-points of opposite edges. The rotation angle α divides the icosahedral rotation operators into five classes. The class C_1 contains only the identity operator (E); the classes C_2 and C_3 contain all rotations about 5-fold symmetry axes and the class C_4 contains all 3-fold symmetry axes rotations, while class C_5 contains the 2-fold symmetry rotations.

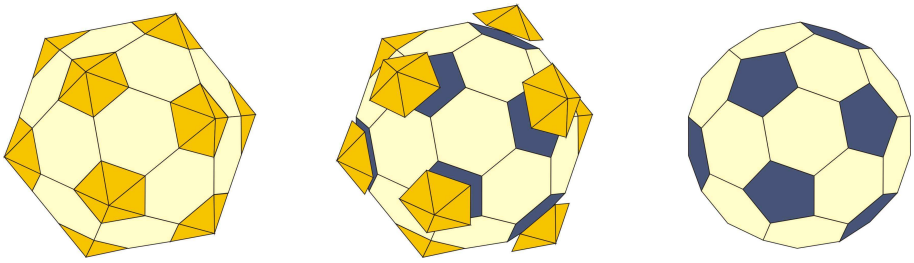

Figure 2.1: The figure on the left is the geometrical shape of a regular icosahedron which can be truncated to produce the C_{60} molecule (right).

	E	$12C_5$	$12C_5^2$	$20C_3$	$15C_2$	i	$12S_{10}^3$	$12S_{10}$	$20S_3$	$15\sigma_v$
A_g	$+1$	$+1$	$+1$	$+1$	$+1$	$+1$	$+1$	$+1$	$+1$	$+1$
T_{1g}	$+3$	$+\phi$	$1-\phi$	0	-1	$+3$	ϕ	$1-\phi$	0	-1
T_{2g}	$+3$	$1-\phi$	$+\phi$	0	-1	$+3$	$1-\phi$	ϕ	0	-1
G_g	$+4$	-1	-1	$+1$	0	$+4$	-1	-1	$+1$	0
H_g	$+5$	0	0	-1	$+1$	$+5$	0	0	-1	$+1$
A_u	$+1$	$+1$	$+1$	$+1$	$+1$	-1	-1	-1	-1	-1
T_{1u}	$+3$	$+\phi$	$1-\phi$	0	-1	-3	$-\phi$	$\phi-1$	0	$+1$
T_{2u}	$+3$	$1-\phi$	$+\phi$	0	-1	-3	$\phi-1$	$-\phi$	0	$+1$
G_u	$+4$	-1	-1	$+1$	0	-4	$+1$	$+1$	-1	0
H_u	$+5$	0	0	-1	$+1$	-5	0	0	$+1$	-1

Table 2.1: Character table for the I_h group, the golden mean $\phi = \frac{1}{2}(1+\sqrt{5})$.

.

The C_{60} molecule also possesses inversion through its centre as a further class of symmetry operations. Interchanging any of the sixty carbon atoms with its opposite atom by inversion leaves C_{60} unchanged. Thus, the inversion operator (i) (or parity operator) can be included as an additional symmetry operator for the C_{60} molecule. Combining this operator with the 60 operations of the group I produces the full 120 element, icosahedral point group I_h with 10 classes included. The classification of the classes of the full group in terms of their character is shown in Table 2.1.

2.4.1 Irreducible representations (irreps)

As mentioned above, identifying the molecule's symmetry in terms of the symmetry operations conforms with the mathematical requirements of the molecule. In other words, using tools provided by group theory to describe and analyse some of the physical properties of such molecules is a powerful technique to facilitate understanding of the whole problem. The irreducible representations (irreps) of the point group are one of these tools. Table 2.1 shows the irreps for the icosahedral point group. In the first column on the left there are ten irreps: two with one-dimension ($A_{g/u}$), two with four-dimensions ($G_{g/u}$), two with five-dimensions ($H_{g/u}$) and four with three-dimensions ($T_{1g/1u}$), ($T_{2g/2u}$). All are subscripted according to whether the basis states of their matrix representations are even (g) or odd (u). Each of the irreps is defined by basis functions that transform among themselves. For example, the irrep T_{1u} related to the components $\{p_x, p_y, p_z\}$ of p-orbital. The complete set of basis functions is most conveniently defined in terms of spherical harmonics wave functions. Therefore, the irreps of the group I_h can be classified in terms of spherical harmonics wave functions as shown in Table 2.2 [38]. This table tells us that each of the irreps of the group I_h can be expressed as spherical harmonics $Y_{l,m}$ with specific angular momentum quantum number.

It is convenient to label the electronic and vibrational states of the C_{60} molecule using the irreps of the icosahedral point group. In the following chapters, JT systems relevant to C_{60} molecules and ions will be classified using such irreps labels. The electronic states will be labelled using uppercase letters, while the vibrational states will be denoted by lowercase letters. For example, the $T \otimes h$ system involves a coupling of an electronic T triplet with a set of five dimensional h-type quintet vibrations.

2.4.2 Electronic structure of C_{60}

Since the JT interactions in C_{60} ions deal with the electronic structure of the molecule, it is worthwhile reviewing the electronic structure of the isolated C_{60} molecule. Hückel molecular orbital (HMO) theory provides a useful starting point for the energy levels of the undoped C_{60} [39], so that we can subsequently consider its anionic and cationic forms. Fig. 2.2 shows that the ground state of neutral

l	Irreps of I_h
0	A_g
1	T_{1u}
2	H_g
3	$T_{2u} \oplus G_u$
4	$G_g \oplus H_g$
5	$T_{1u} \oplus T_{2u} \oplus H_u$
6	$A_g \oplus T_{1g} \oplus G_g \oplus H_g$
7	$T_{1u} \oplus T_{2u} \oplus G_u \oplus H_u$
8	$T_{2g} \oplus G_g \oplus 2H_g$
9	$T_{1u} \oplus T_{2u} \oplus 2G_u \oplus H_u$
10	$A_g \oplus T_{1g} \oplus T_{2g} \oplus G_g \oplus 2H_g$
11	$2T_{1u} \oplus T_{2u} \oplus G_u \oplus 2H_u$
12	$A_g \oplus T_{1g} \oplus T_{2g} \oplus 2G_g \oplus 2H_g$
13	$T_{1u} \oplus 2T_{2u} \oplus 2G_u \oplus 2H_u$
14	$T_{1g} \oplus T_{2g} \oplus 2G_g \oplus 3H_h$
15	$A_u \oplus 2T_{1u} \oplus 2T_{2u} \oplus 2G_u \oplus 2H_u$

Table 2.2: Spherical harmonic functions $Y_{l,m}$ reduced to irreps of I_h. (Based on Ref. [38] with extension to l=15).

C_{60} possesses a closed shell electronic structure with ten electrons in an electronic quintet orbital, giving an A_g ground state. This highest occupied molecular orbital (HOMO) has the irrep of H_u in the I_h group. The C_{60} molecule in this form does not exhibit any vibronic interaction because it is non-degenerate and therefore JT interaction is unexpected for this structure. The lowest unoccupied molecular orbital (LUMO) is an electronic triplet orbital with T_{1u} symmetry. This is a 3-fold degenerate orbital and so it can hold up to six electrons. The JT interaction is possible, therefore, if electrons are added (or removed) from the nuclear species. Once the isolated C_{60} is doped, either cations C_{60}^{n+} or anions C_{60}^{n-} can be formed. The cation C_{60}^{n+} is formed when n electrons are taken from the HOMO of the neutral C_{60} molecule. The removal of electrons will cause vacancies to appear in the HOMO. These vacancies or 'holes' behave as positively charged particles and can be coupled to a vibrational mode via JT interaction. The other doped form

of C_{60} occurs by electron addition to form C_{60}^{n-} anions. These are formed when n electrons are added to the LUMO of C_{60} to form electron-doped molecules. These anions are also coupled to the vibrational modes and thus exhibit JT interactions.

The electronic structure shown in Fig. 2.2 is a good starting point for the theoretical analyses presented in this thesis. However, one should be aware of the vast literature related to the electronic structure of C_{60}. A good general reference is the book by Dresselhaus *et al.* [40]. Specific works of particular interest include the paper by Deng and Yang [41] which gives easy access to the functional forms of the molecular orbitals involved and the band structure calculations of Laouini *et al.* [42] which consider the molecular orbitals in the context of the solid state. Another good paper is that by Green *et al.* [43] which gives the results of density functional calculations of the neutral C_{60} molecules and its negatively charged anions.

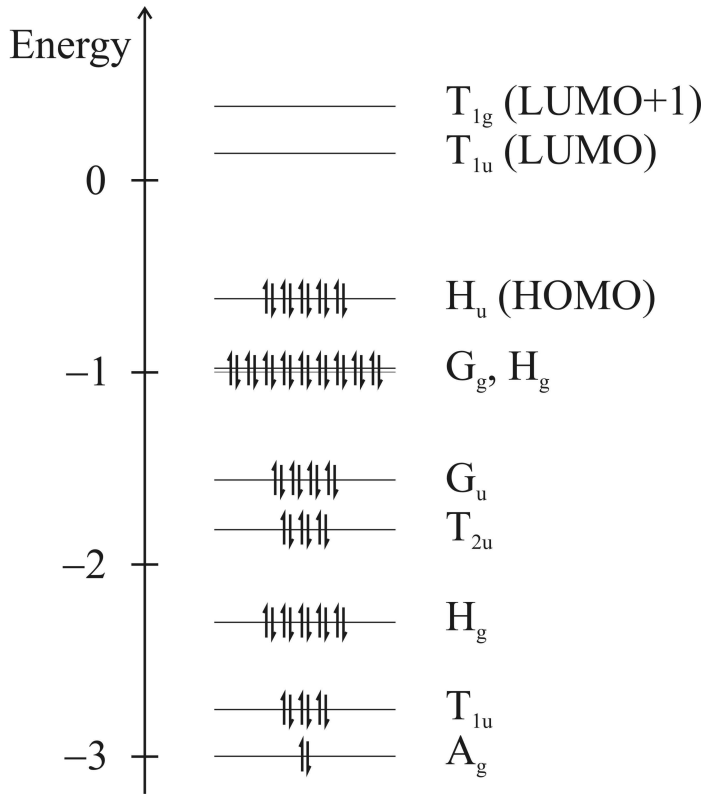

Figure 2.2: Hückel molecular orbital diagram for C_{60} showing the first 36 orbitals of lower energy [44]. Only the first 30 are filled in neutral C_{60}.

2.5 Vibronic coupling in C_{60}

For any polyatomic molecule composed of n atoms, the motion of each atom can be resolved into components along the three directions of a Cartesian coordinate system. Therefore, any molecule consisting of n atoms possesses $3n$ degrees of freedom, including vibrations, translations, and rotations. The vibrational motions of the atoms can always be resolved into fundamental vibrational motions for the entire molecule, called normal modes of vibration. It is well known that any non-linear molecule has three translations and three rotations. Then the number of the normal modes for the non-linear molecules is $3n$ minus the number of the non-vibrational motions (translations and rotations). Therefore, a polyatomic molecule such as C_{60} possesses $3n$-6 normal modes of vibrations [45].

The C_{60} molecule has 180 degrees of freedom, this 180 minus the six modes of translations and rotations leaves 174 normal modes of vibrations. Group theory classifies the 180 degrees of freedom as $a_u + 5t_{1u} + 5t_{2u} + 6g_u + 7h_u + 2a_g + 4t_{1g} + 4t_{2g} + 6g_g + 8h_g$. There is one t_{1u} and one t_{1g} mode that correspond to the translational and rotational modes. Omitting these two modes from the 180 leaves 174 vibrational modes.

It should be noted here that not all the above modes can couple to the electronic orbitals to form JT interactions. The modes of interest that concern us must satisfy specific conditions to be JT normal modes. Suppose that we have an electronic state within icosahedral symmetry with irrep Γ and nuclear coordinates $Q_{\Lambda\lambda}$ where $\lambda = 1, 2, ..., |\Lambda|$ which transform as the irrep Λ. From group theory considerations these coordinates which are allow to be coupled to the electronic Γ state correspond to symmetric Kronecker square $[\Gamma \otimes \Gamma]_S$ which contains Λ in its decomposition [46]. Normal modes which satisfy this condition are called JT active modes. For example, if T_{1u} is the electronic state that is involved in the coupling, the Kronecker product for this irrep is given by $[T_1 \otimes T_1] = [A \oplus H]_S \oplus \{T_1\}_A$. Thus, the T_{1u} electronic state is allowed to couple only to the $2a_g$ and $8h_g$ normal modes. Therefore, the JT interaction takes the form of $T_{1u} \otimes a_g$ and $T_{1u} \otimes h_g$. Coupling to the a_g mode is always considered as a trivial coupling and usually neglected, since the a_g mode is only a breathing mode and thus does not resolve the electronic degeneracies but instead it has the effect of introducing a constant shift in the energy levels. The coupling to $8h_g$ modes usually reduced to a coupling to only

one single effective mode. This is because it has been found that, the corrections that are needed to obtain a good representation of the energy levels when all the eight modes are included in the problem are quite small and do not do much change to the energy levels [47]. Therefore, coupling to a single effective mode can be used with confidence that will produces a good approximation of the energies of the ground states.

Chapter 3

A discussion of pseudorotation in JT systems

In light of what has been mentioned previously, it should be apparent by now that the JT effect is usually treated as a dynamical problem rather than a static one. Theoretically, this approach can be analysed by studying the tunnelling between equivalent distorted configurations by finding the appropriate SASs. Experimentally, the dynamical JT effect could be observed directly via observing the pseudorotation of the molecule using modern ultrafast spectroscopic techniques.

Although pseudorotation phenomena in molecular systems were known [48] some time ago, the causes of this phenomena was not defined until recently. Berry [49] assumed that the APES can be distorted into several equivalent minima with small energy barriers between them and without specifying the origin of these minima, the pseudorotation was observed as a transition between them. Pseudorotation can be detected using ultrafast techniques and is expected to be in a time scale of a few femtoseconds faster than the molecular rotation which itself occurs on a time scale of few picoseconds. To avoid confusion, distinction should be made between the real rotation of the molecule and pseudorotation. The latter is an intramolecular motion in an angular direction in Q space which appears in real space as a fluctuation travelling around the distorted geometric centre of the cluster [see Fig 3.1.(a)]. The former happens when all atoms in the molecule rotate simultaneously around a common axis of rotation usually referred to as a proper axis [see Fig 3.1.(b)].

Pseudorotation in JT systems has three possible forms depending on the shape

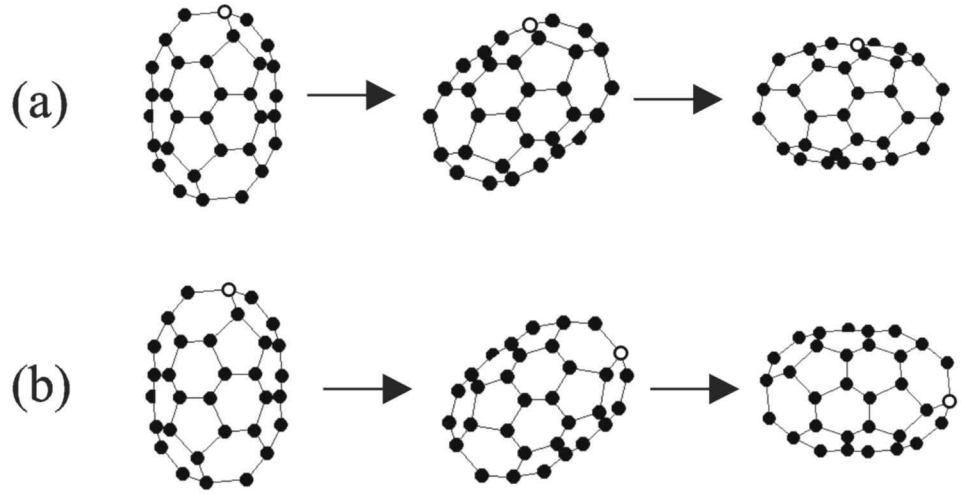

Figure 3.1: (a) Pseudorotation of a distorted C_{60} molecule, and (b) Real rotation of a distorted molecule [50]. One atom is coloured white to distinguish the two motions.

of the APES which, in turn, depends on the strength of the vibronic coupling and also on the order of the Q's that are involved in the coupling [52]. The first kind of pseudorotation is known as *free-rotation*. This happens when the APES has a continuous surface of equivalent minimum points (referred to as a trough) and the system is free to rotate amongst these minima. The motion appears as a rotation of the distorted nuclear framework [see the second sub-figures in (a) and (b) of Fig 3.2]. The second type of pseudorotation is called *hindered rotation*. This occurs when there are potential barriers between discrete minima which are small compared to the quanta associated with the radial vibrations. As a result, the system stays longer at the minima than at the maximum area of the barrier and the motion will appear as slow changes in the distorted nuclear configuration [see the third sub-figures in (a) and (b) of Fig 3.2]. The third pseudorotation form is called *pulsating* (or *fluctuating*) motion. This motion takes place when the height of the potential barrier is larger than the quantum of radial vibration. In this case, the angular motion cannot be separated from the radial motion and therefore the dynamical motion of the system will be described by localised vibrations in the minima accompanied by tunnelling between them. This motion appears as

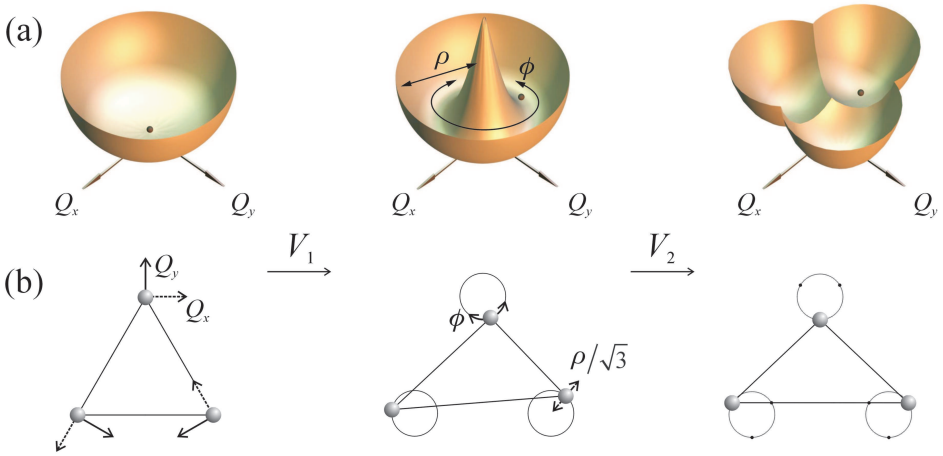

Figure 3.2: (a) Represents the $E \otimes e$ system (the black spot) in the LAPES in Q space with consecutive inclusion of first linear (V_1) and then quadratic V_2 coupling. (b) Represent the orientation of a triatomic molecule X_3 in real space. The first sub-figure in (a) and (b) shows the system when there is no coupling. The second sub-figure in (a) shows a free rotation of the system around the bottom of the trough whereas the second sub-figure in (b) shows the corresponding distortion of the X_3 molecule in real space. Each of the three atoms moves freely along a circle of radius $\rho/\sqrt{3}$. The third sub-figure in (a) represents the hindered rotation where the system is locked into one of the isoenergetic wells due to the small height of the potential barriers between them while the third sub-figure in (b) shows bold points on the circles which indicate the positions of the wells where atoms are allowed to rest for a longer time before moving to another position in the real space. This figure is taken from Ref. [51].

a periodic change in the orientation of the distorted nuclear configuration and as a pulse travelling between the equivalent wells in the APES. The APES will have a shape similar to that in Fig 3.2 part 3(a) but with high walls rather than the lower walls. This kind of motion leads to what is called *tunnelling splitting*, which is one of the most important observables in the JT effect. It has the effect of splitting the energy levels of the ground states. The mechanism of this effect happens when there is an APES with a set of n-fold degenerate minima. Tunnelling between these minima reduces the n-fold degeneracy resulting in new states with symmetries associated with the point group that the system belongs to. For example, consider the $T_{1u} \otimes h_g$ system subject to a JT interaction resulting in minima of D_{5d} symmetry. Here there are 6 wells in the APES. It is clear that there are no 6-fold degenerate irreps in the icosahedral point group and that this degeneracy is only accidental. Tunnelling between wells will remove this degeneracy producing a triplet T_{1u} and a triplet T_{2u}.

Pseudorotation in the $T_{1u} \otimes h_g$ JT system has been examined theoretically by Hands *et al.* [2] using a simple technique involving the time-evolution operator. Applying this operator on a well state shows which wells the system is allowed to visit and which ones cannot be visited during the tunnelling journey and therefore this allows the dynamics of the pseudorotation to be followed. This theory of the time-evolution operator will be briefly discussed in Section 3.1. Application of the theory to JT systems will be given in further sections. The $T_{1u} \otimes h_g$ JT system is given in Section 3.3 as an example of how this theory has been applied and therefore how has the system evolves with time.

3.1 The time-evolution operator

The theory of the time-evolution operator [53, 54] depends on the assumption that there is a physical system with an initial state at time t_0 defined as $|\psi(t_0)\rangle$. How does this state change to $|\psi(t)\rangle$ at any later time t?

The two states can be related by means of a linear operator $U_t(t, t_0)$ such that

$$|\psi(t)\rangle = U_t(t, t_0)|\psi(t_0)\rangle \qquad (t > t_0), \tag{3.1.1}$$

where we infer from this equation that the operator $U_t(t, t_0))$ is a unitary operator

that satisfies

$$U_t(t,t_0)U_t^\dagger(t,t_0) = U_t^\dagger(t,t_0)U_t(t,t_0) = I, \tag{3.1.2}$$

where I is the unit operator, the operator that leaves any state unchanged. The problem is to find an expression for $U_t(t,t_0)$. To do this, we substitute Eq. (3.1.1) into the time-dependent Schrödinger equation

$$\mathrm{i}\hbar\frac{\partial|\psi(t)\rangle}{\partial t} = \mathcal{H}|\psi(t)\rangle \tag{3.1.3}$$

to get

$$\mathrm{i}\hbar\frac{\partial}{\partial t}\left(U_t(t,t_0)|\psi(t_0)\rangle\right) = \mathcal{H}\left(U_t(t,t_0)|\psi(t_0)\rangle\right), \tag{3.1.4}$$

or

$$\frac{\partial U_t(t,t_0)}{\partial t} = -\frac{\mathrm{i}}{\hbar}\mathcal{H}U_t(t,t_0). \tag{3.1.5}$$

The solution of this differential equation depends on whether or not the Hamiltonian involves time. Generally, all the Hamiltonians in our study do not depend on time and then it can be easily seen that integration of Eq. (3.1.5) leads to

$$U_t(t,t_0) = \exp[-\mathrm{i}\mathcal{H}(t-t_0)/\hbar]. \tag{3.1.6}$$

$U_t(t,t_0)$ is known as the time-evolution operator or propagator and it can be used to follow the temporal evolution of a system for any given initial state.

3.2 Time-evolution in JT systems

As stated earlier, any JT system can be defined by a Hamiltonian that has the general form of Eq. (2.2.15). Note that, it has been explained that the SASs represent a good approximation to the true eigenstates of the system in the dynamical motion. Therefore, according to this approximation we may write

$$\mathcal{H}|\Gamma_i\rangle = \varepsilon_i|\Gamma_i\rangle, \tag{3.2.1}$$

where ε_i is the energy of the ith SAS and $|\Gamma_i\rangle$ is the ith SAS having the general form

$$|\Gamma_i\rangle = \sum_{j=1}^{n} a_j^{(i)}|w_j\rangle. \tag{3.2.2}$$

In Eq. (3.2.2), the $a_j^{(i)}$ are a set of real coefficients appearing in front of each well in the SAS and $|w_j\rangle$ is the jth well in the LAPES. Now, from the above equation,

it is clear that the n expressions for the symmetry-adapted states can be inverted to give expressions for the states associated with the wells as

$$|w_i\rangle = \sum_{j=1}^{n} b_i^{(j)} |\Gamma_j\rangle \tag{3.2.3}$$

where $b_i^{(j)}$ are real coefficients. Now, in order to study the temporal evolution of a well state, the time-evolution operator can be applied to the well state as

$$U_t(t,t_0)|w_i\rangle = \sum_{j=1}^{n} b_i^{(j)} \exp[-\mathrm{i}\mathcal{H}(t-t_0)/\hbar]|\Gamma_j\rangle. \tag{3.2.4}$$

On expanding the exponential as a power series using the identity

$$\exp[-x] = 1 - \frac{x}{1!} + \frac{(-x)^2}{2!} + \ldots., \tag{3.2.5}$$

the right hand side of Eq. (3.2.4) is

$$\begin{aligned} \exp[-\mathrm{i}\mathcal{H}(t-t_0)/\hbar]|\Gamma_j\rangle &= (1 - \frac{\mathrm{i}\mathcal{H}(t-t_0)}{\hbar} + \frac{(-\mathrm{i}\mathcal{H}(t-t_0)/\hbar)^2}{2!} + \ldots)|\Gamma_j\rangle \\ &= (1 - \frac{\mathrm{i}\varepsilon_i(t-t_0)}{\hbar} + \ldots)|\Gamma_j\rangle, \end{aligned} \tag{3.2.6}$$

where the last equality follows using Eq. (3.2.1). Thus, the temporal evolution of a well state is given by

$$U_t(t,t_0)|w_i\rangle = \sum_{j=1}^{n} b_i^{(j)} \exp[-\mathrm{i}\varepsilon_j(t-t_0)/\hbar]|\Gamma_j\rangle. \tag{3.2.7}$$

From quantum mechanics, the probability P_{if} that a system initially localised in a well $|w_i\rangle$ has become localised in another well $|w_f\rangle$ a time t later is

$$P_{if} = |\langle w_f|U_t|w_i\rangle|^2. \tag{3.2.8}$$

Multiplying Eq. (3.2.7) by $\langle w_f|$ gives

$$\begin{aligned} \langle w_f|U_t|w_i\rangle &= \sum_{k=1}^{n} b_f^{(k)}\langle\Gamma_k| \quad \sum_{j=1}^{n} b_i^{(j)} \exp[-\mathrm{i}\varepsilon_j t/\hbar] \quad |\Gamma_j\rangle \\ &= \sum_{j=1}^{n} b_f^{(j)} b_i^{(j)} \exp[-\mathrm{i}\varepsilon_j t/\hbar], \end{aligned} \tag{3.2.9}$$

where we have taken $t_0 = 0$. On taking the modulus square of Eq. (3.2.9) we obtain

$$\begin{aligned} P_{if} &= \sum_{j=1}^{n} b_f^{(j)} b_i^{(j)} \exp[+\mathrm{i}\varepsilon_j t/\hbar] \sum_{k=1}^{n} b_f^{(k)} b_i^{(k)} \exp[-\mathrm{i}\varepsilon_k t/\hbar] \\ &= \sum_j \sum_k b_f^{(j)} b_i^{(j)} b_f^{(k)} b_i^{(k)} \exp[-\mathrm{i}(\varepsilon_k - \varepsilon_j)t/\hbar]. \end{aligned} \tag{3.2.10}$$

The jth and kth summations generate three conditions for this equation; either $j = k$ or $j < k$ or $j > k$. Therefore, the above equation becomes

$$\begin{aligned} P_{if} &= \sum_{j=1}^{n} \left(b_f^{(j)} b_i^{(j)} \right)^2 \\ &+ \sum_{j<k} b_f^{(j)} b_i^{(j)} b_f^{(k)} b_i^{(k)} \exp[-\mathrm{i}(\varepsilon_k - \varepsilon_j)t/\hbar] \\ &+ \sum_{j>k} b_f^{(j)} b_i^{(j)} b_f^{(k)} b_i^{(k)} \exp[-\mathrm{i}(\varepsilon_k - \varepsilon_j)t/\hbar]. \end{aligned} \tag{3.2.11}$$

The last term in this equation can be written with $j \longleftrightarrow k$

$$\sum_{j<k} b_f^{(k)} b_i^{(k)} b_f^{(j)} b_i^{(j)} \exp[\mathrm{i}(\varepsilon_j - \varepsilon_k)t/\hbar], \tag{3.2.12}$$

as j and k are dummy variables. Using the identity

$$2\cos\theta = \exp[\mathrm{i}\theta] + \exp[-\mathrm{i}\theta], \tag{3.2.13}$$

the final form of the probability is either

$$\begin{aligned} P_{if} &= \sum_{j=1}^{n} \left(b_i^{(j)} b_f^{(j)} \right)^2 \\ &+ 2 \sum_{j<k} b_i^{(j)} b_i^{(k)} b_f^{(j)} b_f^{(k)} \cos[(\varepsilon_j - \varepsilon_k)t/\hbar], \end{aligned} \tag{3.2.14}$$

or, alternatively,

$$P_{if} = \sum_{j=1}^{n} \left(b_i^{(j)} b_f^{(j)} \right)^2 + 2 \sum_{j<k} b_i^{(j)} b_i^{(k)} b_f^{(j)} b_f^{(k)} \{1 - 2\sin^2[(\varepsilon_j - \varepsilon_k)t/2\hbar]\}. \tag{3.2.15}$$

This equation can be used to study the temporal development of a system initially localised in a particular well. As can be seen from this equation, the temporal evolution of the probability depends on the tunnelling splitting $\varepsilon_j - \varepsilon_k$ between the SASs. This quantity usually given the symbol Δ and it can be found by taking the difference between the energies of the SASs. For example, for the $T_{1u} \otimes h_g$ system the SASs are T_{1u} and T_{2u} and $\Delta = E_{T_{2u}} - E_{T_{1u}}$.

3.3 Application to C_{60}^{-}

A simple example of pseudorotation is that described by Hands *et al.* [2] for the C_{60}^{-} anion. In this example, the application of Eq. (3.2.15) to the $T_{1u} \otimes h_g$ JT system when distorted to D_{5d} symmetry [22] will be given. In this case, the system is undergoing tunnelling between 6 wells in the APES and therefore six SASs appear due to this tunnelling. The time-evolution theory outlined above has already been applied to this system [2]. The 6 SASs can be written in a matrix representation such that

$$\begin{bmatrix} |T_{1ux}\rangle/N_{T1u} \\ |T_{1uy}\rangle/N_{T1u} \\ |T_{1uz}\rangle/N_{T1u} \\ |T_{2ux}\rangle/N_{T2u} \\ |T_{2uy}\rangle/N_{T2u} \\ |T_{2uz}\rangle/N_{T2u} \end{bmatrix} = \begin{bmatrix} 0 & 0 & \phi^{-1} & \phi^{-1} & 1 & -1 \\ 1 & -1 & 0 & 0 & \phi^{-1} & \phi^{-1} \\ \phi^{-1} & \phi^{-1} & 1 & -1 & 0 & 0 \\ 0 & 0 & 1 & 1 & -\phi^{-1} & \phi^{-1} \\ -\phi^{-1} & \phi^{-1} & 0 & 0 & 1 & 1 \\ 1 & 1 & -\phi^{-1} & \phi^{-1} & 0 & 0 \end{bmatrix} \cdot \begin{bmatrix} |A';0\rangle \\ |B';0\rangle \\ |C';0\rangle \\ |D';0\rangle \\ |E';0\rangle \\ |F';0\rangle \end{bmatrix} \tag{3.3.1}$$

where $|T_{1,2ui}\rangle$ represents the i^{th} symmetry adapted states and $N_{T_{1,2}u}$ represents the corresponding normalisation constants, ϕ is the golden mean and $|A';0\rangle$ is the untransformed state for well A. This is a matrix form of Eq. (3.2.2), so that the matrix elements represent the coefficients $a_j^{(i)}$. Inverting the above equation gives

$$\begin{bmatrix} |A';0\rangle \\ |B';0\rangle \\ |C';0\rangle \\ |D';0\rangle \\ |E';0\rangle \\ |F';0\rangle \end{bmatrix} = \frac{\phi}{2(1+\phi^2)} \begin{bmatrix} 0 & \phi & 1 & 0 & -1 & \phi \\ 0 & -\phi & 1 & 0 & 1 & \phi \\ 1 & 0 & \phi & \phi & 0 & -1 \\ 1 & 0 & -\phi & \phi & 0 & 1 \\ \phi & 1 & 0 & -1 & \phi & 0 \\ -\phi & 1 & 0 & 1 & \phi & 0 \end{bmatrix} \cdot \begin{bmatrix} |T_{1ux}\rangle/N_{T1u} \\ |T_{1uy}\rangle/N_{T1u} \\ |T_{1uz}\rangle/N_{T1u} \\ |T_{2ux}\rangle/N_{T2u} \\ |T_{2uy}\rangle/N_{T2u} \\ |T_{2uz}\rangle/N_{T2u} \end{bmatrix} \tag{3.3.2}$$

This matrix represents Eq. (3.2.3). By using the probability expression given in Eq. (3.2.15) it has been found that the probability of a system initially localised in well A being found in an adjacent well, say well B at a time t later is given by [2]

$$P_{AB}(t) = \frac{1}{5}\left[S^2 + (1-S^2)\sin^2\left(\frac{\Delta t}{2\hbar}\right)\right], \tag{3.3.3}$$

and the probability that the system remains in well A is

$$P_{AA}(t) = 1 - (1-S^2)\sin^2\left(\frac{\Delta t}{2\hbar}\right). \tag{3.3.4}$$

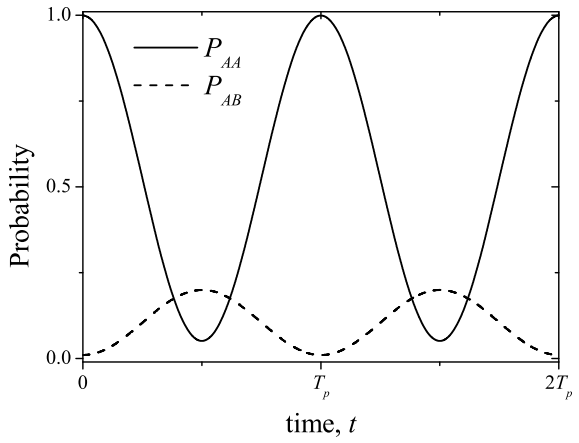

Figure 3.3: Diagram showing the dynamics of the $T_{1u} \otimes h_g$ system initially localised in well A. The continues curve shows the P_{AA} which is the probability of finding the system still in well A after a time t and the dashed curve shows the P_{AB} the probability of finding the system in an adjacent well (well B) [50].

Here, S is the phonon overlap between adjacent pentagonal wells and is given by

$$S = \exp\left[-6\left(\frac{V_1'}{5-4\sqrt{2}V_2'}\right)^2\right], \tag{3.3.5}$$

and Δ is the tunnelling splitting given by the expression

$$\Delta = -\frac{\hbar\omega S \ln S}{(1-S^2)}(2-\sqrt{2}V_2' + \sqrt{2/5}V_3'). \tag{3.3.6}$$

V_1' is the dimensionless linear coupling parameter and V_2' and V_3' are the dimensionless quadratic parameters respectively. A plot of the above expressions of the probabilities is shown in Fig. 3.3. It is very obvious from the figure that, if the system is starting off in well A is being found in well B after a time t varies as $\sin^2$.

We note from Eq. (3.3.4) that at $t = 0$, $P_{AA} = 1$. In other words, the theory assumes that initially the system is completely localised in well A. However, the wells are not orthogonal and so there will always be a finite probability of finding the system in one of the other wells no matter how strongly localised the initial state. Thus, the results presented should ideally all be renormalised so that at any particular time the sums of probabilities of finding the system in the wells is equal to unity.

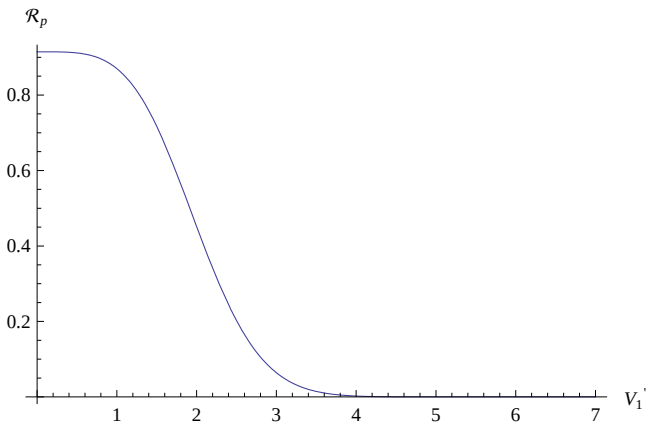

Figure 3.4: Dimensionless pseudorotation rates as a function of the linear coupling constant $V_1^{'}$ for the case of pentagonal minima. Quadratic constants $V_2^{'} = 0.3$ and $V_3^{'} = 0.4$ have been assumed.

As time proceeds the probability of finding the system localised in that well starts to decrease until it reaches the minimum value, simultaneously, the probability of finding the system in well B increases until reaches the maximum value. In this case, it can be said that the system achieved the maximum occupation of well B. Then after a period of time the system travels back to its initial well state. This process will be repeated again starting from the same initial well following the same trend. The probabilities of finding the system in any of the five wells are all equal as they are all equivalent as far as A is concerned.

The time that the system takes to complete one period of this journey of pseudorotation in this particular case is given by

$$T_p = \frac{2\pi\hbar}{\Delta}. \tag{3.3.7}$$

This equation shows that there is an inverse relation between the tunnelling splitting and the period that the system takes to finish one pseudorotation circuit. We can also define a pseudorotation rate R_p for this system as the inverse of the pseudorotation period $R_p = T_p^{-1} = \Delta/2\pi\hbar$. A dimensionless pseudorotation rate has also been defined [2]

$$\mathcal{R}_p = \frac{2\pi}{\omega} T_p^{-1} = \frac{\Delta}{\hbar\omega} \tag{3.3.8}$$

which is more convenient for plotting. This expression has been plotted for the D_{5d} case [2] as shown in Fig. 3.4. The figure shows that as the value of the linear coupling $V_1^{'}$ increases a decrease in the pseudorotation rate occurs until tends to zero. Mathematically, that occurs when $V_1^{'} \to \infty$. This is can be explained more

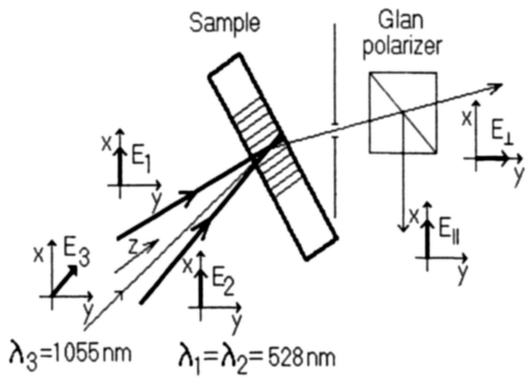

Figure 3.5: The transient grating experiments. E_1 and E_2 are pump beams, E_3 is the probe pulse, $E_{\|}$ and $E_{\perp}$ are the detected diffraction signals.

clearly by explain the physics behind it. In the limit when $V_1' \to \infty$, the coupling in this case is considered to be a very strong coupling that will cause the barriers separating between the wells to become very high associated with deepening of the wells. Therefore, the overlap between wells $S \to 0$ and the tunnelling splitting Δ also tends to zero. Thus, the system will be found localised into either well A, B, C, D, E, or F.

3.4 Experimental Techniques

A suggested technique to observe the pseudorotation experimentally is via the ultrafast experiment called the pump-probe spectroscopy [1, 55]. This technique has already been successfully used by Rubtsov *et al.* to measure experimentally the rate at which the C_{60} and C_{70} molecules rotationally diffuse in various liquids [1, 55]. Effectively, it measures how quickly the molecules rotate in solution. The general idea is explained using the apparatus shown in Fig. 3.5.

In Rubtsov *et al.*'s experiments two pump laser beams (E_1, E_2 having wavelengths $\lambda_1 = \lambda_2 = 528\,\text{nm}$) are applied to the sample so that at $t = 0$ a strong pulse of photons interacts with the target molecules. This interaction produces a diffraction grating within the sample. As time progresses, this grating degrades because of the rotational and translational diffusion of the molecules. Thus, these experiments employ what are called transient grating techniques. After a time delay Δt (of a few fs or ps) a probe beam (E_3 having wavelength $\lambda_3 = 1055\,\text{nm}$)

is applied which is used to measure the strength of the grating. If Δt is small, the grating is strong and so the effect on the probe is strong. As Δt increases, the grating deteriorates due to molecular rotation and a weaker interaction with the probe occurs. The experiment involves varying Δt and measuring the signal arising from the grating-probe interaction. The resulting trace allows the rotational motion to be analysed.

If similar pump-probe experiments were performed on solutions containing C_{60} ions, then the resulting signal would be expected to contain contributions from both real rotation and pseudorotation. For example, for C_{60}^{-} the pseudorotation of the molecule would be expected to degrade the transient grating much more quickly than real rotation. This is simply because the actual amount of atomic motion required to accomplish pseudorotation is much less than that required to achieve real rotation. Thus, a faster decay of the pump-probe signal from a sample of C_{60}^{-} ions (compared to neutral C_{60}) would be a clear indication of pseudorotation. More importantly, a thorough analysis of the decay rates should yield a quantitative value for the pseudorotation rate which, in turn, provides information about the coupling constants that dictates the pseudorotation rates.

Chapter 4

$T \otimes (e \oplus t_2)$ JT system in cubic symmetry

In order to illustrate the ideas of pseudorotation more clearly, we look now at the well known vibronic $T \otimes (e \oplus t_2)$ JT system. The APES contains many minima and tunnelling between equivalent minima may occur resulting in pseudorotation. The interaction in the $T \otimes (e \oplus t_2)$ system can be predicted from the Kronecker product of the T-orbital with itself as $[T]^2 = A + E + T_2$. The coupling takes place when an electron with a T-type orbital couples to two types of vibrational modes namely e-type with (Q_θ, Q_ϵ) coordinates and t_2-type with (Q_4, Q_5, Q_6) coordinates. Coupling to the a-mode is ignored here as the a-mode is trivially a breathing mode.

There are many reasons for studying this system in this thesis. Firstly, this system has cubic symmetry which is less complicated compared to other molecular symmetries (such as icosahedral). Therefore, the time evolution of the JT system can be interpreted more easily both analytically and pictorially. Also, the problem shows a variety of characteristics that can be divided in three different cases according to the magnitude of the coupling strengths. Each case causes different distortions in the APES and thus a variety of well configurations can be investigated dynamically. Another reason to investigate the $T \otimes (e \oplus t_2)$ JT system is that this system has been studied theoretically in detail for many years by many authors, see Refs. [56, 57, 58] for example and therefore the available information such as the SASs in the literature regarding this interaction will be a very good base for our new calculations of pseudorotation rates. Thus, investigating the dynamical behaviour of the $T \otimes (e \oplus t_2)$ system will serve as a good introduction to

the more advanced systems having more complicated symmetries.

The $T \otimes (e \oplus t_2)$ cubic system has three types of extremal points on the LAPES namely tetragonal (D_{4h}), trigonal (D_{3d}) and orthorombic (D_{2h}) [59]. The (D_{4h}) points become minima and the system will be represented by a $T \otimes e$ JT effect, when the coupling to the e-mode dominates. The (D_{3d}) points become minima and the system will be represents as $T \otimes t_2$, when the t_2-mode dominates. When the (D_{2h}) points are minima, the system will be denoted as $T \otimes (e \oplus t_2)$, when coupling to both modes (e, t_2) is present.

In this chapter, the pseudorotation for the $T \otimes (e \oplus t_2)$ system involving the three cases will be studied using the theory outlined in Chapter 3 by applying the quantum mechanical time evolution operator with the help of a previously obtained SASs [60] to derive analytical expressions of the pseudorotation probabilities and the corresponding rates.

4.1 The transformed Hamiltonian for $T \otimes (e \oplus t_2)$

The transformed Hamiltonian for this system has been derived by Bates *et al.* [3] and written in terms of the electronic basis states $|x;0\rangle, |y;0\rangle$ and $|z;0\rangle$ in five-dimensional space and it takes the form

$$\tilde{\mathcal{H}}_1 = \begin{bmatrix} -A_\theta + \sqrt{3}A_\epsilon & \sqrt{3}A_6 & \sqrt{3}A_5 \\ +\frac{\mu\hbar^2}{2}\sum_i(\omega_i\alpha_i)^2 & & \\ \sqrt{3}A_6 & -A_\theta - \sqrt{3}A_\epsilon & \sqrt{3}A_4 \\ & +\frac{\mu\hbar^2}{2}\sum_i(\omega_i\alpha_i)^2 & \\ \sqrt{3}A_5 & \sqrt{3}A_4 & 2A_\theta \\ & & +\frac{\mu\hbar^2}{2}\sum_i(\omega_i\alpha_i)^2 \end{bmatrix}, \quad (4.1.1)$$

where μ is the reduced mass of each oscillator of frequency ω and the A_i are defined as

$$\begin{aligned} A_\theta &= \frac{\hbar V_E}{2}\alpha_\theta, \\ A_\epsilon &= \frac{\hbar V_E}{2}\alpha_\epsilon, \\ A_4 &= \frac{\hbar V_T}{2}\left(1 - \frac{\hbar V_{BL}}{2V_T}(\alpha_\theta - \sqrt{3}\alpha_\epsilon)\right)\alpha_4, \\ A_5 &= \frac{\hbar V_T}{2}\left(1 - \frac{\hbar V_{BL}}{2V_T}(\alpha_\theta + \sqrt{3}\alpha_\epsilon)\right)\alpha_5, \\ A_6 &= \frac{\hbar V_T}{2}\left(1 - \frac{\hbar V_{BL}}{2V_T}(-2\alpha_\theta)\right)\alpha_6. \end{aligned} \tag{4.1.2}$$

α_i represents the i^{th} coordinates of the well in the LAPES, the constants V_E and V_T describe the linear coupling to the e and t_2 vibrations respectively, V_{BL} is the bilinear (quadratic) constant which describes the coupling to both vibrations. It has been found that the bilinear term is the one which plays the most important rôle in changing the shape of the APES [56] for this system so including any higher terms in Q will not add any further information when solving the problem.

Minimising this Hamiltonian using the Öpik and Pryce method [4] has produced the positions of the minimum points (wells) on the APES in Q-space [3]. As mentioned, under certain condition of the coupling strength, the system becomes localised into one of the minima either tetragonal, trigonal or orthorhombic. In quantum mechanics, if the system is prepared in one of the minima, then the system can evolve by tunnelling between the potential wells. The following sections take each symmetry in turn.

4.1.1 The $T \otimes e$ JT system

When a cubic molecule is dynamically distorted along a C_4 axis (see Fig. 4.1), tetragonal wells of D_{4h} symmetry will be generated in the APES consists of three wells intersecting at $Q_\theta = Q_\varepsilon = 0$ (see Fig.3.10 Ref. [48]). The system will be localised in the bottom of one of these wells. The corresponding untransformed ground states of these minima are given as [60]

$$|x';0\rangle, \quad |y';0\rangle, \quad |z';0\rangle. \tag{4.1.3}$$

These states are mutually orthogonal to each other and they are appropriate eigenstates for both the infinite and finite coupled $T \otimes e$ JT system. As a result of this, the system will be found trapped in one of the three equivalent wells and therefore no tunnelling is taking place between the minima. Thus, since the system is not tunnelling it is not necessary to construct any combinations of SASs.

Comparing this case in the $T \otimes e$ JT system to the case in Ref. [51] for the $E \otimes e$ JT system, it should be noticed that, although the APES of this system is showing three wells similar in number to that in the $E \otimes e$ system, the latter system is free to pseudorotate between the three wells when the quadratic coupling is taken into account [51], in this case the system is not allowed to undergo a tunnelling motion between these wells. This is because the wavefunctions in the three wells of the $T \otimes e$ JT system are mutually orthogonal and they are not mixed by the tetragonal displacement[48].

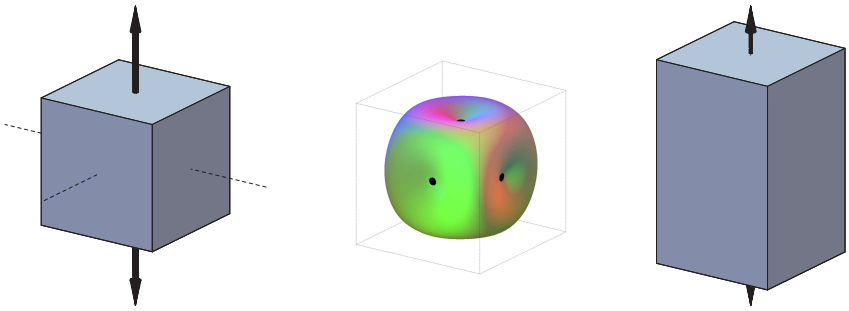

(a) (b) (c)

Figure 4.1: (a)Cubic molecule with a distortion axis C_4 in real space. (b)The black dots show the positions of the orthogonal well states in the APES in the Q-space. (c)A distorted molecule with D_{4h} symmetry when the coupling to the e mode dominates.

4.1.2 The $T \otimes t_2$ JT System

If the molecule is dynamically distorted around a C_3 axis by the $T \otimes t_2$ JT effect, trigonal wells of D_{3d} symmetry appear in the APES with four-fold degeneracy Fig. 4.2. This degeneracy splits via the tunnelling between the four trigonal wells and therefore the appropriate eigenstates for the system in this case are the linear combinations of the ground states localised in the four wells. Using the projection operator technique, a triplet T_1 and a singlet A_2 SASs are produced and given in

Ref. [33] namely

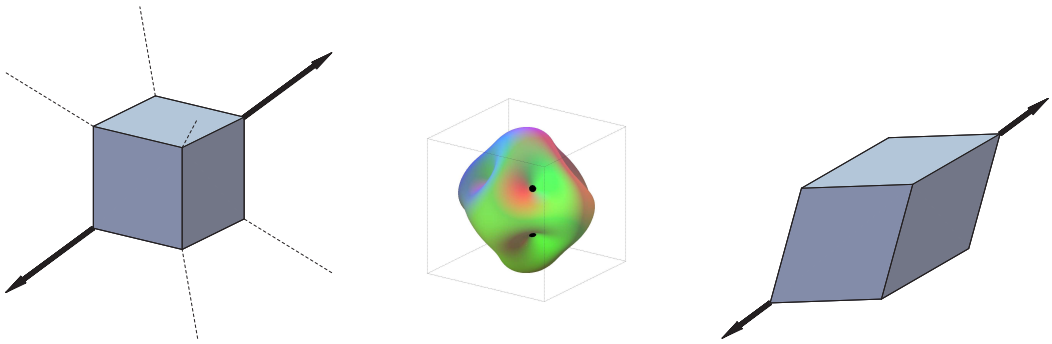

(a) (b) (c)

Figure 4.2: (a)Cubic molecule with a distortion axis C_3 in real space. (b)The four triagonal wells are represented by black dots in the APES in the Q-space. (c)A distorted molecule of D_{3d} symmetry when coupling with the t_2 mode dominates.

$$\begin{aligned}
|T_{1x}\rangle &= N^t_{T_1}[\,|A';0\rangle + |B';0\rangle - |C';0\rangle - |D';0\rangle], \\
|T_{1y}\rangle &= N^t_{T_1}[\,|A';0\rangle - |B';0\rangle + |C';0\rangle - |D';0\rangle], \\
|T_{1z}\rangle &= N^t_{T_1}[-|A';0\rangle + |B';0\rangle + |C';0\rangle - |D';0\rangle], \\
|A_{2a}\rangle &= N^t_{A_2}[\,|A';0\rangle + |B';0\rangle + |C';0\rangle + |D';0\rangle],
\end{aligned} \tag{4.1.4}$$

where

$$\begin{aligned}
N^t_{T_1} &= \frac{1}{2\sqrt{1+\frac{S_t}{3}}}, \\
N^t_{A_2} &= \frac{1}{2\sqrt{1-S_t}},
\end{aligned} \tag{4.1.5}$$

are the normalisation constants for the trigonal case, $|X';0\rangle$ is the Glauber state defined in Eq. (2.3.18) which forms the untransformed state associated with the well, S_t is the overlap between the oscillator parts of any two adjacent wells. The superscript and subscript t refer to the trigonal wells. The oscillator overlap between any adjacent wells has been found using Eq. (2.3.23) and is given by [33]

$$S_t = \exp\left[-\frac{16}{9}\left(\frac{K_T}{\hbar\omega_T}\right)^2\right]. \tag{4.1.6}$$

where K_T is a constant involves the linear coupling constant V_T given by

$$K_T = \frac{\sqrt{3\hbar}V_T}{2\sqrt{2\mu\omega_T}}. \tag{4.1.7}$$

The energy of the T_1 SASs states is given by [60]

$$E_{T_1} = \hbar\omega_E + \frac{3}{2}\hbar\omega_T - \frac{4}{9}\left(\frac{K_T^2}{\hbar\omega_T}\right)\left(\frac{9+7S_t}{3+S_t}\right), \tag{4.1.8}$$

while for the A_2 SASs the energy is

$$E_{A_2} = \hbar\omega_E + \frac{3}{2}\hbar\omega_T - \frac{4}{9}\left(\frac{K_T^2}{\hbar\omega_T}\right)\left(\frac{3-7S_t}{1-S_t}\right). \tag{4.1.9}$$

Here, the T_1 state is always the lower in energy than the singlet A_2 state and therefore the tunnelling splitting between these states is given by [60]

$$\Delta = E_{A_2} - E_{T_1} = -\frac{4S_t \ln S_t}{(1-S_t)(3+S_t)}\hbar\omega_T. \tag{4.1.10}$$

Using the above expressions of the normalised SASs in Eq. (4.1.4) and following similar procedure to that outlined in Chapter 3 , expressions for the normalised states that are associated with each of the four trigonal wells are obtained and have the form:

$$\begin{aligned}
|A';0\rangle &= \frac{|A_{2a}\rangle}{4N^t_{A_2}} + \frac{|T_{1x}\rangle + |T_{1y}\rangle - |T_{1z}\rangle}{4N^t_{T_1}},\\
|B';0\rangle &= \frac{|A_{2a}\rangle}{4N^t_{A_2}} + \frac{|T_{1x}\rangle - |T_{1y}\rangle + |T_{1z}\rangle}{4N^t_{T_1}},\\
|C';0\rangle &= \frac{|A_{2a}\rangle}{4N^t_{A_2}} - \frac{|T_{1x}\rangle - |T_{1y}\rangle - |T_{1z}\rangle}{4N^t_{T_1}},\\
|D';0\rangle &= \frac{|A_{2a}\rangle}{4N^t_{A_2}} - \frac{|T_{1x}\rangle + |T_{1y}\rangle + |T_{1z}\rangle}{4N^t_{T_1}}.
\end{aligned} \tag{4.1.11}$$

Now, in order to study the evolution of the system initially localised in one of the minimum wells, the time evolution operator Eq. (3.1.6) is applied to obtained expressions of the probabilities of finding the system in another well at later time t by using Eq. (3.2.15). These probabilities are:

$$\begin{aligned}
P_{AA}(t) &= 1 - \frac{1}{4}(1-S_t)(3+S_t)\sin^2\left(\frac{\Delta t}{2\hbar}\right),\\
P_{AB}(t) &= \frac{S_t^2}{9} + \frac{1}{12}(1-S_t)(3+S_t)\sin^2\left(\frac{\Delta t}{2\hbar}\right),
\end{aligned} \tag{4.1.12}$$

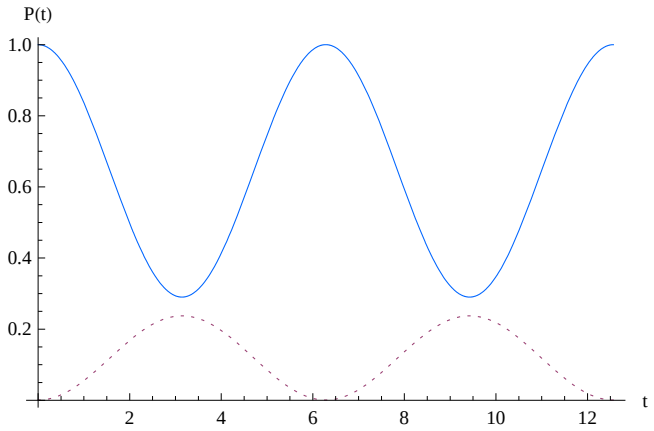

Figure 4.3: The internal pseudorotation of a moderately coupled $T \otimes t_2$ with $K_T = 1.2\hbar\omega_T$.

In this case, it can be seen from Fig. 4.2, that the wells are equally separated and therefore the phonon overlaps between them are also equal. As this is the situation, there is no need to find the probabilities P_{AC} and P_{AD} since they are identical to that for P_{AB}. From the results above, it is clear that the system is in dynamical motion due to the pseudorotation between the different wells. In general, and as can be seen from Eq. (4.1.12) pseudorotation depends on the phonon overlap which in turn depends on the separation between the wells.

The expressions for the probabilities given in Eq. (4.1.12) are plotted in Fig. 4.3. The diagram clearly shows a sinusoidal pseudorotation behaviour between the wells similar to that for the $T_1 \otimes h_g$ system in Chapter 3. It tells us that, at time $t = 0$ the probability $P_{AA}(t)$ of finding the system still localised in well A is unity, which is an expected result since the system must be found localised in one of the wells. The probability of finding the system localised in well A is then decreasing with simultaneous increasing of the probability of finding the system in well B (or C, D). After the system is fully localised in well B and as the time increasing the system begins to migrate back to its original state after completing one revolution of pseudorotation. The time for this is again given by the formula in Eq. (3.3.7).

The dimensionless pseudorotation rate $\mathcal{R}_p$ from Eq. (3.3.8) is plotted in Fig. 4.4 as a function of linear coupling. As expected, increasing of the strength of the linear coupling increases the barriers between the wells in the APES which in turn reduces the overlap between the wells. This therefore, decreases the pseudorotation of the system between the wells. The trend continues until infinite coupling where

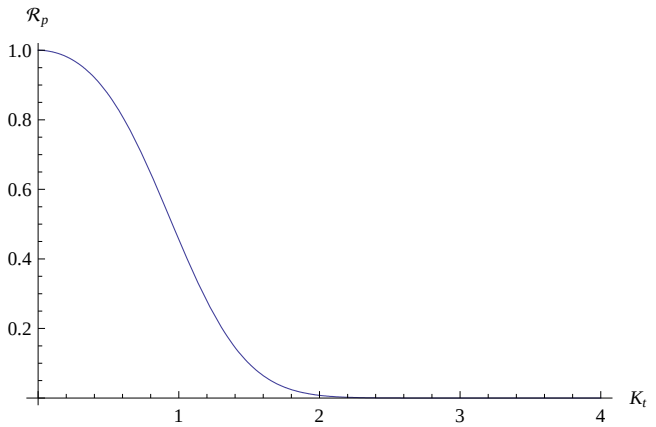

Figure 4.4: Dimensionless pseudorotation rate as a function of the coupling constant for the case of trigonal minima.

the system achieves the zero pseudorotation. Here, the system becomes locked into one of the four trigonal wells showing static behaviour.

A previous calculation given in Ref. [59] for multi-dimensional tunnelling systems like $T \otimes t_2$ gives the most probable tunnelling path that the system is taking during the tunnelling. By calculating what is termed the path of steepest descent, the minimum energy path is obtained. Further details can be found in Ref. [61]. However, it has been found that, when the t_2 mode in the $T \otimes (e + t_2)$ system dominates, the system has two possible types of classical paths of steepest descent connecting the D_{3d} triagonal wells. The first one is via the D_{2h} saddle point, while the other one is via the D_{4h} saddle point. There is no interchanging between these two types of tunnelling paths when t_2 dominates and the system shows that the path via the D_{2h} saddle point is always the one favoured [59]. The calculations shows that the tunnelling integral along the path via the D_{2h} saddle point always has a smaller value than that along the path via a D_{4h} saddle points. This is clearly shown in both Fig. 4.5 and table 1 in Ref. [59]. This situation can also be deduced from Fig. 4.2.(b) which shows the trigonal wells in the APES separated by two different saddle points. The D_{4h} saddle points have higher potential barriers at large distances from the minima than the D_{2h} saddle points. The tunnelling splitting between the energies of the system is found to be related to the tunnelling path integral via the relation [62]

$$\Delta = \hbar\omega \exp[-I_T] \tag{4.1.13}$$

where ω is the frequency of the vibration of the particle in the well and I_T is

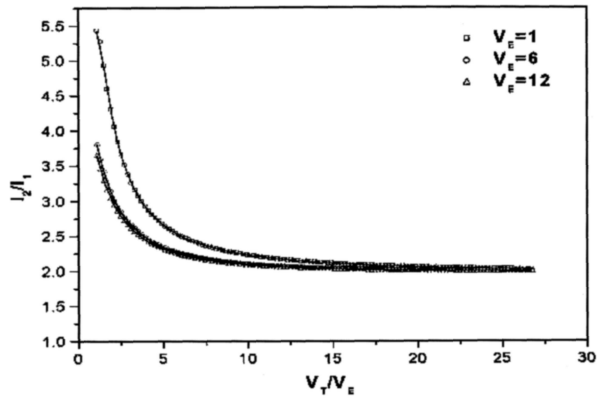

Figure 4.5: The ratio of the action integrals I_2/I_1 as a functions of V_T/V_E with different choices of V_E when t_2 mode dominates. I_1 and I_2 are the action integral of the path via a D_{4h} and D_{2h} saddle points respectively. As shown in the figure I_2 is always bigger than I_1 [59].

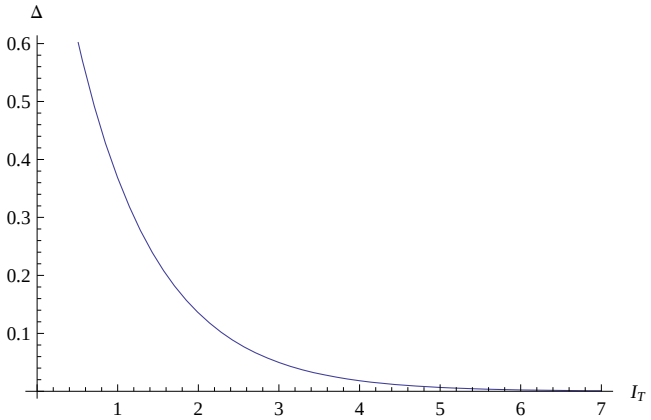

Figure 4.6: The figure shows the tunnelling splitting Δ changes as a function of the tunnelling path integral I_T.

the tunnelling path integral. Fig. 4.6 shows the variation of Δ as a function of I_T. There is a relation between the pseudorotation rate of the molecule and the tunnelling splitting via $R_p = \Delta/2\pi\hbar$. Thus, this equation with Eq. (4.1.13) show that, as the path integral becomes larger, the pseudorotation rate of the system becomes smaller and thus the system then takes a longer time to travel from one well to another. Since the time that a system takes to pseudorotate is expected to be of the order of femtoseconds, the tunnelling path that the system takes will be expected to be via the saddle points which have a lower potential barriers and smaller separations between the minima.

Thus, this shows another good reason for studying the pseudorotation rate of the system as it gives valuable information of the favoured tunnelling path that is taken when it pseudorotates.

4.1.3 The $T \otimes (e + t_2)$ JT System

In this case, when the coupling to e and t_2 modes are both involved, a distortion in the direction of C_2 axis via the $T \otimes (e + t_2)$ JT effect occurs, the system is then said to experience orthorhombic D_{2h} symmetry (see Fig. 4.7). The APES for this symmetry contains six wells. These wells are presented in Fig. 4.7.(b) and divided into non-orthogonal and orthogonal wells. For each well state, there are four nearest neighbour wells of non-orthogonal states and one next nearest neighbour well of an orthogonal state. It has been found that, in the infinite coupling limit, the system is found to be relaxing into one of the six orthorhombic wells [3] and no tunnelling occurs between them. When the coupling is finite, the system starts to tunnel and movement between the wells takes place. This process leads the system to have states that are linear combination from those localised in the wells that the system visits during the tunnelling. These states [3] have been found to be the triplets T_1 and T_2 given by

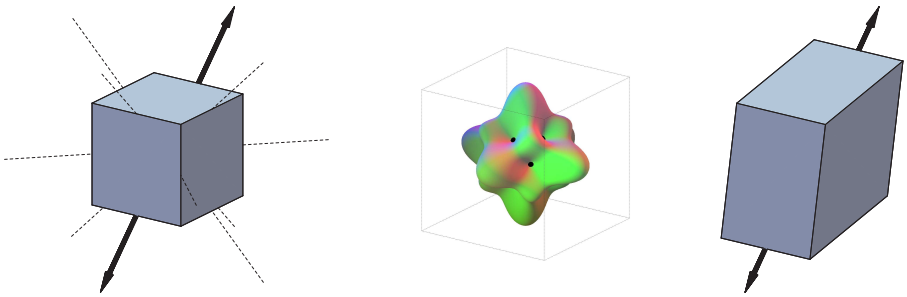

(a) (b) (c)

Figure 4.7: (a)Cubic molecule with a distortion axis C_2 in real space. (b)The black dots represents the positions of the orthorhombic wells in the APES in the Q-space. (c)A distorted molecule with D_{2h} symmetry.

$$\begin{aligned}
|T_{1x}\rangle &= N^o_{T_1}[\,|a';0\rangle + |b';0\rangle + |e';0\rangle - |f';0\rangle], \\
|T_{1y}\rangle &= N^o_{T_1}[\,|a';0\rangle - |b';0\rangle + |c';0\rangle + |d';0\rangle], \\
|T_{1z}\rangle &= N^o_{T_1}[\,|c';0\rangle - |d';0\rangle + |e';0\rangle + |f';0\rangle],
\end{aligned} \tag{4.1.14}$$

$$\begin{aligned}
|T_{2x}\rangle &= N^o_{T_2}[\,|a';0\rangle + |b';0\rangle - |e';0\rangle + |f';0\rangle], \\
|T_{2y}\rangle &= N^o_{T_2}[\,-|a';0\rangle + |b';0\rangle + |c';0\rangle + |d';0\rangle], \\
|T_{2z}\rangle &= N^o_{T_2}[\,-|c';0\rangle + |d';0\rangle + |e';0\rangle + |f';0\rangle],
\end{aligned} \tag{4.1.15}$$

where the normalisation constants are defined as

$$\begin{aligned}
N^o_{T_1} &= \frac{1}{2\sqrt{1+S_o}}, \\
N^o_{T_2} &= \frac{1}{2\sqrt{1-S_o}}.
\end{aligned} \tag{4.1.16}$$

The superscript and subscript letter o refers to the orthorhombic case, $|x';0\rangle$ is the Glauber form of the state associated with the x orthorhombic well and S_o is the phonon overlap between the oscillators part of any two of the orthorhombic wells that do not have orthogonal orbits and given by [33]

$$S_o = \exp\left[-\frac{3}{2}\left(\frac{K_E}{\hbar\omega_E}\right)^2 - \left(\frac{K_T}{\hbar\omega_T}\right)^2\right]. \tag{4.1.17}$$

Here, K_E and K_T are constants involving the linear coupling parameters V_E and

V_T as

$$K_E = -\frac{\sqrt{\hbar}V_E}{2\sqrt{2\mu\omega_E}}, \tag{4.1.18}$$

and

$$K_T = \frac{\sqrt{3\hbar}V_T}{2\sqrt{2\mu\omega_T}}. \tag{4.1.19}$$

The energies of the triplets states are [60]

$$\begin{aligned} E_{T_i} &= \hbar\omega_E + \frac{3}{2}\hbar\omega_T - 4N_{T_i}^2([1-(-1)^i\frac{5}{2}S_o]\frac{K_E^2}{\hbar\omega_E} + [1-2(-1)^i S_o]\frac{K_T^2}{\hbar\omega_T} \\ &\quad +2[4-(-1)^i S_o]\frac{V_{BL}}{V_E V_T}\frac{K_E^2}{\hbar\omega_E}\frac{K_T^2}{\hbar\omega_T}), \end{aligned} \tag{4.1.20}$$

for $i = 1$ and 2. The the energy gap between T_1 and T_2 is [60]

$$\Delta = E_{T_2} - E_{T_1} = \frac{S_o}{(1-S_o^2)}\left(3\frac{K_E^2}{\hbar\omega_E} + 2\frac{K_T^2}{\hbar\omega_T} - 12\frac{K_E^2}{\hbar\omega_E}\frac{K_T^2}{\hbar\omega_T}\frac{V_{BL}}{V_E V_T}\right). \tag{4.1.21}$$

In order to study the evolution of the system with respect to time, the associated states with each of the six orthorhombic wells must be derived first of all. These are obtained by inverting the relations given in Eq. (4.1.14). Again following the same procedure as outlined at the end of Chapter 3 for the $T \otimes h$ system, the well states are

$$\begin{aligned} |a';0\rangle &= \frac{|T_{1x}\rangle + |T_{1y}\rangle}{4N_{T_1}^o} + \frac{|T_{2x}\rangle - |T_{2y}\rangle}{4N_{T_2}^o}, \\ |b';0\rangle &= \frac{|T_{1x}\rangle - |T_{1y}\rangle}{4N_{T_1}^o} + \frac{|T_{2x}\rangle + |T_{2y}\rangle}{4N_{T_2}^o}, \\ |c';0\rangle &= \frac{|T_{1y}\rangle + |T_{1z}\rangle}{4N_{T_1}^o} + \frac{|T_{2y}\rangle - |T_{2z}\rangle}{4N_{T_2}^o}, \\ |d';0\rangle &= \frac{|T_{1y}\rangle - |T_{1z}\rangle}{4N_{T_1}^o} + \frac{|T_{2y}\rangle + |T_{2z}\rangle}{4N_{T_2}^o}, \\ |e';0\rangle &= \frac{|T_{1x}\rangle + |T_{1z}\rangle}{4N_{T_1}^o} - \frac{|T_{2x}\rangle - |T_{2z}\rangle}{4N_{T_2}^o}, \\ |f';0\rangle &= -\frac{|T_{1x}\rangle - |T_{1z}\rangle}{4N_{T_1}^o} + \frac{|T_{2x}\rangle + |T_{2z}\rangle}{4N_{T_2}^o}. \end{aligned} \tag{4.1.22}$$

The time evolution of this system when it is initially localised in one of the orthorhombic wells can be studied by deriving the probabilities of finding the system

in another well after a time t. This can be done trivially by applying Eq. (3.2.15), with the result that these probabilities are

$$P_{aa}(t) = 1 - (1 - S_o^2)\sin^2\left(\frac{\Delta t}{2\hbar}\right), \tag{4.1.23}$$

$$P_{ab}(t) = 0, \tag{4.1.24}$$

$$P_{ac}(t) = \frac{S_o^2}{4} + \frac{1}{4}(1 - S_o^2)\sin^2\left(\frac{\Delta t}{2\hbar}\right). \tag{4.1.25}$$

The system here is behaving in a different way from that when the t_2 mode dominates. It is clear from the results that, if the system starts in a given well, then it is only possible to be found localised later in a time t in the non-orthogonal state wells. For example, if the system is initially localised in well a, then it can be found later only in either well c, d, e or f. Finding the system localised in well b is forbidden as indicated in Eq. (4.1.23) because it is orthogonal to well a. Thus, if the system is localised into one well then it has the opportunity to be found at any well after later time except the orthogonal one. This behaviour seems to be that experimentally exhibited by the carbonyl compound $Fe(CO)_4$ [63, 64]. Isotopically substituted carbon monoxide was used to investigate the change in geometry that occurs as we progress between different equivalent distorted minima [65]. It was found that starting from one particular minima the system could migrate to an adjacent minima but not directly to the minima opposite.

$Fe(CO)_4$ is distorted from the high symmetry tetrahedral geometry into a C_{2v} geometry which can be achieved in six equivalent ways [66], see Fig. 4.8. The figure shows six C_{2v} equivalent minima. At the centre of the figure is a dot representing the system in its undistorted tetrahedral geometry T_d. One of the lowest energy paths for the conversion AA-EE is also shown. The direct conversion from the AA to EE does not occur. The experimental observation is that indirect conversion via AE actually occurs.

The internal dynamics for this system are shown in Fig. 4.9. The system shows regular tunnelling when it starts off in well a and moves towards well c then back to well a again completing one period of pseudorotation T_p. The probabilities of finding the system in the wells d, e or f have the same expression as that for well c. The process of pseudorotation repeats itself as time progresses and, as there is only one tunnelling level for this system, it is safe to use the same equation Eq. (3.3.8) to represents the pseudorotation rate. This equation is plotted in Fig. 4.10 to show the changes of the pseudorotation rate while the coupling

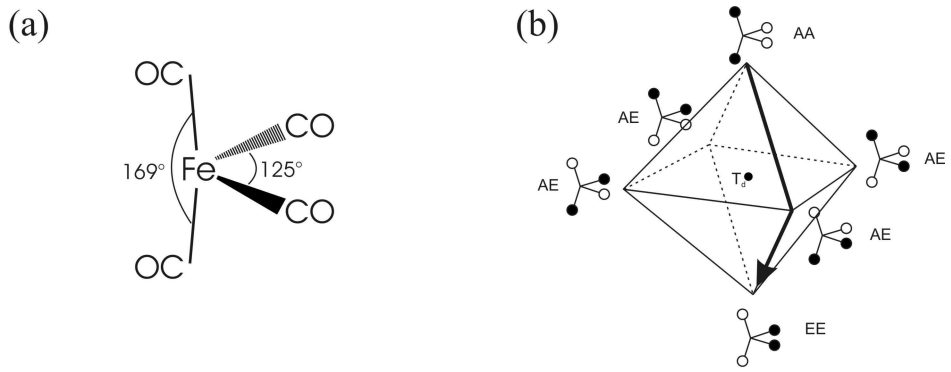

Figure 4.8: (a) Structure of singlet [$Fe(CO)_4$], determined by electron diffraction [64]. The two CO molecules above and below the iron atom are the axial molecules (A) and the other two are the equatorial molecules (E). (b) Showing the allowed paths connecting C_{2v} minima [66].

strength is increasing. The figure shows decreasing in the pseudorotation rate of the system as the coupling constant increases in a similar manner as that for the $T \otimes t_2$ system. The pseudorotation between the wells in this system follows two paths similar to that for the $T \otimes t_2$ system, one path is via the D_{3d} saddle points and the other via the D_{4h} saddle points (see Fig. 4.7.(b)). As the heights of the D_{4h} saddle points are very large compared to those of D_{3d}, the system is then expected to follow the D_{3d} path rather than the D_{4h} path.

4.2 Summary

In general, for any JT system when the vibronic coupling is infinite, the vibronic states obtained are good eigenstates for the system in its static limit. But, when the coupling is finite, the obtained states should be manipulated so that it can suit the dynamical situation of the system. In the case when the system shows D_{4h} tetragonal wells, the states obtained are mutually orthogonal and they form a good eigenstates for all infinite and finite coupled $T \otimes e$ systems. Therefore, there is no need to find any linear combination of the states in the wells. The system here shows no pseudorotation between the wells and it stays in the state that it starts in. When the system is localised in one of the D_{3d} trigonal wells, then the probabilities of finding it at time t later in any of the other three wells

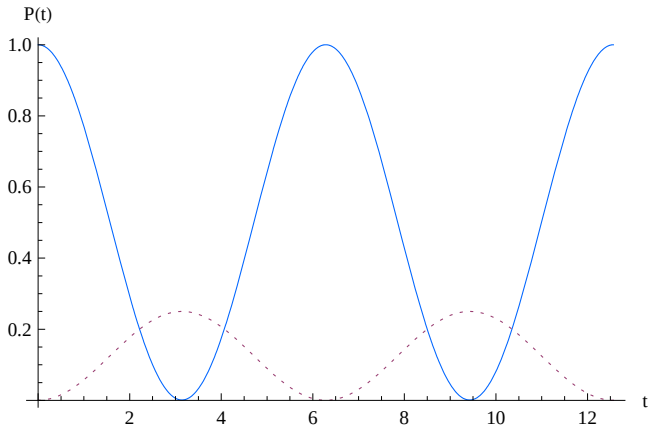

Figure 4.9: Internal dynamics of a moderately coupled $T \otimes (e + t_2)$ with $K_T = 1.4\hbar\omega_T, K_E = \hbar\omega_E$ and $V_{BL} = 0.04 V_E V_T$.

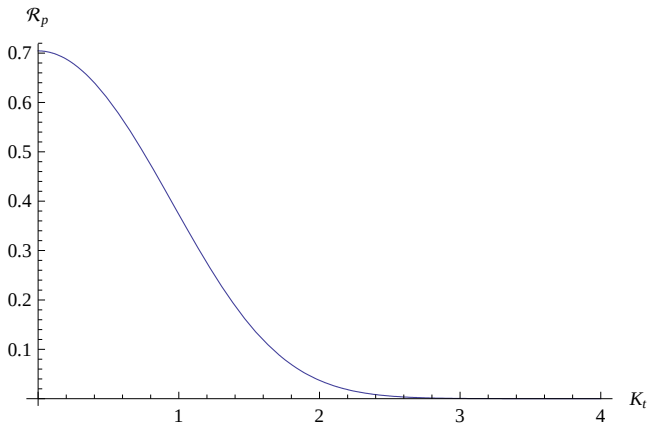

Figure 4.10: Pseudorotation rate as a function of the coupling constant for the $T \otimes (e + t_2)$ system.

are equal. The summation of the probabilities is $\sum_{X=A}^{D} P_{AX}(t) = 1 + \frac{S_t^2}{3}$ which is time independent as expected. In this case, the system is allowed to pseudorotate freely between wells following the smallest classical path via the D_{2h} saddle points. When the system contains D_{2h} orthorhombic wells, tunnelling only occurs between the non orthogonal well states while transitions between the orthogonal well states are impossible. Again, the summation of the probabilities is $\sum_{X=a}^{f} P_{ax}(t) = 1 + S_o^2$ as expected also time independent.

According to these transitions between the wells in both the $T \otimes t_2$ and $T \otimes (e \oplus t_2)$ JT systems, the molecule which exhibits such an intramolecular rotation will then show a motion of the distortion of the outer nuclear framework which appears as a periodic change in the orientation of the distorted nuclear configuration. Such a molecule is the Methane cations CH_4^+ modelled with $T \otimes (e + t_2)$ JT system. The rovibronic structure of this molecule has been investigated in which the pseudorotation could potentially be measured (for further information see Ref. [67]).

Chapter 5

The Quadratic $p^2 \otimes h$ JT Interaction: A model for C_{60}^{2-}

Fullerene derivatives form very interesting materials due to the many unexpected electronic properties that they possess. These molecules can exhibit unusual behaviour especially when they are doped with the alkali impurities to produce the alkali doped fullerenes A_nC_{60}. For example, the A_3C_{60} salts are metals with a half-filled LUMO that show superconductivity at low temperatures [68]. Such compounds are K_3C_{60} and Rb_3C_{60} which become superconductors at temperatures below 18K and 28K respectively [69]. On the other hand, the A_2C_{60} and the A_4C_{60} compounds such as Na_2C_{60} and Cs_4C_{60}, which are related to each other by electron-hole symmetry [70], are non-magnetic insulators. This behaviour in the latter compounds is somewhat unexpected and surprising as well because, according to band theory calculations [71, 72], the electrons occupy the LUMO (T_{1u}) which is just partially filled. Therefore, these compounds would be expected to be metals rather than insulators. This is the case because the Coulomb repulsion between the two electrons and the JT interactions open band gaps cooperatively, and are non-magnetic because the JT coupling overcomes the known Hunds's rule ordering [73, 74]. Hund's first rule states that for a given electron configuration the term with maximum spin multiplicity (high-spin) has the lowest energy. It has been found that compounds containing negative ions like C_{60}^{n-} where $n = 2, 4$ disobey this rule when they undergo JT distortions as the energy gained from this distortion is large enough to reverse the situation from a high-spin to a low-spin ground state [75].

The C_{60}^{2-} system has therefore a singlet spin ground state (^1A_g,^1H_g) and a close-lying triplet excited state ($^3T_1$) [76]. Although this electronic structure has been confirmed experimentally for this ion, many theoretical studies on C_{60}^{2-} systems still deal with it as if Hund's rule remains valid. These studies give values for the energies of the molecular terms some of which are (given in meV): (-114.1, 114.1, 456.6) in Ref. [77], (-275, 175, 848), (-117, 73, 359) and (-122, 77, 375) in Ref. [78] for the $^3T_1$,^1H_g,^1A_g terms respectively.

Many spectroscopic experiments such as ESR, NMR, X-ray diffraction and neutron scattering [70, 79] have shown the distorted symmetries of the molecular structure for the doubly doped C_{60} molecule. It has been predicted that the different properties between the body centred tetragonal A_4C_{60} and the face cubic centred A_3C_{60} systems for example, are due to their different structures [80, 73]. As there is a strong correlation between the distorted molecular structure and the pseudorotation of the dynamical JT effect, studying the pseudorotation phenomenon in such systems will be a good step to understand some of their underlying properties. Also, as vibrational spectroscopy is exclusively sensitive to the distorted molecules due to the splitting between the energy levels, it can detect the motion of the atoms when the distortion of the molecular framework takes place. These spectroscopic results can be compared with the theoretical calculations which can lead to an estimate of the vibronic coupling strength.

In this chapter, the JT effect in the fullerene anion C_{60}^{2-} will be investigated in detail by analysing the LAPES when a higher order (quadratic) coupling is included in the problem. Section 5.1 shows how the C_{60}^{2-} doubly doped anion is formed when the two electrons occupy the T_{1u} LUMO and obey Hund's rule. Also, the electronic states for the system which form the bases for the matrix representation of the interaction Hamiltonian are derived using the tables of Fowler and Ceulemans [27]. This is achieved by considering the Coulomb repulsion between the two electrons. This ion was investigated in an earlier work [81, 82], but only using a linear coupling Hamiltonian. At this level of approximation, the APES takes the form of a two-dimensional trough with an equipotential energy surface upon which the system moves freely around the trough whilst performing a free pseudorotation [83].

However, including quadratic terms in the problem, causes the equipotential energy points on the trough to be warped to form minima. These minima are

found to have either D_{5d} or D_{3d} symmetry in the absence of Coulomb interactions depending upon the values of the mixing angle β which mixes the two sets of the CG coefficients corresponding to the two h_g modes. The work leading to these results is given in Section 5.2.1. The minimisation of the complicated Hamiltonian is dealt with using advanced computer programmes (Mathematica, Maple) which apply the shift transformation technique outlined in Chapter 2 to obtain analytical expressions for the energy and the corresponding vibronic eigenstates for the system in its static limit. It should be noted that, since the JT interaction is assumed to be stronger than the Coulomb interaction, for simplicity the effect of the term splitting which arises from Coulomb repulsion will be neglected through this chapter, although the e-e interaction is not negligible in the doubly doped fullerenes. Studying the system when performing dynamical motion is accomplished using the projection operator technique in order to find the linear combination of the wells that the system is visiting whilst tunnelling. The SASs produced as a result of this tunnelling and the corresponding energies for both D_{5d} or D_{3d} minima are given in Section 5.2.2. Since the system is undergoing tunnelling between wells, it is undergoing a pseudorotation motion as well. The probabilities that the system can be found at a later time t when it is initially prepared in one particular well are derived in Section 5.3. Also in this section the behaviour of the system while it pseudorotates between wells is also discussed.

5.1 The JT Effect in C_{60}^{2-}

Before discussing the JT interaction in the C_{60}^{2-} anion it is worthwhile to re-examine the electronic structure of the C_{60}^{2-} molecule. The electronic structure for the isolated C_{60} molecule is given in Chapter 2. When the C_{60} molecule is doped with two electrons, these electrons occupy the empty triplet T_{1u} (LUMO) Fig. 5.1, forming the C_{60}^{2-} anion. From group theory, coupling to $2a_g$ and $8h_g$ modes is expected. This is obviously a very complicated problem to solve analytically. Therefore, the model is approximated to that in which coupling to a single effective h_g mode is only taken into account as discussed earlier in Section 2.5. The coupling problem reduces to that of a single h_g mode and termed the $p^2 \otimes h$ JT effect using the notation used in Ref. [82]. In this notation, the superscript denotes that two electrons occupy a p-type electronic orbital coupled to an h_g-type vibrational

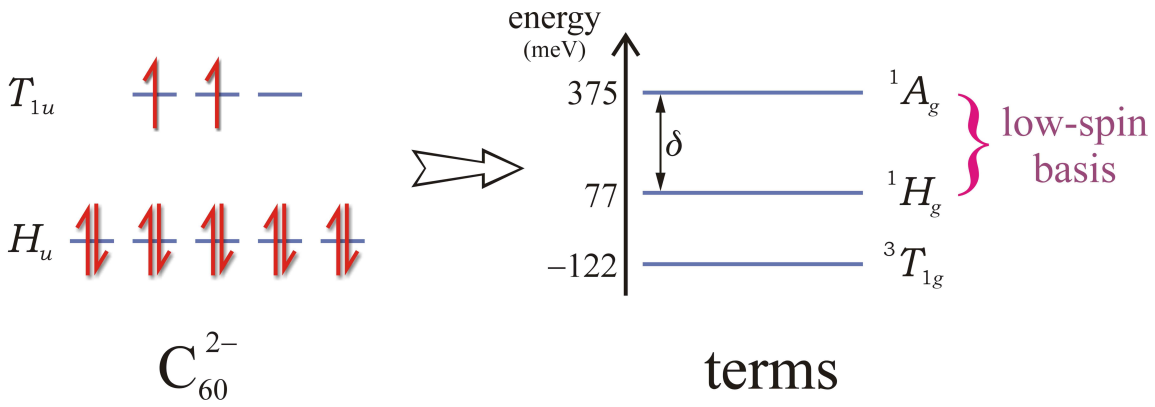

Figure 5.1: Diagrammatic representation of the doubly occupied T_{1u} LUMO of C_{60} pertinent to the $p^2 \otimes h$ system of interest. The electrons may couple to produce both high- and low-spin terms and Hund's rule is thought to be obeyed. The energies shown are taken from Ref. [78]. The energy difference δ between the low-spin basis states $\{^1A_g, ^1H_g\}$ amounts to 298 meV.

mode. The notation p is used here because of the analogy between the p atomic orbital and the T_{1u} molecular orbital.

Representing this system via the interaction Hamiltonian is quite complicated. The difficulty appears when we start constructing the electronic bases for the interaction Hamiltonian. Both the spin and the orbital angular momenta should be considered first for both electrons. Then coupling between the orbital states and the spin states should follow. This will produce rather complicated bases states which in turn will lead to cumbersome work in constructing the Hamiltonian. Another difficulty arises when the quadratic terms of the normal mode coordinates Q_iQ_j are included in the problem. This arises because the h_g mode appears twice in the Kronecker product as $H \otimes H = [A+G+2H]$, which means that the quadratic terms of the coordinates can be included in the problem with two independent sets of coefficients [27]. This therefore produces two more types of interaction Hamiltonians as will as the linear interaction Hamiltonian.

5.1.1 Electronic basis states and the linear interaction Hamiltonian

In order to find the linear interaction Hamiltonian that represents the coupling, the basis is chosen by considering the Coulomb repulsion between the two electrons in the T_{1u} orbital. Such an interaction will give rise to terms that are obtained from coupling the spin and orbital angular momenta of the two electrons together. To obtain these terms for the C_{60}^{2-} system, we first consider the coupling between the spin angular momenta. The total spin states can either be triplet symmetric states with $S = 1$, or singlet anti-symmetric states with $S = 0$. Both spin states will be further coupled to the orbital states for the two electrons. The orbital states can be found using the Kronecker product $T \otimes T = [A + H]_S \oplus \{T\}_A$. The anti-symmetric part of the Kronecker product couples to the symmetric triplet spin states to give the high-spin term $^3T_{1g}$, while the symmetric part couples to the anti-symmetric singlet spin states to give the low-spin terms ^1A_g and ^1H_g. These terms are presented in Fig. 5.1. The first diagram in Fig. 5.1 shows the HOMO and the LUMO of the C_{60} molecule when the two added electrons occupy the LUMO. The other diagram shows the relative energies of electronic states [78] following the usual Hund's rule. The term δ represents the energy splitting (term splitting) between the low-spin terms $\{^1A_g, ^1H_g\}$.

The JT coupling of the high-spin $^3T_{1g}$ term to the h_g mode has been investigated in detail by Dunn and Bates [22] by studying the analogous $T_{1u} \otimes h_g$ JT problem. Therefore, only the coupling of the low-spin terms $\{^1A_g, ^1H_g\}$ to the h_g vibrations will be considered in this work.

The next step is to find the wave functions associated with these terms which form a basis for the matrix of the interaction Hamiltonian. These wave functions are a result of multiplying the spin states by the orbital states. The resulting wave functions must be anti-symmetric in order to obey Pauli's exclusion principle.

The spin wave functions can be derived following the basic quantum mechanics rules. For example, if we consider two electrons with spins ($s_1 = s_2 = \frac{1}{2}$) and ($m_{s_1} = m_{s_2} = \pm\frac{1}{2}$), coupling between the two spins gives a maximum value of the spin (S=1) with ($M_S = 1, 0, -1$). One of the spin states can be represented in a

bra-ket notation for the values $(S = 1, M_S = 1)$ as

$$\begin{aligned} |S, M_S\rangle &= |s_1, m_{s_1}\rangle|s_2, m_{s_2}\rangle, \\ |1, 1\rangle &= |\frac{1}{2}, \frac{1}{2}\rangle|\frac{1}{2}, \frac{1}{2}\rangle. \end{aligned} \tag{5.1.1}$$

By operating on this state with the lowering spin operator defined as

$$S_-|s, m_s\rangle = \hbar\sqrt{s(s+1) - m_s(m_s-1)}\ |s, m_s - 1\rangle, \tag{5.1.2}$$

we obtain

$$S_- = (S_{1_-} + S_{2_-})|\frac{1}{2}, \frac{1}{2}\rangle|\frac{1}{2}, \frac{1}{2}\rangle \tag{5.1.3}$$

which leads to a state of the form

$$|1, 0\rangle = \frac{1}{\sqrt{2}}\left[|\frac{1}{2}, \frac{1}{2}\rangle|\frac{1}{2}, -\frac{1}{2}\rangle + |\frac{1}{2}, -\frac{1}{2}\rangle|\frac{1}{2}, \frac{1}{2}\rangle\right]. \tag{5.1.4}$$

The process is repeated again giving

$$|1, -1\rangle = |\frac{1}{2}, -\frac{1}{2}\rangle|\frac{1}{2}, -\frac{1}{2}\rangle. \tag{5.1.5}$$

The wave function associated with the triplet spin can be written now in a similar way by dropping the spin quantum number s and using the notations $|+\rangle$ and $|-\rangle$ to represent $m_s = +\frac{1}{2}$ and $m_s = -\frac{1}{2}$ respectively. Thus, we obtain

$$\begin{aligned} |M_s = 1\rangle &= |+\rangle|+\rangle, \\ |M_s = 0\rangle &= \frac{1}{\sqrt{2}}[|+\rangle|-\rangle + |-\rangle|+\rangle], \\ |M_s = -1\rangle &= |-\rangle|-\rangle, \end{aligned} \tag{5.1.6}$$

and for the singlet spin (S=0) the spin wave function is written as

$$|M_s = 0\rangle = \frac{1}{\sqrt{2}}[|+\rangle|-\rangle - |-\rangle|+\rangle]. \tag{5.1.7}$$

Now, the orbital wave functions for the CG coefficients for the product $T_1 \otimes T_1$ are derived using the tables of Fowler and Ceulemans [27]. This produces the

following states

$$
\begin{aligned}
|A_a\rangle &= \frac{1}{\sqrt{3}}\left[|T_1x\rangle_1|T_1x\rangle_2 + |T_1y\rangle_1|T_1y\rangle_2 + |T_1z\rangle_1|T_1z\rangle_2\right], \\
|T_{1x}\rangle &= \frac{1}{\sqrt{2}}[|T_1y\rangle_1|T_1z\rangle_2 - |T_1z\rangle_1|T_1y\rangle_2], \\
|T_{1y}\rangle &= \frac{1}{\sqrt{2}}[-|T_1x\rangle_1|T_1z\rangle_2 + |T_1z\rangle_1|T_1x\rangle_2], \\
|T_{1z}\rangle &= \frac{1}{\sqrt{2}}[|T_1x\rangle_1|T_1y\rangle_2 - |T_1y\rangle_1|T_1x\rangle_2], \\
|H_\theta\rangle &= \frac{\phi^{-1}}{2}|T_1x\rangle_1|T_1x\rangle_2 - \frac{\phi}{2}|T_1y\rangle_1|T_1y\rangle_2 + \frac{1}{2}|T_1z\rangle_1|T_1z\rangle_2, \\
|H_\epsilon\rangle &= \frac{\phi^2}{2\sqrt{3}}|T_1x\rangle_1|T_1x\rangle_2 - \frac{\phi^{-2}}{2\sqrt{3}}|T_1y\rangle_1|T_1y\rangle_2 - \frac{\sqrt{5}}{2\sqrt{3}}|T_1z\rangle_1|T_1z\rangle_2, \\
|H_4\rangle &= \frac{1}{\sqrt{2}}[|T_1y\rangle_1|T_1z\rangle_2 + |T_1z\rangle_1|T_1y\rangle_2], \\
|H_5\rangle &= \frac{1}{\sqrt{2}}[|T_1x\rangle_1|T_1z\rangle_2 + |T_1z\rangle_1|T_1x\rangle_2], \\
|H_6\rangle &= \frac{1}{\sqrt{2}}[|T_1x\rangle_1|T_1y\rangle_2 + |T_1y\rangle_1|T_1x\rangle_2],
\end{aligned}
\tag{5.1.8}
$$

where $|A_a\rangle$, $|T_{1x}\rangle \ldots$ *etc* are the electronic orbital states. The term $|T_1x\rangle_1|T_1x\rangle_2$ tells us that both electrons occupy the state $|T_1x\rangle$.

Now, the overall states must be anti-symmetric. Therefore, the triplet (symmetric) spin wave functions must be multiplied by the anti-symmetric orbital wave functions while, the singlet (anti-symmetric) spin states must be multiplied by the symmetric orbital wave functions. Therefore, the final resulting basis states can

be written as

$$
\begin{aligned}
|^1A_a; M_s = 0\rangle &= \frac{1}{\sqrt{6}}[|T_1x\rangle_1^+|T_1x\rangle_2^- + |T_1y\rangle_1^+|T_1y\rangle_2^- + |T_1z\rangle_1^+|T_1z\rangle_2^- \\
&\quad -|T_1x\rangle_1^-|T_1x\rangle_2^+ - |T_1y\rangle_1^-|T_1y\rangle_2^+ - |T_1z\rangle_1^-|T_1z\rangle_2^+] \\
|^3T_{1x}; M_s = 1\rangle &= \frac{1}{\sqrt{2}}[|T_1y\rangle_1^+|T_1z\rangle_2^+ - |T_1z\rangle_1^+|T_1y\rangle_2^+] \\
|^3T_{1y}; M_s = 1\rangle &= \frac{1}{\sqrt{2}}[-|T_1x\rangle_1^+|T_1z\rangle_2^+ + |T_1z\rangle_1^+|T_1x\rangle_2^+] \\
|^3T_{1z}; M_s = 1\rangle &= \frac{1}{\sqrt{2}}[|T_1x\rangle_1^+|T_1y\rangle_2^+ - |T_1y\rangle_1^+|T_1x\rangle_2^+] \\
|^3T_{1x}; M_s = 0\rangle &= \frac{1}{2}[|T_1y\rangle_1^-|T_1z\rangle_2^+ - |T_1z\rangle_1^-|T_1y\rangle_2^+] \\
|^3T_{1y}; M_s = 0\rangle &= \frac{1}{2}[-|T_1x\rangle_1^-|T_1z\rangle_2^+ + |T_1z\rangle_1^-|T_1x\rangle_2^+] \\
|^3T_{1z}; M_s = 0\rangle &= \frac{1}{2}[|T_1x\rangle_1^-|T_1y\rangle_2^+ - |T_1y\rangle_1^-|T_1x\rangle_2^+] \\
|^3T_{1x}; M_s = -1\rangle &= \frac{1}{\sqrt{2}}[|T_1y\rangle_1^-|T_1z\rangle_2^- - |T_1z\rangle_1^-|T_1y\rangle_2^-] \\
|^3T_{1y}; M_s = -1\rangle &= \frac{1}{\sqrt{2}}[-|T_1x\rangle_1^-|T_1z\rangle_2^- + |T_1z\rangle_1^-|T_1x\rangle_2^-] \\
|^3T_{1z}; M_s = -1\rangle &= \frac{1}{\sqrt{2}}[|T_1x\rangle_1^-|T_1y\rangle_2^- - |T_1y\rangle_1^-|T_1x\rangle_2^-] \qquad (5.1.9) \\
|^1H_\theta; M_s = 0\rangle &= \frac{1}{2\sqrt{2}}[\phi^{-1}|T_1x\rangle_1^+|T_1x\rangle_2^- - \phi|T_1y\rangle_1^+|T_1y\rangle_2^- + |T_1z\rangle_1^+|T_1z\rangle_2^- \\
&\quad - \phi^{-1}|T_1x\rangle_1^-|T_1x\rangle_2^+ + \phi|T_1y\rangle_1^-|T_1y\rangle_2^+ - |T_1z\rangle_1^-|T_1z\rangle_2^+] \\
|^1H_\epsilon; M_s = 0\rangle &= \frac{1}{2\sqrt{6}}[\phi^2|T_1x\rangle_1^+|T_1x\rangle_2^- - \phi^{-2}|T_1y\rangle_1^+|T_1y\rangle_2^- - \sqrt{5}|T_1z\rangle_1^+|T_1z\rangle_2^- \\
&\quad - \phi^2|T_1x\rangle_1^-|T_1x\rangle_2^+ + \phi^{-2}|T_1y\rangle_1^-|T_1y\rangle_2^+ + \sqrt{5}|T_1z\rangle_1^-|T_1z\rangle_2^+] \\
|^1H_4; M_s = 0\rangle &= \frac{1}{2}[|T_1y\rangle_1^+|T_1z\rangle_2^- - |T_1z\rangle_1^+|T_1y\rangle_2^- - |T_1y\rangle_1^-|T_1z\rangle_2^+ - |T_1z\rangle_1^-|T_1y\rangle_2^+] \\
|^1H_5; M_s = 0\rangle &= \frac{1}{2}[|T_1x\rangle_1^+|T_1z\rangle_2^- + |T_1z\rangle_1^+|T_1x\rangle_2^- - |T_1x\rangle_1^-|T_1z\rangle_2^+ - |T_1z\rangle_1^-|T_1x\rangle_2^+] \\
|^1H_6; M_s = 0\rangle &= \frac{1}{2}[|T_1x\rangle_1^+|T_1y\rangle_2^- + |T_1y\rangle_1^+|T_1x\rangle_2^- - |T_1x\rangle_1^-|T_1y\rangle_2^+ - |T_1y\rangle_1^-|T_1x\rangle_2^+]
\end{aligned}
$$

In these expressions, $|T_1x\rangle_1^+|T_1y\rangle_2^-$ represents the product state where electron 1 is in the $|T_1x\rangle$ orbital with spin $+\frac{1}{2}$ and electron 2 is in the $|T_1y\rangle_2^-$ orbital with spin $-\frac{1}{2}$. Only the low-spin basis is used to derive the matrix representation of the JT interaction Hamiltonian whereas, the high-spin bases will be ignored in this problem because of the analogy between the coupling problem of this term with the $T_{1u} \otimes h_g$ coupling as was previously mentioned.

The total Hamiltonian for the system may be given in the form of a 6×6 matrix.

It has the general form

$$\mathcal{H}_{total} = \mathcal{H}_{vib} + \mathcal{H}_{JT} + \mathcal{H}_{TS}, \tag{5.1.10}$$

where $\mathcal{H}_{vib}$ is the Hamiltonian that has been defined in Eq. (2.2.14), $\mathcal{H}_{JT}$ is the JT interaction Hamiltonian which has the general form

$$\mathcal{H}_{JT} = V_1\mathcal{H}_1(\mathbf{Q}) + V_2\mathcal{H}_2(\mathbf{Q}^2) + V_3\mathcal{H}_3(\mathbf{Q}^2), \tag{5.1.11}$$

where V_i are the vibronic coupling constants, which determine the relative importance of each contribution to the coupling, and $\mathcal{H}_i$ are the interaction matrices. Finally, $\mathcal{H}_{TS}$ is the term splitting Hamiltonian that arise from Coulomb interaction. In this section the effect of this Hamiltonian will be ignored and the problem will be achieved without the inclusion of the term splitting δ. Using the above basis states with the tables in Ref. [27], the linear interaction matrix for the system takes the form

$$\mathcal{H}_1(\mathbf{Q}) = \sqrt{2}\begin{bmatrix} 0 & Q_\theta & Q_\epsilon & Q_4 & Q_5 & Q_6 \\ Q_\theta & f_1 & f_2 & \frac{\sqrt{3}}{4\phi}Q_4 & \frac{-\sqrt{3}\phi}{4}Q_5 & \frac{\sqrt{3}}{4}Q_6 \\ Q_\epsilon & f_2 & -f_1 & \frac{\phi^2}{4}Q_4 & \frac{-1}{4\phi^2}Q_5 & \frac{-\sqrt{5}}{4}Q_6 \\ Q_4 & \frac{\sqrt{3}}{4\phi}Q_4 & \frac{\phi^2}{4}Q_4 & f_3 & -\sqrt{\frac{3}{8}}Q_6 & -\sqrt{\frac{3}{8}}Q_5 \\ Q_5 & \frac{-\sqrt{3}\phi}{4}Q_5 & \frac{-1}{4\phi^2}Q_5 & -\sqrt{\frac{3}{8}}Q_6 & f_4 & -\sqrt{\frac{3}{8}}Q_4 \\ Q_6 & \frac{\sqrt{3}}{4}Q_6 & \frac{-\sqrt{5}}{4}Q_6 & -\sqrt{\frac{3}{8}}Q_5 & -\sqrt{\frac{3}{8}}Q_4 & -(f_3+f_4) \end{bmatrix},$$

where,

$$\begin{aligned} f_1 &= \frac{3\sqrt{3}Q_\theta + \sqrt{5}Q_\epsilon}{8}, \\ f_2 &= \frac{\sqrt{5}Q_\theta - 3\sqrt{3}Q_\epsilon}{8}, \\ f_3 &= \frac{\sqrt{3}Q_\theta + \phi^3 Q_\epsilon}{4\phi}, \\ f_4 &= \frac{-\left(\sqrt{3}\phi^3 Q_\theta + Q_\epsilon\right)}{4\phi^2}. \end{aligned}$$

Studying this linear Hamiltonian by itself produces a continuous trough with radius $\rho = 2K$ and minimum energy of $E_{JT} = -2K^2$ [83], where K is defined as $K = \frac{\sqrt{2}}{\sqrt{5}}V_1$. Each point on the trough corresponds to a different distorted configuration. The system in this case is rotating around the trough in two perpendicular directions in a free pseudorotation; at the same time it is vibrating across the

trough in the other three perpendicular directions. However, this system has been investigated in detail and the corresponding energy and eigenstate have been obtained in Ref. [81].

5.1.2 The quadratic interaction Hamiltonians for C_{60}^{2-}

In the previous section, the linear interaction Hamiltonian was constructed using the basis states arising from the coupling between ${}^1A$ and ${}^1H$ terms. The quadratic interaction matrices can be written by making simple substitutions in the linear matrix of the form

$$\mathcal{H}_2(\mathbf{Q}^2) = \mathcal{H}_1(\mathbf{Q} \mapsto \mathbf{A}), \tag{5.1.12}$$

$$\mathcal{H}_3(\mathbf{Q}^2) = \mathcal{H}_1(\mathbf{Q} \mapsto \mathbf{B}), \tag{5.1.13}$$

where the individual components in the linear interaction matrix are mapped so that, for example, for $\mathcal{H}_2$, $Q_\theta \mapsto A_\theta$, $Q_\epsilon \mapsto A_\epsilon \ldots etc$ with

$$\begin{aligned}
A_\theta &= \frac{1}{2\sqrt{6}}\left(3Q_\theta^2 - 3Q_\epsilon^2 - Q_4^2 - Q_5^2 + 2Q_6^2\right), \\
A_\epsilon &= \frac{-1}{2\sqrt{2}}\left(2\sqrt{3}Q_\theta Q_\epsilon - Q_4^2 + Q_5^2\right), \\
A_4 &= \frac{-1}{\sqrt{6}}\left(Q_\theta Q_4 - \sqrt{3}Q_\epsilon Q_4 + 2\sqrt{2}Q_5 Q_6\right), \\
A_5 &= \frac{-1}{\sqrt{6}}\left(Q_\theta Q_5 + \sqrt{3}Q_\epsilon Q_5 + 2\sqrt{2}Q_4 Q_6\right), \\
A_6 &= \frac{2}{\sqrt{6}}\left(Q_\theta Q_6 - \sqrt{2}Q_4 Q_5\right),
\end{aligned} \tag{5.1.14}$$

and

$$\begin{aligned}
B_\theta &= \frac{1}{2\sqrt{2}}\left(2Q_\theta Q_\epsilon + \sqrt{3}Q_4^2 - \sqrt{3}Q_5^2\right), \\
B_\epsilon &= \frac{1}{2\sqrt{2}}\left(Q_\theta^2 - Q_\epsilon^2 + Q_4^2 + Q_5^2 - 2Q_6^2\right), \\
B_4 &= \frac{1}{\sqrt{2}}\left(Q_\epsilon + \sqrt{3}Q_\theta\right)Q_4, \\
B_5 &= \frac{1}{\sqrt{2}}\left(Q_\epsilon - \sqrt{3}Q_\theta\right)Q_5, \\
B_6 &= -\sqrt{2}Q_\epsilon Q_6.
\end{aligned} \tag{5.1.15}$$

where the A_i and B_i components are derived again using the tables given in Ref. [27].

As already discussed, $\mathcal{H}_2$ and $\mathcal{H}_3$ arise due to the fact that the Kronecker product $H \otimes H$ contains the H irrep twice. The relative strength of these two quadratic terms are governed by the quadratic coupling constants V_2 and V_3. Unfortunately, no attempts to calculate these parameters have so far appeared in the literature for the appropriate modes of C_{60}^{2-} and therefore, they will be treated as general as possible in this thesis.

It is well known that by including higher order coupling terms in such problems, it causes the trough of minimum energy points to be warped to form minima. The symmetry of those minima is unknown until the APES associated with the Hamiltonian given in Eq. (5.1.10) is investigated. This can be conveniently done by using the shift transformation technique which will be discussed in the next section.

5.2 The unitary shift transformation and energy minimisation

The Hamiltonian given in Eq. (5.1.10) can be investigated in order to find the minima in the ground APES by applying the theory of the shift transformation that was outlined in Section 2.3.1. The transformation has the effect of displacing each of the coordinates Q_i by an amount equal to $-\hbar\alpha_i$ and the outcome of this process is that the transformed Hamiltonian $\tilde{\mathcal{H}}$ is a function of the unknown constants α_i. The six eigenvalues of this Hamiltonian are, therefore, also functions of these constants. The symmetry of the system, however, means that there are always several minima $\{\alpha_{min}^{(j)}\}$, the number of which indicates the symmetry of the distorted ion. However, the aim in this section is to provide analytic expressions for the constants $\alpha_{min}^{(j)}$ and the energies associated with each minimum. This can be accomplished by investigating the $\tilde{\mathcal{H}}$ using a numerical minimisation program. The general idea of this programme is relatively simple and depends on allowing the parameters α to vary in order to minimise the lowest eigenvalue, to indicate a minimum in the APES. The transformed Hamiltonian $\tilde{\mathcal{H}}(a_i)$ is a function of the parameters $a_\theta, a_\epsilon, a_4, a_5, a_6$, where a_i are dimensionless values defined as $a_i = \frac{\mu\hbar\omega^2}{V_1}\alpha_i$; we set up these parameters by initial arbitrary numbers a_i^0, then the programme can be run in order to find the eigenvalues corresponding to these

parameters. The lowest energy among these eigenvalues is then our current energy $\mathcal{E}(a_i^0)$. The programme can be run again after we let one of the values of a_i^0 to vary by a small factor κ as $a_i^0 \longrightarrow a_i^0 + \kappa$ and then we calculate the energy $\mathcal{E}(a_i^0 + \kappa)$. If the new energy is found to be lower, then the programme will be adjusted to move to a new point until it achieves the lowest energy corresponding to the changing of that parameter. The same procedure will be repeated for each parameters a_i^0 successively. Eventually, if there are no further changes in a_i which lead to a further lowering of the energy, then the final achieved energy can be accepted to be the true energy of the minimum.

This approach is especially useful here as it allows us to investigate the effect of the two quadratic interaction matrices $\tilde{\mathcal{H}}_2$ and $\tilde{\mathcal{H}}_3$ separately. Thus, to account for the general coupling problem, it is useful to defined the vibronic coupling constants in their polar form by:

$$\begin{aligned} V_2 &= V_{\text{tot}} \cos\beta, \\ V_3 &= V_{\text{tot}} \sin\beta, \end{aligned} \tag{5.2.1}$$

where V_{tot} is a positive number representing the overall magnitude of the quadratic coupling. The mixing angle β has the effect of mixing the two sets of CG coefficients that appear in the Kronecker product $H \otimes H$. If we select representative values for the coupling constants, we can minimise the energy numerically using the above outlined method. The numerical minimaisation routine obtained from this method is represented as $\{\bigcirc\}$ for the D_{3d} symmetry and $\{\square\}$ for the D_{5d} symmetry in Fig. 5.2, where we have assumed dimensionless coupling constants amounting to

$$\begin{aligned} V_1' &= \frac{-V_1}{\sqrt{\mu\hbar\omega^3}} = 1, \\ V_{\text{tot}}' &= \frac{V_{\text{tot}}}{\mu\omega^2} = 0.1. \end{aligned} \tag{5.2.2}$$

5.2.1 The adiabatic potential energy surface (APES)

Fig. 5.2 illustrates the symmetry of the minima in the APES as a function of the mixing angle β. It shows that, when $0 \lesssim \beta \lesssim 0.641$, the APES of the system has D_{5d} symmetry lower in energy than the D_{3d} symmetry. In the region where $0.641 \lesssim \beta \lesssim 3.78$, the D_{3d} symmetry becomes lower in energy than the D_{5d}

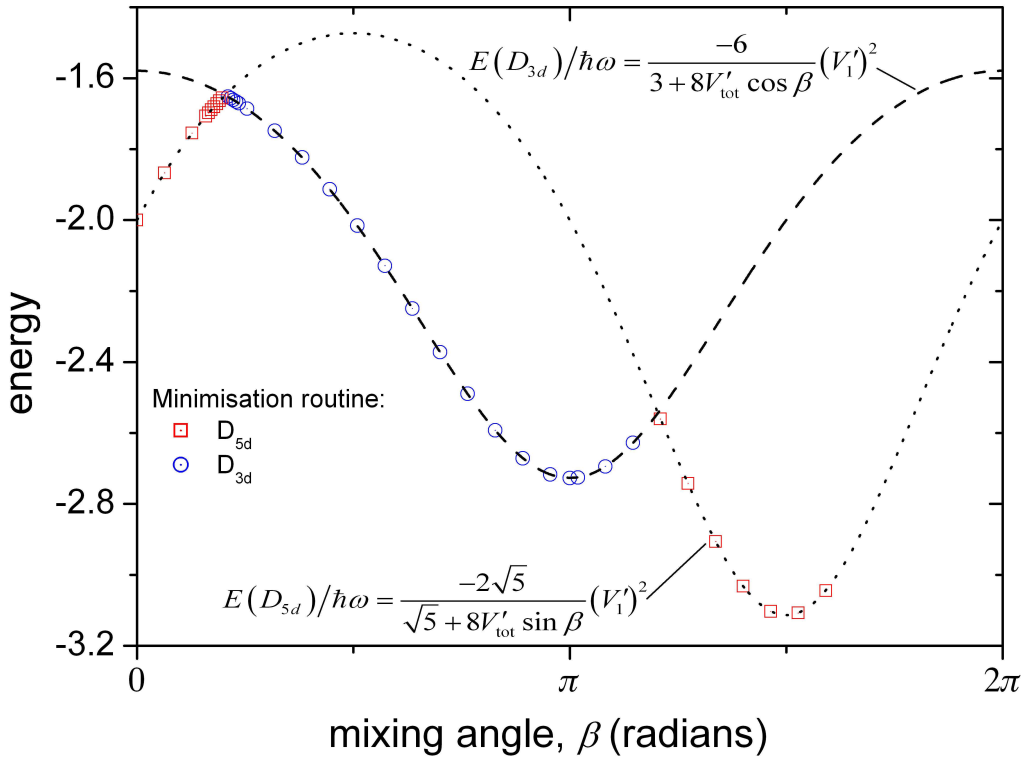

Figure 5.2: Energies and symmetry of the minima found by numerically minimising the transformed Hamiltonian $\tilde{\mathcal{H}}_1$ as a function of the mixing angle β. The values used for the dimensionless coupling constants are $V'_1 = 1$ and $V'_{tot} = 0.1$ and the energy difference due to Coulombic interactions has been ignored ($\delta = 0$). The energy is given in units of $\hbar\omega$ and the lines represent analytical expressions of the energy for both types of minima.

symmetry and therefore the system prefers to be confined to D_{3d} minima. In the range when $\beta \gtrsim 3.78$, the system localises again D_{5d} minima.

The problem has also been investigated theoretically by applying a simple method summarised as follow. Let first assume that the problem will be investigated for the D_{5d} case. Here, one of the D_{5d} minimum points $\{a_\theta, a_\epsilon, a_4, a_5, a_6\}$ takes the general form as $\{0, 2\zeta, 0, 0, \sqrt{6}\zeta\}$, where ζ represents the required value to minimised the energy. The ratio $\frac{a_\epsilon}{a_6} = \frac{\sqrt{2}}{\sqrt{3}}$, by substituting this value with $a_\theta = a_4 = a_5 = 0$ in the transformed Hamiltonian which is a function of a_i produces a Hamiltonian as a function of the a_6 alone. The eigenvalues and the corresponding eigenstates can then be found. The lowest eigenvalues which is a function of the a_6 will be chosen. Minimising this value with respect to a_6 and then solving the equation when it is equal to zero for a_6. Since the value of a_6 is obtained, the value of a_ϵ is then equal to $\frac{\sqrt{2}}{\sqrt{3}}a_6$. Substituting the a_6 again in the eigenvalue expression results an analytical expression for the D_{5d} symmetry of the following form

$$E\left(D_{5d}\right) = \frac{-2\sqrt{5}}{\sqrt{5} + 8V'_{\text{tot}} \sin\beta} \left(V'_1\right)^2 \hbar\omega \tag{5.2.3}$$

Similarly, by following the previous steps for the D_{3d} case, an analytical expression for the minimum energy is found as

$$E\left(D_{3d}\right) = \frac{-6}{3 + 8V'_{\text{tot}} \cos\beta} \left(V'_1\right)^2 \hbar\omega. \tag{5.2.4}$$

An interesting observation here is that when these expressions are plotted for the same previous values of V'_1 and V'_{tot}, it shows a perfect fit to the dashed and dotted lines which represent the numerical values that were obtained from the minimisation programme, as shown in Fig. 5.2. Either D_{5d} or D_{3d} minima occur only if one of the conditions is satisfied either $\sqrt{5}V_2 > 3V_3$ or $\sqrt{5}V_2 < 3V_3$ respectively. For example, when $V_3 = 0$, $\mathcal{H}_2$ produces D_{5d} minima in the APES provided that $V_2 > 0$. However, if $V_2 < 0$, it will produce D_{3d} minima. This can be seen very clearly in Fig. 5.3, when $V_3 = 0$ we should be looking only along the V_2 axis. Similarly, when $V_2 = 0$, $\mathcal{H}_3$ by itself produces D_{3d} minima in the APES if $V_3 > 0$ and D_{5d} minima if $V_3 < 0$. This is obvious from Fig. 5.3 when we look along the V_3 axis. Overall, only minima of D_{5d} or D_{3d} symmetry have been obtained. A critical mixing angle β can be found when the two energies of both symmetries become equally (i.e when $E\left(D_{5d}\right) = E\left(D_{3d}\right)$) from this a mixing angle is found to be $\beta = \tan^{-1}(\sqrt{5}/3)$. This angle divided the region into two parts as shown

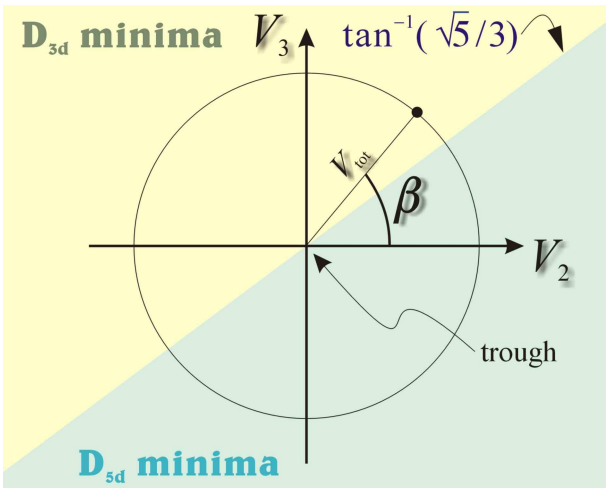

Figure 5.3: Diagrammatic representation of the symmetry of the minima as a function of the mixing angle. At the origin, the quadratic constants are zero and so there is a continuous two-dimensional trough of minima with energy $E_{\text{trough}} = -2\left(V_1'\right)^2 \hbar\omega$. The minima are of D_{3d} symmetry in the range $0.641 \lesssim \beta \lesssim 3.78$, and D_{5d} elsewhere.

in Fig. 5.3 where the different symmetries are allowed to exist. The upper half represents the region of the D_{3d} symmetry where $0.641 \lesssim \beta \lesssim 3.78$. The lower half represents the D_{5d} region for the rest values of β. It is also noticeable that when $\beta = 0$, $V_3 \longrightarrow 0$ and the energy of the D_{5d} minima is equal to $-2\left(V_1'\right)^2 \hbar\omega$. This is independent of the quadratic coupling strength V_{tot}' (provided that $V_{\text{tot}}' \lesssim 0.4$, above which the quadratic part outweighs the contribution from $\mathcal{H}_{\text{vib}}$ and the minimisation routine diverges to $-\infty$ as $\boldsymbol{\alpha} \to \infty$). This energy is identical to the energy of the two-dimensional trough obtained in the absence of quadratic coupling, even though quadratic coupling is present and is undoubtedly warping the APES. A rationalisation of this behaviour may be made by considering the nature of the warping produced by the quadratic term only, as shown in Fig. 5.4. When $\beta = 0$ (top part of Fig. 5.4), D_{5d} minima are obtained with an energy of $-2\left(V_1'\right)^2 \hbar\omega$. Changing the value of V_{tot}' has no effect on this minimum energy, but it will affect the 'height' of the D_{3d} 'hills' between the minima, thus, warping is increased but the minima stay at the same energy. A similar argument can be used to explain why the D_{3d} minima produced when $\beta = \pi/2$ also have an energy of $-2\left(V_1'\right)^2 \hbar\omega$ [Eq. (5.2.3)] provided the value of V_{tot}' is not excessive.

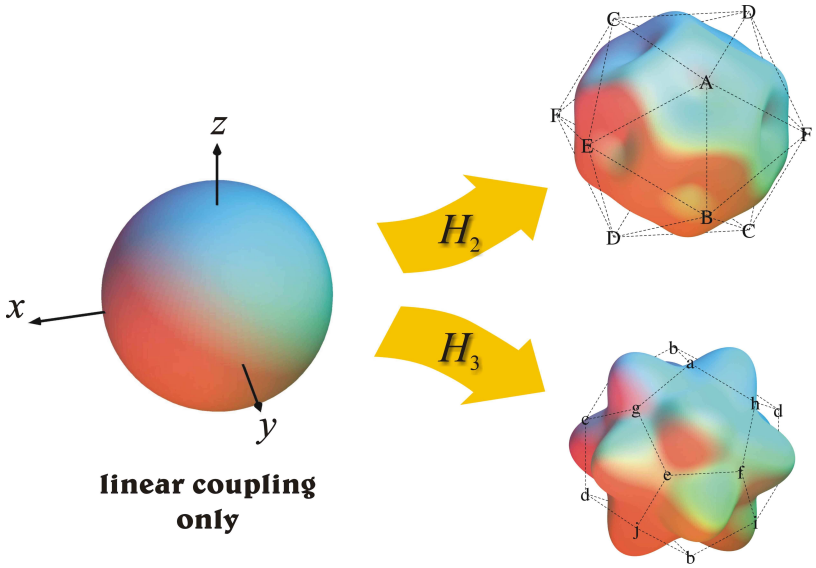

Figure 5.4: Warping of the spherical APES obtained from the linear coupling model by the quadratic interaction Hamiltonians. The cases shown correspond to $\beta = 0$ (top) and $\beta = \pi/2$ (bottom). For clarity, and later use, the minima are labelled {A, B, ..., F, a, b, ..., j}.

5.2.2 Well positions and electronic states

The values of the minimum points for the wells can be obtained using the theoretical method outlined above when it was required to obtain the analytical results for the energies. The rest of the minimum points of the wells can therefore be obtained easily by applying the symmetry operators on one of the minimum point and this can be worked for both symmetries. These values with the corresponding eigenvectors are obtained and tabulated in Tables 5.1 and 5.2. In order to reduce the complexity of the problem, we shall present results for two specific cases, exemplifying the behaviour in the presence of D_{5d} and D_{3d} minima as follow.

D_{5d} minima

Table 5.1 gives the positions of the pentagonal wells of D_{5d} symmetry and the associated electronic states. The vibronic states can be easily found using Eq. (2.3.18).

Table 5.1: Electronic states and well positions for the D_{5d} symmetry case. Term splitting has been ignored and $\zeta = \frac{-\sqrt{2}}{\sqrt{5}+8V'_{\rm tot}\sin\beta}$.

Label	Shift, $\boldsymbol{\alpha}$[a]	Electronic state
A	$(-\sqrt{3}\zeta, -\zeta, \sqrt{6}\zeta, 0, 0)$	$(\frac{-1}{\sqrt{3}}, \frac{-1}{\sqrt{5}}, \frac{-1}{\sqrt{15}}, \frac{\sqrt{2}}{\sqrt{5}}, 0, 0)$
B	$(-\sqrt{3}\zeta, -\zeta, -\sqrt{6}\zeta, 0, 0)$	$(\frac{-1}{\sqrt{3}}, \frac{-1}{\sqrt{5}}, \frac{-1}{\sqrt{15}}, \frac{-\sqrt{2}}{\sqrt{5}}, 0, 0)$
C	$(\sqrt{3}\zeta, -\zeta, 0, \sqrt{6}\zeta, 0)$	$(\frac{-1}{\sqrt{3}}, \frac{1}{\sqrt{5}}, \frac{-1}{\sqrt{15}}, 0, \frac{\sqrt{2}}{\sqrt{5}}, 0)$
D	$(\sqrt{3}\zeta, -\zeta, 0, -\sqrt{6}\zeta, 0)$	$(\frac{-1}{\sqrt{3}}, \frac{1}{\sqrt{5}}, \frac{-1}{\sqrt{15}}, 0, \frac{-\sqrt{2}}{\sqrt{5}}, 0)$
E	$(0, 2\zeta, 0, 0, \sqrt{6}\zeta)$	$(\frac{-1}{\sqrt{3}}, 0, \frac{2}{\sqrt{15}}, 0, 0, \frac{\sqrt{2}}{\sqrt{5}})$
F	$(0, 2\zeta, 0, 0, -\sqrt{6}\zeta)$	$(\frac{-1}{\sqrt{3}}, 0, \frac{2}{\sqrt{15}}, 0, 0, -\frac{\sqrt{2}}{\sqrt{5}})$

[a] In units of $V_1/\hbar\mu\omega^2$.

D_{3d} minima

Table 5.2 presents the positions of the trigonal wells of D_{3d} symmetry and the corresponding electronic states.

5.2.3 Symmetry-adapted states

The general theory outlining the use of projection operators in order to find the SASs is found in Section 2.3.3. A specific application to JT systems has also been made before in Refs. [84] and [22].

SASs for D_{5d} minima

Symmetry adapted states of H and A symmetry are obtained after using the projection operator technique. These six states are linear combination of the six

Table 5.2: Electronic states and well positions for the D_{3d} symmetry case. Term splitting has been ignored and $\eta = \frac{-2\sqrt{3}}{3+8V'_{\rm tot}\cos\beta}$.

Label	Shift, $\boldsymbol{\alpha}$[a]	Electronic state
a	$(\frac{1}{\sqrt{2}}\eta, -\sqrt{\frac{3}{2}}\eta, \eta, 0, 0)$	$(\frac{-1}{\sqrt{3}}, \frac{1}{3}, \frac{-1}{\sqrt{3}}, \frac{\sqrt{2}}{3}, 0, 0)$
b	$(\frac{1}{\sqrt{2}}\eta, -\sqrt{\frac{3}{2}}\eta, -\eta, 0, 0)$	$(\frac{-1}{\sqrt{3}}, \frac{1}{3}, \frac{-1}{\sqrt{3}}, \frac{-\sqrt{2}}{3}, 0, 0)$
c	$(\frac{1}{\sqrt{2}}\eta, \sqrt{\frac{3}{2}}\eta, 0, \eta, 0)$	$(\frac{-1}{\sqrt{3}}, \frac{1}{3}, \frac{1}{\sqrt{3}}, 0, \frac{\sqrt{2}}{3}, 0)$
d	$(\frac{1}{\sqrt{2}}\eta, \sqrt{\frac{3}{2}}\eta, 0, -\eta, 0)$	$(\frac{-1}{\sqrt{3}}, \frac{1}{3}, \frac{1}{\sqrt{3}}, 0, \frac{-\sqrt{2}}{3}, 0)$
e	$(-\sqrt{2}\eta, 0, 0, 0, \eta)$	$(\frac{-1}{\sqrt{3}}, \frac{-2}{3}, 0, 0, 0, \frac{\sqrt{2}}{3})$
f	$(-\sqrt{2}\eta, 0, 0, 0, -\eta)$	$(\frac{-1}{\sqrt{3}}, \frac{-2}{3}, 0, 0, 0, \frac{-\sqrt{2}}{3})$
g	$(0, 0, \eta, \eta, \eta)$	$(\frac{-1}{\sqrt{3}}, 0, 0, \frac{\sqrt{2}}{3}, \frac{\sqrt{2}}{3}, \frac{\sqrt{2}}{3})$
h	$(0, 0, \eta, -\eta, -\eta)$	$(\frac{-1}{\sqrt{3}}, 0, 0, \frac{\sqrt{2}}{3}, \frac{-\sqrt{2}}{3}, \frac{-\sqrt{2}}{3})$
i	$(0, 0, -\eta, \eta, -\eta)$	$(\frac{-1}{\sqrt{3}}, 0, 0, \frac{-\sqrt{2}}{3}, \frac{\sqrt{2}}{3}, \frac{-\sqrt{2}}{3})$
j	$(0, 0, -\eta, -\eta, \eta)$	$(\frac{-1}{\sqrt{3}}, 0, 0, \frac{-\sqrt{2}}{3}, \frac{-\sqrt{2}}{3}, \frac{\sqrt{2}}{3})$

[a] In units of $V_1/\hbar\mu\omega^2$.

well states given by

$$\begin{aligned}
|H_\theta\rangle &= \frac{N_H}{2}\left[|A';0\rangle + |B';0\rangle - |C';0\rangle - |D';0\rangle\right], \\
|H_\epsilon\rangle &= \frac{N_H}{2\sqrt{3}}\left[|A';0\rangle + |B';0\rangle + |C';0\rangle + |D';0\rangle - 2|E';0\rangle - 2|F';0\rangle\right], \\
|H_4\rangle &= \frac{N_H}{\sqrt{2}}\left[-|A';0\rangle + |B';0\rangle\right], \\
|H_5\rangle &= \frac{N_H}{\sqrt{2}}\left[-|C';0\rangle + |D';0\rangle\right], \\
|H_6\rangle &= \frac{N_H}{\sqrt{2}}\left[-|E';0\rangle + |F';0\rangle\right], \\
|A_a\rangle &= \frac{N_A}{\sqrt{6}}\left[|A';0\rangle + |B';0\rangle + |C';0\rangle + |D';0\rangle + |E';0\rangle + |F';0\rangle\right],
\end{aligned} \tag{5.2.5}$$

where N_H and N_A are normalisation constants given by

$$\begin{aligned}
N_H &= \frac{\sqrt{5}}{\sqrt{5 - S_p}}, \\
N_A &= \frac{1}{\sqrt{1 + 5S_p}}.
\end{aligned} \tag{5.2.6}$$

Here, S_p is the phonon overlap between any two pentagonal wells and given by

$$S_p = \exp[-6V_1'^2\zeta^2]. \tag{5.2.7}$$

SASs for D_{3d} minima

For D_{3d} minima, ten SASs of H, G and A symmetry are obtained. They are linear combinations of the ten well states and given by

$$\begin{aligned}
|H_\theta\rangle &= \frac{N_H}{\sqrt{12}}\,[\,|a';0\rangle + |b';0\rangle + |c';0\rangle + |d';0\rangle - 2|e';0\rangle - 2|f';0\rangle],\\
|H_\epsilon\rangle &= \frac{N_H}{2}\,[-|a';0\rangle - |b';0\rangle + |c';0\rangle + |d';0\rangle],\\
|H_4\rangle &= \frac{N_H}{\sqrt{6}}\,[\,|a';0\rangle - |b';0\rangle + |g';0\rangle + |h';0\rangle - |i';0\rangle - |j';0\rangle],\\
|H_5\rangle &= \frac{N_H}{\sqrt{6}}\,[\,|c';0\rangle - |d';0\rangle + |g';0\rangle - |h';0\rangle + |i';0\rangle - |j';0\rangle],\\
|H_6\rangle &= \frac{N_H}{\sqrt{6}}\,[\,|e';0\rangle - |f';0\rangle + |g';0\rangle - |h';0\rangle - |i';0\rangle + |j';0\rangle],\\
|G_a\rangle &= \frac{N_G}{2\sqrt{15}}\,[2(|a';0\rangle + |b';0\rangle + |c';0\rangle + |d';0\rangle + |e';0\rangle + |f';0\rangle)\\
&\qquad -3(|g';0\rangle + |h';0\rangle + |i';0\rangle + |j';0\rangle)],\\
|G_x\rangle &= \frac{N_G}{\sqrt{12}}\,[2(\,|a';0\rangle - |b';0\rangle) - (|g';0\rangle + |h';0\rangle) + |i';0\rangle + |j';0\rangle],\\
|G_y\rangle &= \frac{N_G}{\sqrt{12}}\,[2(\,|c';0\rangle - |d';0\rangle) - |g';0\rangle + |h';0\rangle - |i';0\rangle + |j';0\rangle],\\
|G_z\rangle &= \frac{N_G}{\sqrt{12}}\,[2(\,|e';0\rangle - |f';0\rangle) - |g';0\rangle + |h';0\rangle + |i';0\rangle - |j';0\rangle],\\
|A_a\rangle &= \frac{N_A}{\sqrt{30}}\,[\,|a';0\rangle + |b';0\rangle + |c';0\rangle + |d';0\rangle + |e';0\rangle + |f';0\rangle\\
&\qquad +|g';0\rangle + |h';0\rangle + |i';0\rangle + |j';0\rangle].
\end{aligned} \tag{5.2.8}$$

where N_H, N_G and N_A are normalisation constants given by

$$\begin{aligned}
N_H &= \frac{1}{\sqrt{1 + \frac{5}{9}S_t - \frac{2}{9}S_t^2}},\\
N_G &= \frac{1}{\sqrt{1 - \frac{10}{9}S_t - \frac{2}{9}S_t^2}},\\
N_A &= \frac{1}{\sqrt{\frac{1}{3} + \frac{5}{9}S_t + \frac{2}{9}S_t^2}}.
\end{aligned} \tag{5.2.9}$$

S_t is the phonon overlap between any two adjacent trigonal wells and is of the form

$$S_t = \exp[-V_1^{'2}\eta^2]. \tag{5.2.10}$$

5.2.4 Energies of the SASs

The energy of the SASs can be found by taking the matrix elements of the total Hamiltonian divided by the norm of the states; Mathematically

$$E_\Gamma = \frac{\langle \Gamma_i | \mathcal{H}_{total} | \Gamma_i \rangle}{\langle \Gamma_i | \Gamma_i \rangle}. \tag{5.2.11}$$

$|\Gamma_i\rangle$ is the SAS of Γ symmetry and the subscript i refers to the i^{th} component. These calculations are not trivial in this system, since the total Hamiltonian Eq. (5.1.10) consists of four different 6×6 Hamiltonians. For example, to find the energy of the states $|H_\theta\rangle$ in Eq. (5.2.5) for the pentagonal case, Eq. (5.2.11) is written as

$$E_H = \frac{\langle H_\theta | \mathcal{H}_{vib} | H_\theta \rangle + \langle H_\theta | \mathcal{H}_1 | H_\theta \rangle + \langle H_\theta | \mathcal{H}_2 | H_\theta \rangle + \langle H_\theta | \mathcal{H}_3 | H_\theta \rangle}{\langle H_\theta | H_\theta \rangle}. \tag{5.2.12}$$

As the $|H_\theta\rangle$ is a normalised state, the denominator of this equation is equal to unity. The first term in Eq. (5.2.12) can be expanded as

$$\begin{aligned} \langle H_\theta | \mathcal{H}_{vib} | H_\theta \rangle &= \frac{N_H^2}{4} [\langle A';0 | \mathcal{H}_{vib} | A';0 \rangle + \langle A';0 | \mathcal{H}_{vib} | B';0 \rangle - \langle A';0 | \mathcal{H}_{vib} | C';0 \rangle \\ &- \langle A';0 | \mathcal{H}_{vib} | D';0 \rangle + \ldots]. \end{aligned} \tag{5.2.13}$$

The term $\langle A';0|\mathcal{H}_{vib}|A';0\rangle$ is the matrix element of $\mathcal{H}_{vib}$ for the well state A. $\langle A';0|\mathcal{H}_{vib}|B';0\rangle$ is the matrix element between the well states A and B. These terms can be written in more simplified forms as $S\langle A'|\mathcal{H}_{vib}|B'\rangle$, where S is the phonon overlap between the oscillators in the wells found using Eq. (2.3.23). The other terms in Eq. (5.2.12) can be similarly expanded. The calculations are cumbersome since they need to be undertaken for each Hamiltonian in Eq. (5.1.10) and will not be discussed further. Below are expressions of the energies obtained for the two cases of D_{5d} and D_{3d} minima.

D_{5d} minima

The matrix elements of the total Hamiltonian Eq. (5.1.10) for D_{5d} minima are presented in Table 5.3. Substituting them into Eq. (5.2.12) yields the energies of the H and A pentagonal SASs. They are found to be

$$\begin{aligned} E_H^p &= \frac{H_{AA} - \frac{1}{5} S_p H_{AB}}{1 - \frac{1}{5} S_p}, \\ E_A^p &= \frac{H_{AA} + S_p H_{AB}}{1 + S_p}. \end{aligned} \tag{5.2.14}$$

Table 5.3: The matrix elements for the D_{5d} minima.

Hamiltonian	$\langle A';0\|H\|A';0\rangle/\hbar\omega$	$\langle A';0\|H\|B';0\rangle/\hbar\omega$
$\mathcal{H}_{vib}$	$5V_1'^2\zeta^2 + \frac{5}{2}$	$-V_1'^2\zeta^2 + \frac{5}{2}$
$\mathcal{H}_1$	$2\sqrt{10}V_1'^2\zeta$	$2\sqrt{10}V_1'^2\zeta$
$\mathcal{H}_2$	0	$6V_1'^2V_2'\zeta^2$
$\mathcal{H}_3$	$-\sqrt{10}(1+\sqrt{\frac{5}{2}}\zeta)V_1'^2\zeta$	$-\frac{\sqrt{10}}{4}(1+\sqrt{\frac{5}{2}}\zeta)V_1'^2\zeta$
$\mathcal{H}_{total}$	$\sqrt{10}V_1'^2\zeta + \frac{5}{2}$	$[(-\frac{9}{4}+6V_2')\zeta + \frac{7}{4}\sqrt{10}]V_1'^2\zeta + \frac{5}{2}$

Note: The electronic and the phonon overlaps are not included in the calculated matrix elements.

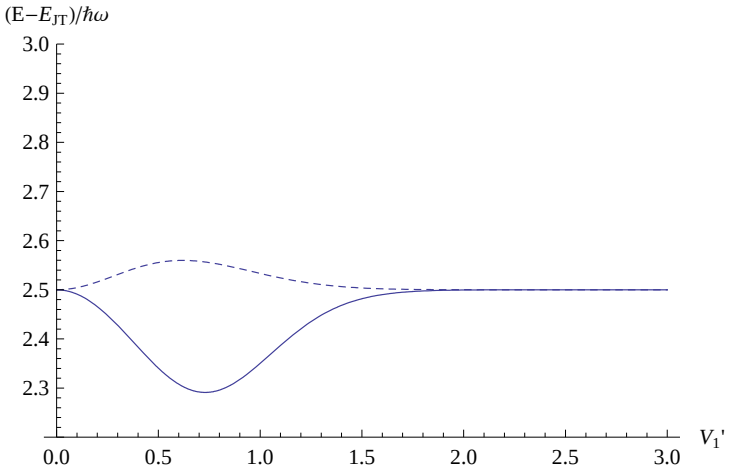

Figure 5.5: Energies of the SASs derived for D_{5d} minima ignoring the differences between the term energies. It has been assumed that $V_1' = 10V_{\text{tot}}'$ and the mixing angle is $\beta = 0$ ($V_3' = 0$). The dotted curve represents the H state and the solid curve represents the A state.

Table 5.4: The matrix elements for the D_{3d} minima.

	$\langle a';0\|H\|a';0\rangle/\hbar\omega$	$\langle a';0\|H\|b';0\rangle/\hbar\omega$	$\langle a';0\|H\|c';0\rangle/\hbar\omega$
$\mathcal{H}_{vib}$	$\frac{3}{2}V_1'^2+\frac{5}{2}$	$\frac{1}{2}V_1'^2\eta^2+\frac{5}{2}$	$-\frac{1}{2}V_1'^2\eta^2+\frac{5}{2}$
$\mathcal{H}_1$	$2\sqrt{3}V_1'^2\eta$	$2\sqrt{3}V_1'^2\eta$	$2\sqrt{3}V_1'^2\eta$
$\mathcal{H}_2$	$-\sqrt{3}(1+\frac{\sqrt{3}}{2}\eta)V_1'^2\eta$	$3V_1'^2V_2'\eta^2$	$V_1'^2V_2'\eta^2$
$\mathcal{H}_3$	0	$\frac{1}{\sqrt{5}}V_1'^2V_3'\eta^2$	$\frac{1}{\sqrt{5}}V_1'^2V_3'\eta^2$
$\mathcal{H}_{total}$	$\sqrt{3}V_1'^2\eta+\frac{5}{2}$	$(\frac{1}{2}+3V_2'+\frac{V_3'}{\sqrt{5}}+\frac{2\sqrt{3}}{\eta})V_1'^2\eta^2+\frac{5}{2}$	$(\frac{-1}{2}+V_2'+\frac{V_3'}{\sqrt{5}}+\frac{2\sqrt{3}}{\eta})V_1'^2\eta^2+\frac{5}{2}$

Note: The electronic and the phonon overlaps are not included in the calculated matrix elements.

It should be noted that $H_{AA}=\langle A';0|H_{total}|A';0\rangle$, $H_{AB}=\langle A';0|H_{total}|B';0\rangle\ldots etc.$ Also the matrix element H_{AB} is equal to the H_{AC}, because the wells in the pentagonal case are equally separated.

The energies of the SASs for the D_{5d} case are plotted in Fig. 5.5 for the particular mixing angle $\beta=0$ (i.e $V_3'=0$). The figure shows the energies of the symmetry-adapted states (divided by $\hbar\omega$ to create a dimensionless quantity), relative to E_{JT} as a function of the dimensionless linear coupling parameter V_1'. The figure shows that the ground state is of A symmetry. In the strong coupling limit, the energies tend to $\frac{5}{2}\hbar\omega$ representing five harmonic oscillators of the h_g mode as expected. At zero coupling (i.e $V_1'=0$), the A and H states are degenerate with an energy of $\frac{5}{2}\hbar\omega$.

D_{3d} minima

The matrix elements of the Hamiltonian between the states associated with the wells for D_{3d} minima are given in Table 5.4. In this table, $\langle a';0|H|a';0\rangle$ is the matrix element for the same well and $\langle a';0|H|b';0\rangle$ and $\langle a';0|H|c';0\rangle$ for the adjacent ones. Here, $\langle a';0|H|a';0\rangle=H_{aa}$, $\langle a';0|H|b';0\rangle=H_{ab}\ldots etc$; the matrix element H_{ab} is different from the matrix element H_{ac} due to the differences in the separations between the triagonal wells as will be discussed in the following section. Therefore extra care should be taken when calculating the energy for this case. The energies of the H,G and A trigonal SASs are found to be

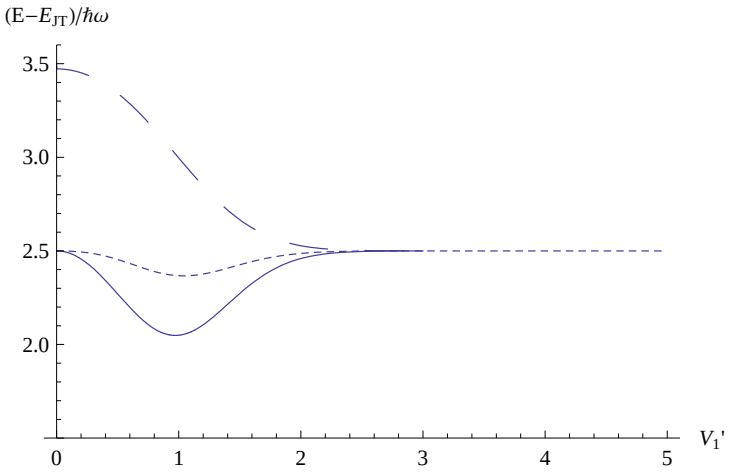

Figure 5.6: Same as in Fig. 5.5, but for the D_{3d} wells arising when $\beta = \pi/2$ ($V_2' = 0$).The dotted curve represents the H state, the solid curve represents the A state and the dashed one represents the G state.

$$\begin{aligned} E_H^t &= \frac{H_{aa} + \frac{5}{9}S_t H_{ab} - \frac{2}{9}S_t^2 H_{ac}}{1 + \frac{5}{9}S_t - \frac{2}{9}S_t^2}, \\ E_G^t &= \frac{H_{aa} - \frac{10}{9}S_t H_{ab} + \frac{1}{9}S_t^2 H_{ac}}{1 - \frac{10}{9}S_t + \frac{1}{9}S_t^2}, \\ E_A^t &= \frac{\frac{1}{3}H_{aa} + \frac{5}{9}S_t H_{ab} + \frac{2}{9}S_t^2 H_{ac}}{\frac{1}{3} + \frac{5}{9}S_t + \frac{2}{9}S_t^2}. \end{aligned} \tag{5.2.15}$$

These energies for the D_{3d} minima are plotted as shown in Fig. 5.6 for the mixing angle, $\beta = \pi/2$ (i.e $V_2' = 0$). It shows the energies of the SASs relative to E_{JT} as a function of the dimensionless linear coupling parameter V_1'. The figure shows that the ground state is of A symmetry. In fact, the behaviour of the A and H states is rather similar irrespective of whether they arise from combinations of D_{5d} or of D_{3d} wells. Also the figure shows the expected trend of the energies where all tend to $\frac{5}{2}\hbar\omega$ again behaving as a five dimensional harmonic oscillator. At zero JT coupling, the states of the A and H symmetry are degenerate which represents the symmetries of the terms of the anion with which we started the problem. It is also seen that, in the case of the D_{3d} minima, the additional wells give rise to a SAS of G symmetry which forms the first excited vibronic state, sometimes referred to as the tunnelling state. If these states are observed spectroscopically, this additional four-fold degenerate state could be used as an indicator of the symmetry of the ion.

5.3 Pseudorotation in C_{60}^{2-} anion without Coulomb interaction

The method outlined in Chapter 3 related to the time evolution of the system will be used here. The theory is applied to both D_{5d} and D_{3d} symmetries in order to investigate the dynamical motion of the ion. The calculations of the probabilities will start by inverting equations (5.2.5) and (5.2.8) to obtain the states of the wells in terms of the SASs; then by using Eq. (3.2.9), the probabilities of the systems initially localised in a specific well and found later in another well will be derived. The results are as follows.

5.3.1 D_{5d} Symmetry

The unnormalised states associated with the pentagonal wells are

$$\begin{aligned}
|A';0\rangle &= \frac{|A_a\rangle}{\sqrt{6}N_A} + \frac{|H_\theta\rangle}{2N_H} + \frac{|H_\epsilon\rangle}{2\sqrt{3}N_H} - \frac{|H_4\rangle}{\sqrt{2}N_H}, \\
|B';0\rangle &= \frac{|A_a\rangle}{\sqrt{6}N_A} + \frac{|H_\theta\rangle}{2N_H} + \frac{|H_\epsilon\rangle}{2\sqrt{3}N_H} + \frac{|H_4\rangle}{\sqrt{2}N_H}, \\
|C';0\rangle &= \frac{|A_a\rangle}{\sqrt{6}N_A} - \frac{|H_\theta\rangle}{2N_H} + \frac{|H_\epsilon\rangle}{2\sqrt{3}N_H} - \frac{|H_5\rangle}{\sqrt{2}N_H}, \\
|D';0\rangle &= \frac{|A_a\rangle}{\sqrt{6}N_A} - \frac{|H_\theta\rangle}{2N_H} + \frac{|H_\epsilon\rangle}{2\sqrt{3}N_H} + \frac{|H_5\rangle}{\sqrt{2}N_H}, \\
|E';0\rangle &= \frac{|A_a\rangle}{\sqrt{6}N_A} - \frac{|H_\epsilon\rangle}{\sqrt{3}N_H} - \frac{|H_6\rangle}{\sqrt{2}N_H}, \\
|F';0\rangle &= \frac{|A_a\rangle}{\sqrt{6}N_A} - \frac{|H_\epsilon\rangle}{\sqrt{3}N_H} + \frac{|H_6\rangle}{\sqrt{2}N_H},
\end{aligned} \tag{5.3.1}$$

where N_A and N_H are the normalisation constants which are defined earlier in the chapter. The above states may be normalised by multiplying them with the normalisation constant

$$N = \frac{1}{\sqrt{1 + \frac{2S_p}{\sqrt{3}}}}. \tag{5.3.2}$$

Now, the above states are used to find the probabilities of the system which are given by

$$\begin{aligned}
P_{AA}(t) &= 1 - \frac{1}{(3+2S_p)^2}\left[(5-S_p)(1+5S_p)\sin^2\left(\frac{\Delta t}{2\hbar}\right)\right], \\
P_{AB}(t) &= \frac{1}{25(3+2S_p)^2}\left[169\ S_p^2 + 5(5-S_p)(1+5S_p)\sin^2\left(\frac{\Delta t}{2\hbar}\right)\right],
\end{aligned} \tag{5.3.3}$$

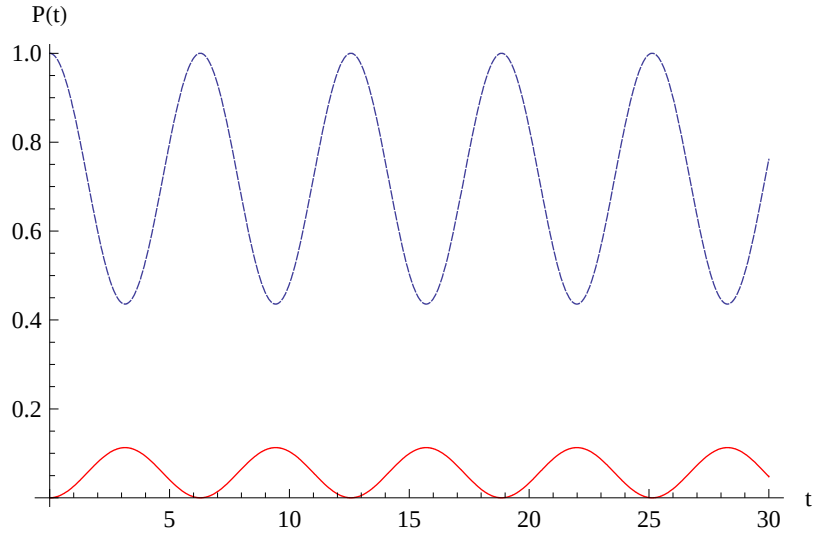

Figure 5.7: Internal dynamics of the D_{5d} symmetry with $V'_{tot} = 0.1$, $V'_1 = 1.5$. The dashed curve represents the P_{AA} and the solid one represents the P_{AB}.

where Δ is the energy difference between the energies of the SASs and given by

$$\Delta = -\frac{6\ S_p \ln S_p}{(5 - S_p)(1 + S_p)}(1 - V'_{tot}). \tag{5.3.4}$$

The pseudorotational dynamics for this case is illustrated in Fig. 5.7 for a moderately strong coupling $V'_1 = 1.5$. An interesting observation is that $P_{AA} \geqslant \frac{4}{9}$ at all times and the probability of finding the system initially localised in well A to remain in the same well later never drops below $\frac{4}{9}$. The figure shows that, at $t = 0$ the system migrates from well A and starts to appear in well B (or in any of the adjacent wells C, D, E or F). After a time $t = \frac{\pi\hbar}{\Delta}$,the probability of finding the system in well B reaches its maximum value. When $t = \frac{2\pi\hbar}{\Delta}$, the system has returned back to its initial state after completing one pseudorotational period $T_p = \frac{2\pi\hbar}{\Delta}$. The dimensionless pseudorotational rate $\mathcal{R}_p$ can be found using Eq. (3.3.8).

Another interesting feature here is that, the sum of the probabilities of being in any of the six well states at time t is

$$\sum_{X=A}^{F} P_{AX} = 1 + \frac{169 S_p^2}{5(3 + 2S_p)^2}. \tag{5.3.5}$$

This sum is independent of time as expected, and as $V'_1 \longrightarrow \infty$ the separation walls between wells becomes higher and the phonon overlap S_p tends to zero. Therefore, the summation tends to one as expected as the system must be localised in one

of the wells. Overall, the system in this case pseudorotates between all wells in a regular pattern similar to that in the C_{60}^{-} with some differences due to the specific circumstances for each problem.

5.3.2 D_{3d} Symmetry

For this case the unnormalised states associated with the trigonal wells are found to be as

$$\begin{aligned}
|a';0\rangle &= \frac{\sqrt{3}|A_a\rangle}{\sqrt{10}N_A} + \frac{\sqrt{2}|H_\theta\rangle - \sqrt{6}|H_\epsilon\rangle + 2|H_4\rangle}{2\sqrt{6}N_H} + \frac{3|G_a\rangle + \sqrt{5}|G_x\rangle}{3\sqrt{15}N_G},\\
|b';0\rangle &= \frac{\sqrt{3}|A_a\rangle}{\sqrt{10}N_A} + \frac{\sqrt{2}|H_\theta\rangle - \sqrt{6}|H_\epsilon\rangle - 2|H_4\rangle}{2\sqrt{6}N_H} + \frac{3|G_a\rangle - \sqrt{5}|G_x\rangle}{3\sqrt{15}N_G},\\
|c';0\rangle &= \frac{\sqrt{3}|A_a\rangle}{\sqrt{10}N_A} + \frac{\sqrt{2}|H_\theta\rangle + \sqrt{6}|H_\epsilon\rangle + 2|H_5\rangle}{2\sqrt{6}N_H} + \frac{3|G_a\rangle + \sqrt{5}|G_y\rangle}{3\sqrt{15}N_G},\\
|d';0\rangle &= \frac{\sqrt{3}|A_a\rangle}{\sqrt{10}N_A} + \frac{\sqrt{2}|H_\theta\rangle + \sqrt{6}|H_\epsilon\rangle - 2|H_5\rangle}{2\sqrt{6}N_H} + \frac{3|G_a\rangle - \sqrt{5}|G_y\rangle}{3\sqrt{15}N_G},\\
|e';0\rangle &= \frac{\sqrt{3}|A_a\rangle}{\sqrt{10}N_A} - \frac{2\sqrt{2}|H_\theta\rangle - 2|H_6\rangle}{2\sqrt{6}N_H} + \frac{3|G_a\rangle + \sqrt{5}|G_z\rangle}{3\sqrt{15}N_G},\\
|f';0\rangle &= \frac{\sqrt{3}|A_a\rangle}{\sqrt{10}N_A} - \frac{2\sqrt{2}|H_\theta\rangle + 2|H_6\rangle}{2\sqrt{6}N_H} + \frac{3|G_a\rangle - \sqrt{5}|G_z\rangle}{3\sqrt{15}N_G},\\
|g';0\rangle &= \frac{\sqrt{3}|A_a\rangle}{\sqrt{10}N_A} + \frac{|H_4\rangle - |H_5\rangle + |H_6\rangle}{\sqrt{6}N_H} - \frac{3|G_a\rangle + \sqrt{5}(|G_x\rangle + |G_y\rangle + |G_z\rangle)}{2\sqrt{15}N_G},\\
|h';0\rangle &= \frac{\sqrt{3}|A_a\rangle}{\sqrt{10}N_A} + \frac{|H_4\rangle - |H_5\rangle - |H_6\rangle}{\sqrt{6}N_H} - \frac{3|G_a\rangle + \sqrt{5}(|G_x\rangle - |G_y\rangle - |G_z\rangle)}{2\sqrt{15}N_G},\\
|i';0\rangle &= \frac{\sqrt{3}|A_a\rangle}{\sqrt{10}N_A} - \frac{|H_4\rangle - |H_5\rangle + |H_6\rangle}{\sqrt{6}N_H} - \frac{3|G_a\rangle - \sqrt{5}(|G_x\rangle + |G_y\rangle - |G_z\rangle)}{2\sqrt{15}N_G},\\
|j';0\rangle &= \frac{\sqrt{3}|A_a\rangle}{\sqrt{10}N_A} - \frac{|H_4\rangle + |H_5\rangle - |H_6\rangle}{\sqrt{6}N_H} - \frac{3|G_a\rangle - \sqrt{5}(|G_x\rangle - |G_y\rangle + |G_z\rangle)}{2\sqrt{15}N_G}.
\end{aligned} \tag{5.3.6}$$

The N_A, N_G and N_H are the normalisation constants for the SASs. These states can be normalised by multiplying them by the normalisation constant

$$N = \frac{1}{\sqrt{1 - \frac{2S_t^2}{15}}}. \tag{5.3.7}$$

The probabilities of the system to evolve to another well at a later time t are found to be

$$\begin{aligned} P_{aa}(t) &= 1 - F_1\left[15\ F_2 - 12\ F_3 + 20\ F_4\right], \\ P_{ab}(t) &= \frac{F_1}{9}\left[9S_t^2(25+4S_t)^2 - 45\ F_2 - 72\ F_3 + 40\ F_4\right], \\ P_{ac}(t) &= \frac{F_1}{9}\left[45\ F_2 + 2\ F_3 + 5\ F_4\right], \end{aligned}$$

where F_1, F_2, F_3 and F_4 are defined by

$$\begin{aligned} F_1 &= \frac{1}{9(15-2S_t^2)^2}, \\ F_2 &= (27 + S_t(60 + 37S_t - 4S_t^3))\sin^2\left(\frac{\Delta_1 t}{2\hbar}\right), \\ F_3 &= (1+S_t)(3+2S_t)(-9+2S_t(5+S_t))\sin^2\left(\frac{\Delta_2 t}{2\hbar}\right), \\ F_4 &= (-9+2S_t(5+S_t))(-9+S_t(-5+2S_t))\sin^2\left(\frac{\Delta_3 t}{2\hbar}\right), \end{aligned} \tag{5.3.8}$$

where Δ_1, Δ_2 and Δ_3 are the energy differences between the SASs A, G and H which are given by

$$\begin{aligned} \Delta_1 &= -\frac{2S_t \ln S_t(-15 - 24S_t - 10S_t^2 + \sqrt{5}(3 + 4S_t(3+2S_t))V_{tot'})}{-27 + S_t(-60 - 37S_t + 4S_t^3)}\hbar\omega, \\ \Delta_2 &= -\frac{5S_t \ln S_t(15 + 6S_t - 5S_t^2 + \sqrt{5}(-3 + S_t(-3+4S_t))V_{tot'})}{(-9+S_t)(-1+S_t)(1+S_t)(3+2S_t)}\hbar\omega, \\ \Delta_3 &= -\frac{3S_t \ln S_t(-45 + 18S_t - 5S_t^2 + \sqrt{5}(9 + S_t(-9+4S_t))V_{tot'})}{(-9+S_t)(-1+S_t)(-9+S_t(-5+2S_t))}\hbar\omega. \end{aligned} \tag{5.3.9}$$

It can be inferred from the above expressions for the probabilities that, the interwell dynamics in the trigonal case is more complicated than that for the pentagonal case. In the trigonal distortion, there are two tunnelling splittings between the states involved rather than one compared to the pentagonal distortion. The wells here can be classified as nearest-neighbour $\{b, g, h\}$ and next nearest-neighbour wells $\{c, d, e, f, i, j\}$ when we start off in well a. The system in this approach is allowed to tunnel to either one of the wells in the first set or to one in the second set. This can be seen clearly from Fig. 5.8. The regime of this trend is as follow; when the time equals zero, the system is initially prepared in well a and the probabilities of finding it in well b and c are very small. As time progresses, the system starts to evolves with a decreasing probability of finding it

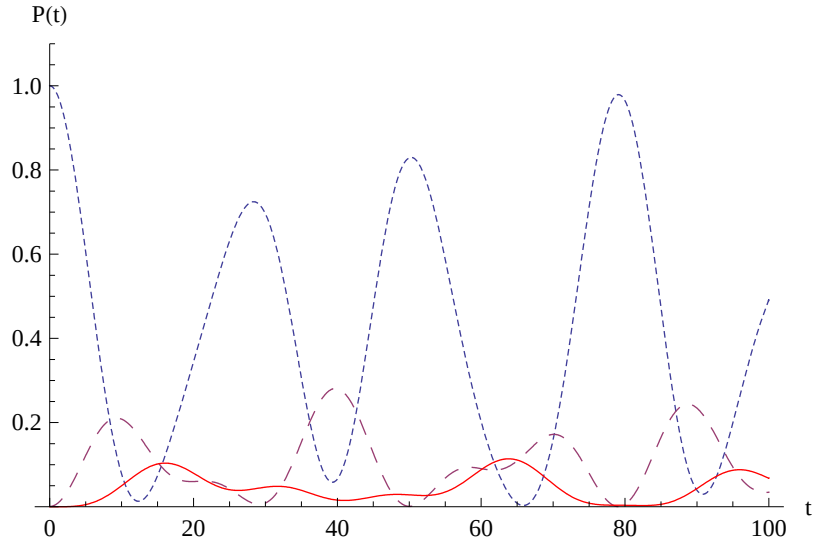

Figure 5.8: Internal dynamics of the D_{3d} symmetry with $V'_{tot} = 0.1$, $V'_1 = 1.5$. The dotted curve represents the P_{aa}; the dashed curve represents the P_{ab} and the solid curve represents the P_{ac}.

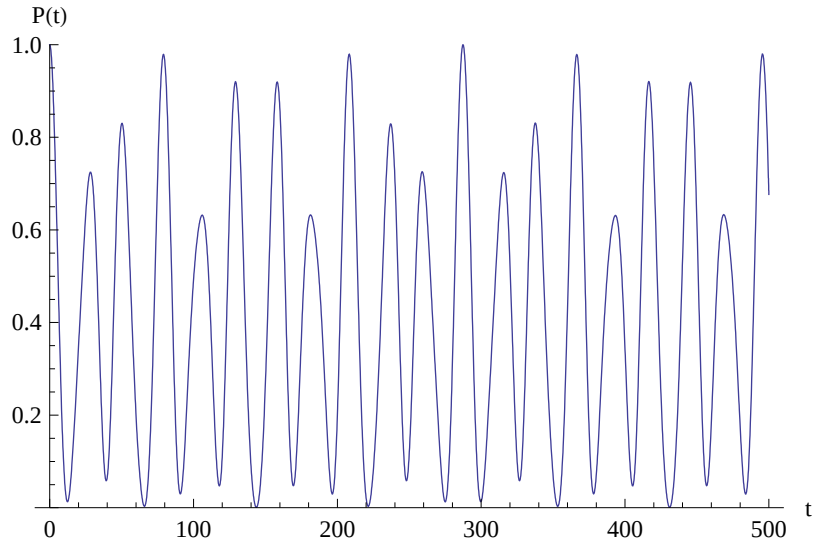

Figure 5.9: Plot for the P_{aa} for a long-term variation as a function of t. The vibronic coupling constants have been takes as $V'_{tot} = 0.1$, $V'_1 = 1.5$.

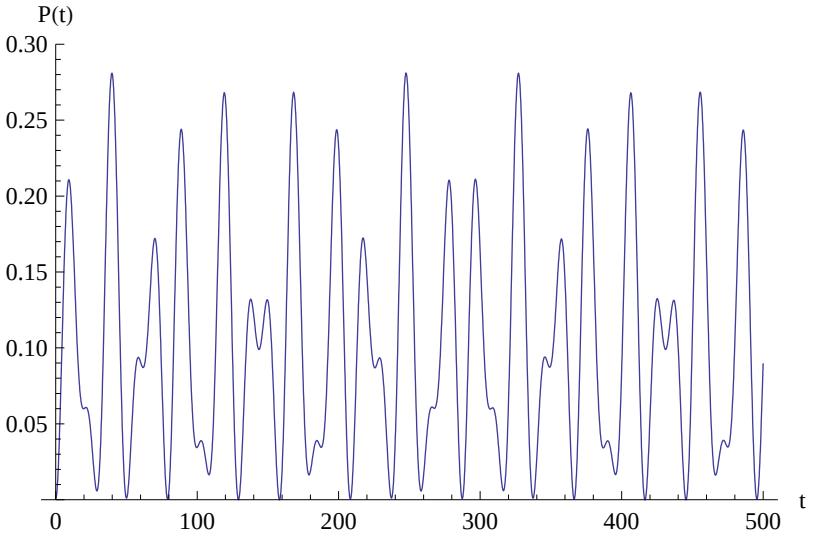

Figure 5.10: Plot for the P_{ab} for a long-term variation as a function of t. The vibronic coupling constants have been takes as $V'_{tot} = 0.1$, $V'_1 = 1.5$.

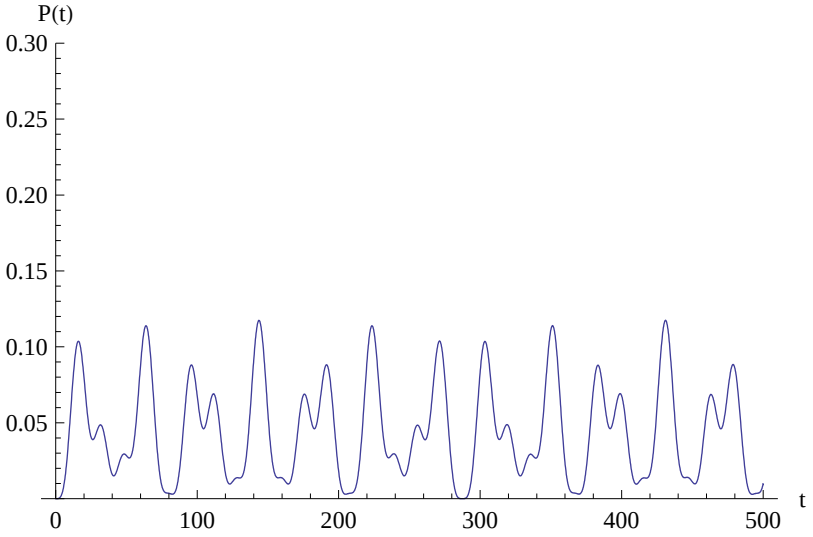

Figure 5.11: Plot for the P_{ac} for a long-term variation as a function of t. The vibronic coupling constants have been takes as $V'_{tot} = 0.1$, $V'_1 = 1.5$.

still localised in well a and increasing of that for both wells b and c. Here, the figure shows that on average, the system is more likely to be in well b than well c as the rate of increase in P_{ac} is smaller than P_{ab}. This is an expected situation as well b is the nearest-neighbour and well c is the next nearest-neighbour to well a. With time increasing, the system has occupied well b and then well c. After a period of time, the system has migrated back to its original well state. It can be seen from the figure that, after the system completes one revolution the state is no more identical to the initial state and this can be seen clearly if the process extended over a period of time as in Fig. 5.9, 5.10 and 5.11. The figures show plots of P_{aa}, P_{ab} and P_{ac} displayed over a longer period of time. The state behaves in such a way that the system reoccurs in the initial state again, an increasingly large percentage of it gets "left behind" in the other wells which leads to a decrease in the rate of the P_{aa} in the second reoccurrence. From the figures, the expected time that the system could repeat this circuit again is $\backsim 285\omega t$.

5.4 Summary and Discussion

In this chapter, an approximate model applicable to C_{60}^{2-} anions has been developed. This model has been treated using numerical and analytical techniques to investigate the minima on the APES. Including the quadratic coupling led to have two different kinds of minima : one with D_{5d} symmetry, and the other with D_{3d} symmetry. The results which has been obtained from the numerical and theoretical methods for these two cases show perfect consistency. Also, the energies and the corresponding eigenstates for both the static and the dynamic JT interaction have been found analytically and plotted as a function of the linear vibronic coupling constant. The plotted energy levels showed an agreement with those obtained previously by O'Brien in Ref. [47].

The pseudorotation of the dynamical systems has also been studied for both cases and the probabilities of finding the systems at time t later have been derived using the time evolution operator. The system involving the D_{5d} minima pseudorotates freely between all wells in a regular pattern, while the D_{3d} minima behave differently due to the complicated shape of the APES.

If we assume that the ion is treated as if the $h_g(2)$ mode is the only mode of importance at ~ 429 cm^{-1} (~ 53.2 meV) as this is thought to be the most strongly

coupled mode in some Refs. [85]. Manini *et al.* [7] have calculated a JT energy for this mode in C_{60} of 6.3 meV, together with a linear coupling constant $g = 0.489$. Comparing theories suggests that in terms of our parameters, $V_1' = \frac{1}{2}g = 0.245$. To check this, it is noted that $E_{JT} \approx -2\left(V_1'\right)^2 \hbar\omega$ and so it is calculated, using the above quantities, $E_{JT} = 6.4$ meV, in good agreement with the value calculated by Manini *et al.* [7].

This work has been partially published in Ref. [86].

Chapter 6

A further investigation of the C_{60}^{2-} anion with e-e repulsion included

In this chapter, we will investigate the previous problem analytically when the term splitting that appears as a result of the e-e repulsion is included in the problem. Including this term complicates the calculations when it is required to obtain analytical expressions for the positions of the minima and the corresponding energies. Nevertheless, the insertion of this term could be important. There are suggestions that it is even stronger than the JT interaction in the doubly-doped ions which add to the Coulomb repulsion to localise electrons although this is not clear [87].

6.1 A general review of the system

In the previous chapter the electronic basis states have been derived for the low-spin terms $\{A, H\}$ when the term splitting has been ignored. When this term is taken into account, splitting between the basis states of these terms occurs leading to a removal of the degeneracy between them. The Hamiltonian which represents this problem has the general form as in Eq. (5.1.10), where the term splitting

Hamiltonian $\mathcal{H}_{TS}$ is represented by

$$\mathcal{H}_{\mathrm{TS}} = \begin{bmatrix} \delta & 0 & 0 & 0 & 0 & 0 \\ 0 & 0 & 0 & 0 & 0 & 0 \\ 0 & 0 & 0 & 0 & 0 & 0 \\ 0 & 0 & 0 & 0 & 0 & 0 \\ 0 & 0 & 0 & 0 & 0 & 0 \\ 0 & 0 & 0 & 0 & 0 & 0 \end{bmatrix}. \tag{6.1.1}$$

This form of the matrix ensures that in the absence of the JT interaction, the electronic states are such that there is an energy difference δ between the $|A\rangle$ state and the $|H\rangle$ state, as shown in Fig. 5.1. The transformed Hamiltonian for this problem is a function of the values of (a_i) which specify the positions of the wells. These values itself are functions of the term splitting δ. It is also found numerically that, for each well, the first components of the corresponding electronic state also varies as a function of δ. For example, the electronic state for well E of the D_{5d} case has the form$\{-\sqrt{\frac{5}{6}}X_1, 0, \sqrt{\frac{2}{3}}, 0, 0, 1\}$, where X_1 represents the variation of the first components with respect to the inclusion of the term splitting. From the theoretical point of view this is quite reasonable as Coulomb repulsion splits the A state away from the H state, while the H state keeps the same position unchanged. Again for simplicity, the problem will be considered for each case of symmetry separately.

6.2 D_{5d} minima

Following the same procedures that were outlined in the previous chapter but including the term splitting this time, it is found that the minimum points have the form shown in Table. 6.1. In this table, σ_1 and X_1 are unknowns depend on the value of δ. These values can be found by considering one of the minima and substituting the shifts and the corresponding electronic state into the eigenvalue equation $\tilde{\mathcal{H}}\psi_{\mathrm{elect}} = E_{JT}\psi_{\mathrm{elect}}$. In this expression, ψ_{elect} is the electronic state and E_{JT} is the energy of the minimum, which coincides with the JT energy. The unknowns σ_1 and X_1 have been chosen to simultaneously obey both this eigenvalue equation and the requirement that σ_1 should minimise E_{JT}. Practically, to find the values of σ_1 and X_1 we start the evaluation by choosing a minimum point (say the minima for well E for the sake of simplicity), and substitute both the positions

Table 6.1: The shifts and their associated electronic states if the minima have D_{5d} symmetry and term splitting is included. σ_1 and X_1 are described in the text.

Label	Shift, $\boldsymbol{\alpha}$[a]	Electronic state
A	$\frac{-2\sigma_1}{\sqrt{10}}\left(-\sqrt{3},-1,\sqrt{6},0,0\right)$	$\left(-\sqrt{\frac{5}{6}}X_1,\frac{-1}{\sqrt{2}},\frac{-1}{\sqrt{6}},1,0,0\right)$
B	$\frac{-2\sigma_1}{\sqrt{10}}\left(-\sqrt{3},-1,-\sqrt{6},0,0\right)$	$\left(-\sqrt{\frac{5}{6}}X_1,\frac{-1}{\sqrt{2}},\frac{-1}{\sqrt{6}},-1,0,0\right)$
C	$\frac{-2\sigma_1}{\sqrt{10}}\left(\sqrt{3},-1,0,\sqrt{6},0\right)$	$\left(-\sqrt{\frac{5}{6}}X_1,\frac{1}{\sqrt{2}},\frac{-1}{\sqrt{6}},0,1,0\right)$
D	$\frac{-2\sigma_1}{\sqrt{10}}\left(\sqrt{3},-1,0,-\sqrt{6},0\right)$	$\left(-\sqrt{\frac{5}{6}}X_1,\frac{1}{\sqrt{2}},\frac{-1}{\sqrt{6}},0,-1,0\right)$
E	$\frac{-2\sigma_1}{\sqrt{10}}\left(0,2,0,0,\sqrt{6}\right)$	$\left(-\sqrt{\frac{5}{6}}X_1,0,\sqrt{\frac{2}{3}},0,0,1\right)$
F	$\frac{-2\sigma_1}{\sqrt{10}}\left(0,2,0,0,-\sqrt{6}\right)$	$\left(-\sqrt{\frac{5}{6}}X_1,0,\sqrt{\frac{2}{3}},0,0,-1\right)$

[a] In units of $V_1/\hbar\mu\omega^2$, so that σ_1 is dimensionless.

of the minima and the corresponding electronic state in the eigenvalue equation

$$\tilde{\mathcal{H}}\psi_{\text{elect}} = E_{JT}\psi_{\text{elect}}. \tag{6.2.1}$$

Next we take the first component of the vector obtained from the product $\tilde{\mathcal{H}}\psi_{\text{elect}}$ and divide by the first component of ψ_{elect} itself to give

$$E_{JT1} = \frac{5X_1\delta + 2\ V_1'^2\sigma_1(-10 + 8\sqrt{5}\ V_3'\sigma_1 + 5X_1\sigma_1)}{5X_1}, \tag{6.2.2}$$

and then apply the same procedure on the second component which gives

$$E_{JT2} = \frac{2\sigma_1\ V_1'^2(-5X_1 + 4\sqrt{5}X_1\ V_3'\ \sigma_1 + 5\ \sigma_1 - 5 + 4\sqrt{5}\ V_3'\ \sigma_1)}{5}. \tag{6.2.3}$$

For ψ_{elect} to be a proper eigenfunction, we must have $E_{JT1} = E_{JT2}$, then Eq. (6.2.2) and Eq. (6.2.3) give

$$2\ \Delta\sigma_1(4\ V_3'\ \sigma_1 - \sqrt{5}) = \sqrt{5}P(X_1) \tag{6.2.4}$$

where Δ is defined as

$$\Delta = \frac{(V_1')^2\hbar\omega}{\delta} \tag{6.2.5}$$

and

$$P(X_1) = \frac{X_1}{(X_1+2)(X_1-1)}. \tag{6.2.6}$$

Now, we need to find value of σ_1 to minimise E_{JT}, in order to satisfy the condition $\frac{\partial E_{JT}}{\partial \sigma_1} = 0$. Applying this to Eq. (6.2.3), an expression of $\frac{\partial X_1}{\partial \sigma_1}$ is found as

$$\frac{\partial X_1}{\partial \sigma_1} = -\frac{X_1(8\ V_3'\ \sigma_1 - \sqrt{5}) + 2\ \sqrt{5}\ \sigma_1 - \sqrt{5} + 8\ V_3'\ \sigma_1}{\sigma_1(4\ V_3'\ \sigma_1 - \sqrt{5})}. \tag{6.2.7}$$

Differentiating Eq. (6.2.4) with respect to σ_1 produces

$$2\ \Delta(8\ V_3'\ \sigma_1 - \sqrt{5}) = \sqrt{5}\ \frac{\partial P(X_1)}{\partial X_1}\frac{\partial X_1}{\partial \sigma_1}. \tag{6.2.8}$$

Then substituting Eq. (6.2.7) into Eq. (6.2.8) we find

$$\sigma_1 = \frac{\sqrt{5}(\frac{P(X_1)}{(\partial P(X_1)/\partial X_1)} + X_1 + 1)}{2\ \sqrt{5} + 8\ V_3'(\frac{P(X_1)}{(\partial P(X_1)/\partial X_1)}. + X_1 + 1)} \tag{6.2.9}$$

On using the definition of $P(X_1)$ and simplifying it we get

$$\sigma_1 = \frac{\sqrt{5}\ F(X_1)}{\sqrt{5} + 8\ V_3'\ F(X_1)}, \tag{6.2.10}$$

where $F(X_1)$ is the function

$$F(x) = \frac{1 + 2x}{2 + x^2}. \tag{6.2.11}$$

With these expressions, E_{JT} has the general form

$$E_{JT}^{(D_{5d})} = \frac{X_1^2}{2 + X_1^2}\delta - \frac{2\sqrt{5}(F(X_1))^2}{(\sqrt{5} + 8\ V_3'\ F(X_1))}\left(V_1'\right)^2 \hbar\omega. \tag{6.2.12}$$

for the case when $V_3' = 0$

$$\sigma_1 = F(X_1), \tag{6.2.13}$$

and therefore

$$E_{JT}^{(D_{5d})} = \frac{X_1^2}{2 + X_1^2}\delta - 2(F\left(X_1\right))^2\left(V_1'\right)^2 \hbar\omega. \tag{6.2.14}$$

Now, X_1 must satisfy a certain condition in order to ensure that the above expression of E_{JT} is the lowest energy of the system. To confirm that the condition in Eq. (6.2.4) must be satisfied, we have

$$2\ \Delta\sigma_1(4\ V_3'\ \sigma_1 - \sqrt{5}) - \sqrt{5}P(X_1) = 0 \tag{6.2.15}$$

and so

$$(X_1 + 2)(X_1 - 1)2\ \Delta\sigma_1(4\ V_3'\ \sigma_1 - \sqrt{5}) - \sqrt{5}X_1 = 0, \tag{6.2.16}$$

using Eq. (6.2.10)

$$2\,\Delta(X_1{+}2)(X_1{-}1)\left(\frac{\sqrt{5}\;F(X_1)}{\sqrt{5}+8\;V_3'\;F(X_1)}\right)\left(\frac{4\;\sqrt{5}\;F(X_1)V_3'}{\sqrt{5}+8\;V_3'\;F(X_1)}-\sqrt{5}\right)-\sqrt{5}X_1=0, \tag{6.2.17}$$

$$\begin{aligned}10\;\Delta\;F(X_1)(-4\;V_3'\;F(X_1)-\sqrt{5})(X_1+2)(X_1-1)\\ -\sqrt{5}X_1(\sqrt{5}+8\;V_3'F(X_1))^2=0.\end{aligned} \tag{6.2.18}$$

When $V_3'=0$, this becomes

$$2\;\Delta\;F(X_1)(X_1+2)(X_1-1)+X_1=0, \tag{6.2.19}$$

on substituting into Eq. (6.2.11)

$$2\;\Delta(1+2X_1)(X_1+2)(X_1-1)+X_1(2+X^2)=0, \tag{6.2.20}$$

yields the cubic equation

$$(1+4\Delta)X_1^3+6\Delta X_1^2+2(1-3\Delta)X_1-4\Delta=0. \tag{6.2.21}$$

Here the (real) root must be taken which yields the lowest energy. If $\Delta\to\infty$, so that the difference between the term energies is negligible compared to the JT energy, then Eq. (6.2.21) has a solution $X_1=1$, which implies that $\sigma_1=1$ and $E_{JT}^{(D_{5d})}=-2\,(V_1')^2\,\hbar\omega$, as found earlier. On the other hand, as $\Delta\to 0$, i.e. if the difference between the term energies overwhelms the JT energy, then Eq. (6.2.21) has the real solution $X_1=0$, which implies that $\sigma_1=1/2$ and $E_{JT}^{(D_{5d})}=-\frac{1}{2}\,(V_1')^2\,\hbar\omega$, which will be negligible compared to δ.

6.3 D_{3d} minima

In this case, the above procedure can be repeated but this time the minima shown in Table 6.2 will be used. The value of σ_2 is found in a similar way to σ_1, to be

$$\sigma_2=\frac{3F(X_2)}{3+8V_2'\;F(X_2)}. \tag{6.3.1}$$

Therefore, the JT energy is found to have the general form

$$E_{JT}^{(D_{3d})}=\frac{X_2^2}{2+X_2^2}\delta-\frac{6(F(X_2))^2}{(3+8\;V_2'\;F(X_2))}\,(V_1')^2\,\hbar\omega. \tag{6.3.2}$$

Table 6.2: The shifts and their associated electronic states if the minima have D_{3d} symmetry and term splitting is included. σ_2 and X_2 are described in the text.

Label	Shift, $\boldsymbol{\alpha}$[a]	Electronic state
a	$\frac{-2\sigma_2}{\sqrt{6}}\left(1,-\sqrt{3},\sqrt{2},0,0\right)$	$\left(-\sqrt{\frac{3}{2}}X_2,\frac{1}{\sqrt{2}},-\sqrt{\frac{3}{2}},1,0,0\right)$
b	$\frac{-2\sigma_2}{\sqrt{6}}\left(1,-\sqrt{3},-\sqrt{2},0,0\right)$	$\left(-\sqrt{\frac{3}{2}}X_2,\frac{1}{\sqrt{2}},-\sqrt{\frac{3}{2}},-1,0,0\right)$
c	$\frac{-2\sigma_2}{\sqrt{6}}\left(1,\sqrt{3},0,\sqrt{2},0\right)$	$\left(-\sqrt{\frac{3}{2}}X_2,\frac{1}{\sqrt{2}},\sqrt{\frac{3}{2}},0,1,0\right)$
d	$\frac{-2\sigma_2}{\sqrt{6}}\left(1,\sqrt{3},0,-\sqrt{2},0\right)$	$\left(-\sqrt{\frac{3}{2}}X_2,\frac{1}{\sqrt{2}},\sqrt{\frac{3}{2}},0,-1,0\right)$
e	$\frac{-2\sigma_2}{\sqrt{6}}\left(-2,0,0,0,\sqrt{2}\right)$	$\left(-\sqrt{\frac{3}{2}}X_2,-\sqrt{2},0,0,0,1\right)$
f	$\frac{-2\sigma_2}{\sqrt{6}}\left(-2,0,0,0,-\sqrt{2}\right)$	$\left(-\sqrt{\frac{3}{2}}X_2,-\sqrt{2},0,0,0,-1\right)$
g	$\frac{-2\sigma_2}{\sqrt{6}}\left(0,0,\sqrt{2},\sqrt{2},\sqrt{2}\right)$	$\left(-\sqrt{\frac{3}{2}}X_2,0,0,1,1,1\right)$
h	$\frac{-2\sigma_2}{\sqrt{6}}\left(0,0,\sqrt{2},-\sqrt{2},-\sqrt{2}\right)$	$\left(-\sqrt{\frac{3}{2}}X_2,0,0,1,-1,-1\right)$
i	$\frac{-2\sigma_2}{\sqrt{6}}\left(0,0,-\sqrt{2},\sqrt{2},-\sqrt{2}\right)$	$\left(-\sqrt{\frac{3}{2}}X_2,0,0,-1,1,-1\right)$
j	$\frac{-2\sigma_2}{\sqrt{6}}\left(0,0,-\sqrt{2},-\sqrt{2},\sqrt{2}\right)$	$\left(-\sqrt{\frac{3}{2}}X_2,0,0,-1,-1,1\right)$

[a] As for Table 5.1, these are given in units of $V_1/\hbar\mu\omega^2$.

For the case when $V_2' = 0$

$$\sigma_2 = F(X_2), \tag{6.3.3}$$

and

$$E_{JT}^{(D_{3d})} = \frac{X_2^2}{2 + X_2^2}\delta - 2F(X_2))^2 \left(V_1'\right)^2 \hbar\omega \tag{6.3.4}$$

where F is the same function as given in Eq. (6.2.11) and X_2 obeys exactly the same equation as X_1 in Eq. (6.2.21).

6.4 Symmetry-adapted states

The SASs for both cases can be obtained using the projection operator, in a similar manner to that presented earlier. Combinations of the vibronic states $|\Gamma'; 0\rangle$ associated with each minimum are taken to formulate these SASs using the definition of the wells presented in Tables 6.1 and 6.2.

Once again, the two separate cases treated in the previous section will be considered, when either $V_2' = 0$ or $V_3 = 0$.

6.4.1 Energies of the SASs from D_{5d} minima

In this case, again the states of A and H symmetry result from taking combinations of the six wells; these states have the same form as that in Eq. (5.2.5), but with different definition of the vibronic state. The corresponding energies are given by

$$\begin{aligned} E_A^p &= \frac{H_{AA} - G(X_1)S_p H_{AB}}{1 - G(X_1)S_p}, \\ E_H^p &= \frac{5H_{AA} + G(X_1)S_p H_{AB}}{5 + G(X_1)S_p}, \end{aligned} \tag{6.4.1}$$

where $G(x)$ is the function

$$G(x) = \frac{2 - 5x^2}{2 + x^2}, \tag{6.4.2}$$

and S_p is the phonon overlap between any two adjacent pentagonal wells given by

$$S_p = \exp\left[-\tfrac{12}{5}\left(\sigma_1 V_1'\right)^2\right]. \tag{6.4.3}$$

In Eq. (6.4.1), $H_{XY} = \langle X'; 0|\mathcal{H}_{total}|Y'; 0\rangle / \langle X'; 0|Y'; 0\rangle$ are the matrix elements of the total Hamiltonian between wells X and Y. Thus, we can derive closed

expressions for these quantities in the form:

$$\begin{aligned} H_{AA} &= \frac{X_1^2}{2+X_1^2}\delta + \left[\tfrac{5}{2} - 2\left(\sigma_1 V_1'\right)^2\right]\hbar\omega, \\ H_{AB} &= \frac{5X_1^2}{5X_1^2-2}\delta + \left\{\tfrac{5}{2} - \sigma_1\left(V_1'\right)^2\left[\tfrac{2}{5}\sigma_1 + \frac{4\left(4X_1-1\right)}{5X_1^2-2}\right.\right. \\ &\qquad \left.\left. - \frac{72\sigma_1 V_{\text{tot}}'}{4\left(5X_1^2-2\right)}\right]\right\}\hbar\omega, \end{aligned} \tag{6.4.4}$$

where V_{tot}' is the dimensionless quadratic coupling constant defined in Eq. (5.2.2).

6.4.2 Energies of the SASs from D_{3d} minima

The SASs here having A, G and H symmetries and also have the same form as these given in Eq. (5.2.8) but again with different meanings of the well state included in the form.

The energies of these states are found to be

$$\begin{aligned} E_A^t &= \frac{H_{aa} + 3g_1(X_2)S_t H_{ab} - 6g_2(X_2)S_t^2 H_{ac}}{1 + 3g_1(X_2)S_t - 6g_2(X_2)S_t^2}, \\ E_G^t &= \frac{H_{aa} - 2g_1(X_2)S_t H_{ab} - g_2(X_2)S_t^2 H_{ac}}{1 - 2g_1(X_2)S_t - g_2(X_2)S_t^2}, \\ E_H^t &= \frac{H_{aa} + g_1(X_2)S_t H_{ab} + 2g_2(X_2)S_t^2 H_{ac}}{1 + g_1(X_2)S_t + 2g_2(X_2)S_t^2}, \end{aligned} \tag{6.4.5}$$

where $g_1(x)$ and $g_2(x)$ are the functions

$$\begin{aligned} g_1(x) &= \frac{2+3x^2}{3\left(2+x^2\right)}, \\ g_2(x) &= \frac{2-3x^2}{3\left(2+x^2\right)}, \end{aligned} \tag{6.4.6}$$

and S_t is the phonon overlap between nearest neighbours, respectively,

$$S_t = \exp\left[-\tfrac{4}{3}\left(\sigma_2 V_1'\right)^2\right], \tag{6.4.7}$$

The matrix elements in Eq. (6.4.5) are found as

$$\begin{aligned}
H_{aa} &= \frac{X_2^2}{2+X_2^2}\delta + \left[\tfrac{5}{2} - 2\left(\sigma_2 V_1'\right)^2\right]\hbar\omega, \\
H_{ab} &= \frac{3X_2^2}{3X_2^2+2}\delta + \left\{\tfrac{5}{2} + \sigma_2\left(V_1'\right)^2\left[\tfrac{2}{3}\sigma_2 - \frac{4\left(4X_2+1\right)}{3X_2^2+2}\right.\right. \\
&\qquad \left.\left. + \frac{4\sqrt{5}\sigma_2 V_{\mathrm{tot}}'}{3\left(3X_2^2+2\right)}\right]\right\}\hbar\omega, \\
H_{ac} &= \frac{3X_2^2}{3X_2^2-2}\delta + \left\{\tfrac{5}{2} - \sigma_2\left(V_1'\right)^2\left[\tfrac{2}{3}\sigma_2 + \frac{4\left(2X_2-1\right)}{3X_2^2-2}\right.\right. \\
&\qquad \left.\left. - \frac{4\sqrt{5}\sigma_2 V_{\mathrm{tot}}'}{3\left(3X_2^2-2\right)}\right]\right\}\hbar\omega. \qquad (6.4.8)
\end{aligned}$$

As a corollary to these expressions, it is noted that the JT energy relative to the D_{3d} minima in the APES can be found most simply using

$$E_{JT} = H_{aa} - \tfrac{5}{2}\hbar\omega. \qquad (6.4.9)$$

The JT energy of the D_{5d} minima can be found from H_{AA} in Eq. (6.4.4) using an analogous expression.

6.5 Discussion

Equations (6.4.1) and (6.4.5) can be used to obtain plots of the energies of the SASs for the two cases considered. This, of course, requires knowledge of the coupling constants and Coulombic term energies. It can also be used to provide a more graphical interpretation of the results for particular values of these parameters.

Let us first assume that the quadratic coupling constant is small compared to its linear counterpart, to the extent that $V_1' = 10V_{\mathrm{tot}}'$. If δ is zero, then the energies of the SASs arising from the combination of the D_{5d} and D_{3d} wells as a function of the dimensionless linear coupling parameter V_1', are as shown previously in Figs. 5.5 and 5.6 respectively.

For the case where δ is non-zero, a particular example, $\delta = 0.5\hbar\omega$ will be taken, which should make the A state higher in energy than the H state in the absence of JT coupling, in the spirit of the variation shown in Fig. 5.1. Keeping the other parameters as before, the resulting plots are as shown in Figs. 6.1 and 6.2. It is

immediately apparent that in both figures, in the limit as $V_1' \to 0$, the A state does attain an energy exceeding that of the H state in a good agreement with that obtained by O'Brien [47] and [81] when the term splitting is taken into account. The H state continues to be the lowest in energy until the limit $V_1' \lesssim 0.5$. From the figures, the crossover between the H state and the A state is predicted to occur at values of $V_1' \approx 0.45$ for the D_{5d} case, whereas, $V_1' \approx 0.5$ for the D_{3d} case. Also it can be seen that, at zero coupling, the A state starts from a relative energy of $3.5\hbar\omega$ while the H state starts from $2.5\hbar\omega$ in both figures. The separation between the A state and the H state occurs due to the inclusion of the term splitting. If the term splitting set to be zero, then the relative energies of both states are 2.5 as shown in Figs. 5.5 and 5.6 again for both cases. All states tend to the correct limit in strong coupling as expected in our theory. The G state in the D_{3d} symmetry is again the first excited vibronic state or the tunnelling state which can be used as an indicator of the symmetry of the ion spectroscopically. It should be noted here that by changing the values of either the term splitting or the quadratic coupling will makes only a trivial changes in the plotted energies which can be ignored and regard the situation as that appeared in Figs. 6.1 and 6.2 for different values of both parameters.

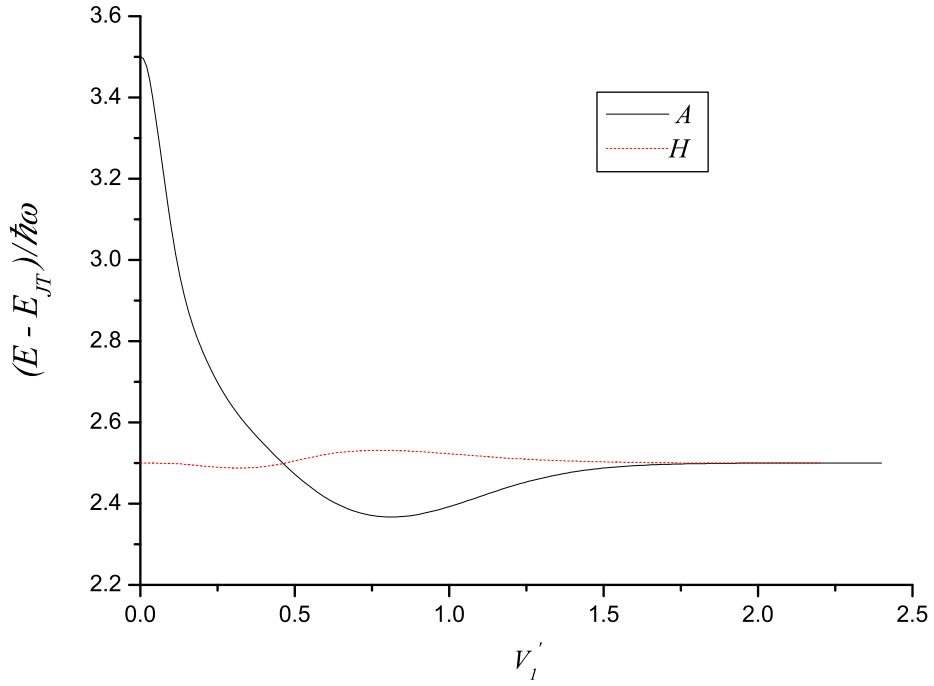

Figure 6.1: Energies of the SASs derived from D_{5d} minima when $\delta = 0.5\hbar\omega$. It has been assumed that $V_1' = 10V_{\text{tot}}'$. The dotted curve represents the H state and the solid curve represents the A state.

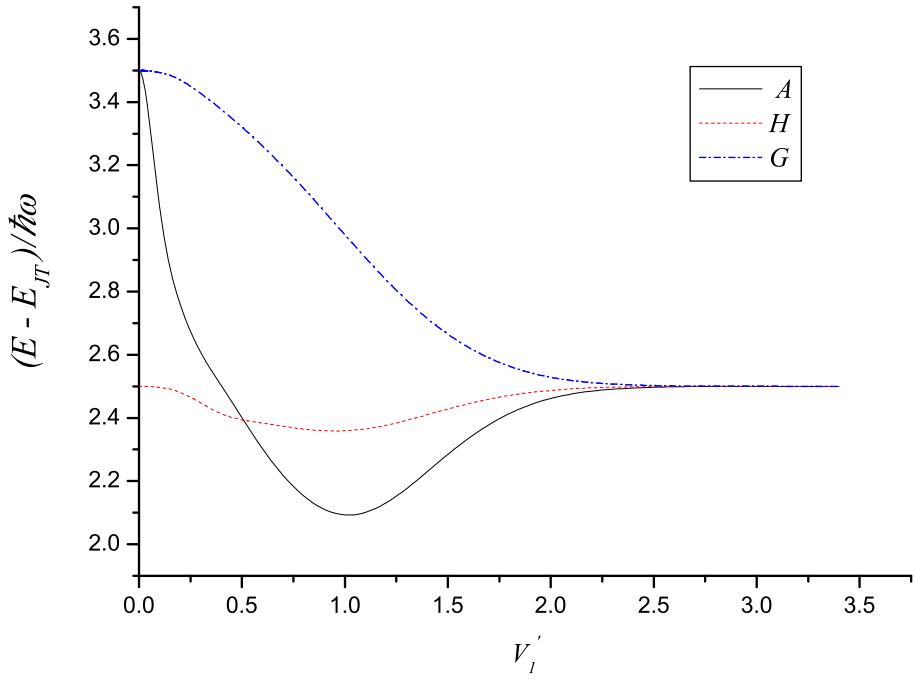

Figure 6.2: As for Fig. 6.1, but for the D_{3d} wells arising. The dotted curve represents the H state, the solid curve represents the A state and the dashed one represents the G state

Chapter 7

The $H \otimes h$ JT system: A model for C_{60}^{+}

Hole-doped derivatives of C_{60} have received less attention compared to their electron-doped counterparts. Although they are difficult to be produced experimentally, nevertheless, they have the ability to exhibit different but interesting properties. Such properties include the superconductivity at high temperatures that is predicted to exceed 50 K [7] higher than that for the electron-doped C_{60} [88, 89]. Superconductivity in these ions is not completely understood, but it is believed that the strong intramolecular JT coupling is related to this behaviour [90]. Therefore investigation of the nature of the JT effect in these ions is of paramount importance.

When electrons are removed from the H_u HOMO of the neutral C_{60} molecule, holes which behave as positively charged particles are produced. The resultant cation is denoted by C_{60}^{n+}, where n refers to the number of holes generated. If only one electron is removed from the H_u orbital, a vacancy will be produced which, in turn can be modelled in the same way as an electron. The cation which results from this removal is the C_{60}^{+}. This cation involves the $H_u \otimes (2a_g + 6g_g + 8h_g)$ JT interaction, in which the vacant hole in the H_u orbital is coupled to $2a_g$, $6g_g$ and $8h_g$ modes of vibration. The coupling to a_g modes will be ignored as mentioned earlier. However, previous theoretical calculations [7, 91] indicate that, in C_{60}^{+}, the coupling to the h_g modes is much stronger than that to the g_g modes, particularly the coupling to the $h_g(1)$ mode (~ 261 cm^{-1}) which is believed to be the strongest. [7]. Therefore, we can restrict our investigation of the C_{60}^{+} cation

by considering the $H_u \otimes h_g$ JT model.

The total Hamiltonian of this system consists of two types of interaction Hamiltonians. This situation arises as the h_g mode appears twice in the Kronecker product $H \otimes H = [A + G + 2H]$, which means that the linear coupling involves two independent sets of coefficients that can be constructed just as with quadratic coupling in the $p^2 \otimes h$ system [27]. The first coupling is labelled as $H_u \otimes h_a$ and the interaction Hamiltonian corresponding to this coupling has been derived from the CG coefficients in the first column of the $H \otimes H$ table in Ref. [27]. The second coupling is referred to as $H_u \otimes h_b$ where the interaction Hamiltonian has been derived from the CG coefficients in the second column of the same table.

In this Chapter, the time evolution operator is used to investigate the dynamical nature of the $H_u \otimes h_g$ JT system in the C_{60}^{+} ion. Analytical expressions for the probabilities of finding the system in different configurations at a later time t is obtained as a function of the vibronic coupling parameters.

7.1 Pseudorotation in the $H \otimes h$ JT system

For the $H_u \otimes h_g$ JT coupling problem, the Hamiltonian of the system takes the form

$$\mathcal{H} = \mathcal{H}_{vib} + \mathcal{H}_1(Q) + \mathcal{H}_2(Q), \tag{7.1.1}$$

where $\mathcal{H}_1(Q)$ and $\mathcal{H}_2(Q)$ are the linear interaction Hamiltonians. It has been found that, after the minimisation procedure of the total Hamiltonian of the system, the ion is distorted and produces an ion with either D_{3d} or D_{5d} geometry [30, 82, 92], depending on the relative contributions of $\mathcal{H}_1$ and $\mathcal{H}_2$ in Eq. (7.1.1). The $\mathcal{H}_1$ represents the interaction that produces the trigonal D_{3d} wells, whereas $\mathcal{H}_2$ generates the D_{5d} pentagonal symmetry.

Pseudorotation takes place between the different configurations. The SASs representing the state of the system in this motion are found in Refs. [93, 92] for both cases of D_{3d} and D_{5d} symmetry. Each case is investigated separately in the following sections.

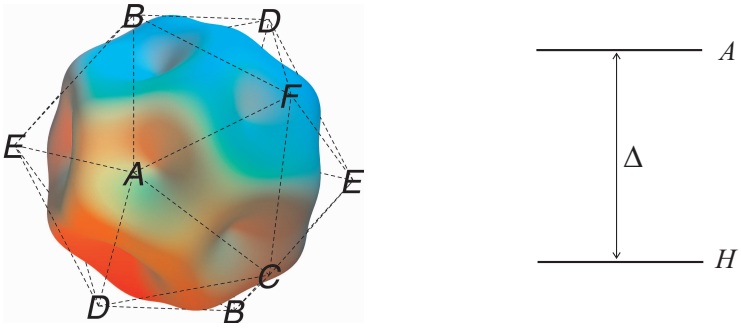

(a) (b)

Figure 7.1: (a) A pictorial representation of the pentagonal wells and (b) the energies of the corresponding symmetry-adapted states formed from these well states. The well labels in (a) correspond to those defined in Ref. [92].

7.1.1 The D_{5d} minima

The D_{5d} wells are represented pictorially in Fig. 7.1.(a). The figure shows the pentagonal wells which are separated equally and labelled as $\{A, B, C, D, E, F\}$. There are six SASs for the system when there is tunnelling between these wells, five of which are of H symmetry and one with A symmetry. They are given by [93]

$$\begin{aligned}
|H_\theta\rangle &= \frac{N_H}{2}\,[\,|A';0\rangle + |B';0\rangle - |C';0\rangle - |D';0\rangle], \\
|H_\epsilon\rangle &= \frac{N_H}{2\sqrt{3}}\,[|A';0\rangle + |B';0\rangle + |C';0\rangle + |D';0\rangle - 2|E';0\rangle - 2|F';0\rangle], \\
|H_4\rangle &= \frac{N_H}{\sqrt{2}}\,[|A';0\rangle - |B';0\rangle], \\
|H_5\rangle &= \frac{N_H}{\sqrt{2}}\,[|C';0\rangle + |D';0\rangle], \\
|H_6\rangle &= \frac{N_H}{\sqrt{2}}\,[-|E';0\rangle + |F';0\rangle], \\
|A_a\rangle &= \frac{N_A}{\sqrt{6}}\,[\,|A';0\rangle + |B';0\rangle + |C';0\rangle + |D';0\rangle + |E';0\rangle + |F';0\rangle],
\end{aligned} \tag{7.1.2}$$

where

$$\begin{aligned}
N_H &= \frac{\sqrt{5}}{\sqrt{5+S_p}}, \\
N_A &= \frac{1}{\sqrt{1-S_p}},
\end{aligned} \tag{7.1.3}$$

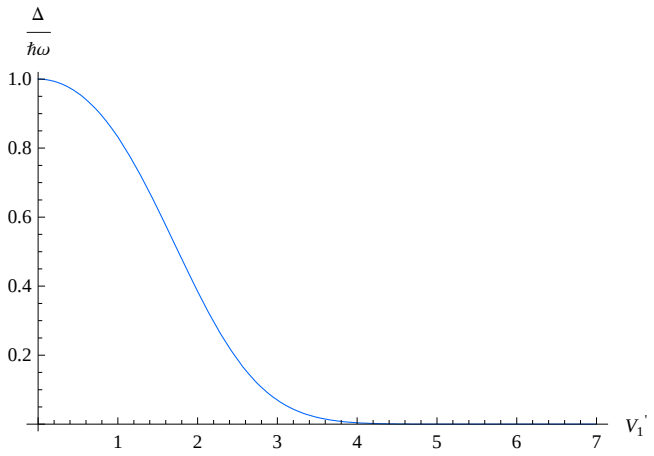

Figure 7.2: A plot of tunnelling splittings (Δ) between the A and H symmetry-adapted states as a function of the dimensionless linear coupling constant $V_1^{'}$.

are the normalisation constants and S_p is the phonon overlap between any two wells and is given by

$$S_p = \exp[-\frac{12}{25}\ V_1^{'2}]. \tag{7.1.4}$$

$V_1^{'}$ is the dimensionless linear coupling constant. Fig. 7.1.(b) depicts the energies of the states and shows that the A state is lying by an amount Δ above the H ground state given by

$$\Delta = -\frac{6\ S_p \ln S_p}{(1-S_p)(5+S_p)}\hbar\omega. \tag{7.1.5}$$

The variation of the tunnelling splitting as a function of $V_1^{'}$ is shown in Fig. 7.2.

The states corresponding to the pentagonal wells are found to be

$$\begin{aligned}
|A';0\rangle &= \frac{|A_a\rangle}{\sqrt{6}N_A} + \frac{|H_\theta\rangle}{2N_H} + \frac{|H_\epsilon\rangle}{2\sqrt{3}N_H} + \frac{|H_4\rangle}{\sqrt{2}N_H}, \\
|B';0\rangle &= \frac{|A_a\rangle}{\sqrt{6}N_A} + \frac{|H_\theta\rangle}{2N_H} + \frac{|H_\epsilon\rangle}{2\sqrt{3}N_H} - \frac{|H_4\rangle}{\sqrt{2}N_H}, \\
|C';0\rangle &= \frac{|A_a\rangle}{\sqrt{6}N_A} - \frac{|H_\theta\rangle}{2N_H} + \frac{|H_\epsilon\rangle}{2\sqrt{3}N_H} - \frac{|H_5\rangle}{\sqrt{2}N_H}, \\
|D';0\rangle &= \frac{|A_a\rangle}{\sqrt{6}N_A} - \frac{|H_\theta\rangle}{2N_H} + \frac{|H_\epsilon\rangle}{2\sqrt{3}N_H} + \frac{|H_5\rangle}{\sqrt{2}N_H}, \\
|E';0\rangle &= \frac{|A_a\rangle}{\sqrt{6}N_A} - \frac{|H_\epsilon\rangle}{\sqrt{3}N_H} - \frac{|H_6\rangle}{\sqrt{2}N_H}, \\
|F';0\rangle &= \frac{|A_a\rangle}{\sqrt{6}N_A} - \frac{|H_\epsilon\rangle}{\sqrt{3}N_H} + \frac{|H_6\rangle}{\sqrt{2}N_H}.
\end{aligned} \tag{7.1.6}$$

The probabilities of finding the system in a particular well at time t can be readily

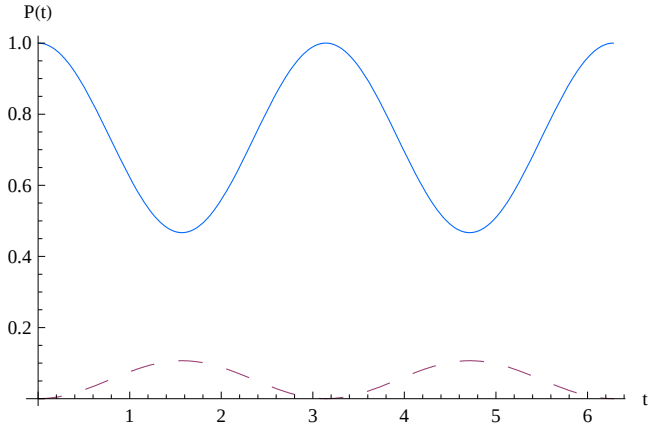

Figure 7.3: Inter-well dynamics for a pentagonal system initially localised in well A. The continuous curve represents P_{AA} and the dashed curve represents P_{AB}. The value of the Phonon overlap used is $S_p = 0.05$.

derived using Eq. (3.2.9). These take the form

$$P_{AA}(t) = 1 - \frac{1}{9}(1 - S_p)(5 + S_p)\ \sin^2\left(\frac{\Delta t}{2\hbar}\right), \tag{7.1.7}$$

and

$$P_{AB}(t) = \frac{S_p^2}{25} + \frac{1}{45}(1 - S_p)(5 + S_p)\ \sin^2\left(\frac{\Delta t}{2\hbar}\right). \tag{7.1.8}$$

From symmetry considerations, the other probabilities of finding the system in the other wells C,D,E and F are equal to P_{AB}. Therefore multiplying P_{AB} by 5 the total probability of the form

$$\sum_{X=A}^{F} P_{AX} = 1 + \frac{S_p^2}{5}. \tag{7.1.9}$$

Again and as expected, the pseudorotation mechanism in this case is similar to that of the D_{5d} case in the $(p^2 \otimes h)$ system. Fig. 7.3 shows that the probability of finding the system in well A subsequently when it is initially localised in well A never drops below $\frac{4}{9}$ in agreement with that for the $(p^2 \otimes h)$ system. From Eq. (7.1.9), it can also be noticed that the sum of the probabilities tends to one as the phonon overlap $S_p \longrightarrow 0$. This is expected as the walls separating the wells in the APES are infinite (i.e.$V_1^{'} = \infty$) so that the system must be found locked in one of the pentagonal wells as expected.

The system completes one pseudorotation of period T_p equal to $\frac{2\pi\hbar}{\Delta}$. The rate at which the system is pseudorotating is the inverse value of T_p and is varying with the coupling constant $V_1^{'}$ in a similar manner as that in Fig. 7.2.

7.1.2 The D_{3d} minima

The D_{3d} minima are shown in Fig. 7.4.(a). The figure shows a pictorial representation of the trigonal wells and the separating distances between them. There are two distances separating the wells into two sets corresponding to well a; the first set includes the nearest-neighbours $\{e, g, j\}$ while the second set contains the next nearest-neighbours $\{b, c, d, f, h, i\}$. At finite coupling, the system is pseudorotating between these wells having SASs given by [93]

$$\begin{aligned}
|H_\theta\rangle &= \frac{N_H}{2\sqrt{3}}\,[-\,|e';0\rangle - |f';0\rangle - |g';0\rangle - |h';0\rangle + 2|i';0\rangle + 2|j';0\rangle],\\
|H_\epsilon\rangle &= \frac{N_H}{2}\,[|e';0\rangle + |f';0\rangle - |g';0\rangle - |h';0\rangle],\\
|H_4\rangle &= \frac{N_H}{\sqrt{6}}\,[-\,|a';0\rangle - |b';0\rangle + |c';0\rangle + |d';0\rangle - |e';0\rangle + |f';0\rangle],\\
|H_5\rangle &= \frac{N_H}{\sqrt{6}}\,[-\,|a';0\rangle + |b';0\rangle - |c';0\rangle + |d';0\rangle - |g';0\rangle + |h';0\rangle],\\
|H_6\rangle &= \frac{N_H}{\sqrt{6}}\,[-\,|a';0\rangle + |b';0\rangle + |c';0\rangle - |d';0\rangle + |i';0\rangle - |j';0\rangle],\\
|G_a\rangle &= \frac{N_G}{\sqrt{15}}\,[-\frac{3}{2}(\,|a';0\rangle + |b';0\rangle + |c';0\rangle + |d';0\rangle)\\
&+ (|e';0\rangle + |f';0\rangle + |g';0\rangle + |h';0\rangle + |i';0\rangle + |j';0\rangle],\\
|G_x\rangle &= \frac{N_G}{2\sqrt{3}}\,[\,|a';0\rangle + |b';0\rangle - |c';0\rangle - |d';0\rangle - 2|e';0\rangle + 2|f';0\rangle],\\
|G_y\rangle &= \frac{N_G}{2\sqrt{3}}\,[\,|a';0\rangle - |b';0\rangle + |c';0\rangle - |d';0\rangle - 2|g';0\rangle + 2|h';0\rangle],\\
|G_z\rangle &= \frac{N_G}{2\sqrt{3}}\,[\,|a';0\rangle - |b';0\rangle - |c';0\rangle + |d';0\rangle + 2|i';0\rangle - 2|j';0\rangle],\\
|A_a\rangle &= \frac{N_A}{\sqrt{10}}\,[\,|a';0\rangle + |b';0\rangle + |c';0\rangle + |d';0\rangle + |e';0\rangle + |f';0\rangle\\
&+ |g';0\rangle + |h';0\rangle + |i';0\rangle + |j';0\rangle],
\end{aligned} \tag{7.1.10}$$

where

$$\begin{aligned}
N_A &= \frac{1}{\sqrt{1 + S_t - 2S_t^2}},\\
N_G &= \frac{\sqrt{3}}{\sqrt{3 - S_t + 2S_t^2}},\\
N_H &= \frac{\sqrt{3}}{\sqrt{3 + S_t + 2S_t^2}}
\end{aligned} \tag{7.1.11}$$

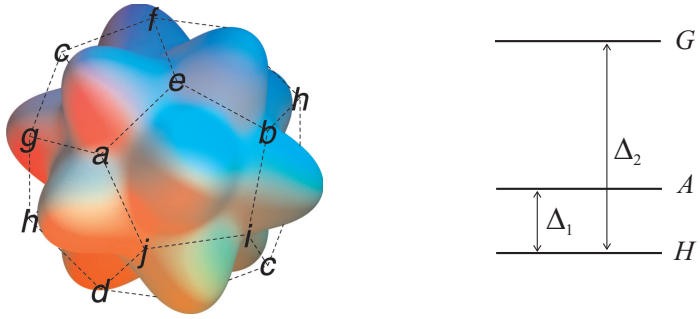

(a) (b)

Figure 7.4: (a) A pictorial representation of the trigonal wells and (b) the energies of the corresponding symmetry-adapted states formed from the well states. The well labels in (a) correspond to those defined in Ref. [93].

are the SASs normalisation constants. S_t is the phonon overlap between the adjacent trigonal wells a and b and is given by

$$S_t = \exp[-\frac{4}{27}V_1''^2]. \tag{7.1.12}$$

The energy separations between the SASs are shown in Fig. 7.4.(b) and given by

$$\Delta_1 = \frac{2(1-8S_t-2S_t^2)S_t \ln S_t}{(1-S_t)(1+2S_t)(3+S_t+2S_t^2)}\hbar\omega, \tag{7.1.13}$$

and

$$\Delta_2 = -\frac{3(3+6S_t-S_t^2)S_t \ln S_t}{(1-S_t)(3+S_t)(3+S_t+2S_t^2)}\hbar\omega. \tag{7.1.14}$$

Δ_1 represents the separation between the A and H SASs and Δ_2 represents the separation between G and H SASs. These expressions are plotted in Fig. 7.5. The figure shows the variation of the tunnelling splittings as a function of the dimensionless linear coupling constant V_1''. It also shows the value of the coupling constant ($V_1'' \approx 3.77$) for the $H-A$ crossover ($\Delta_1 = 0$) [94].

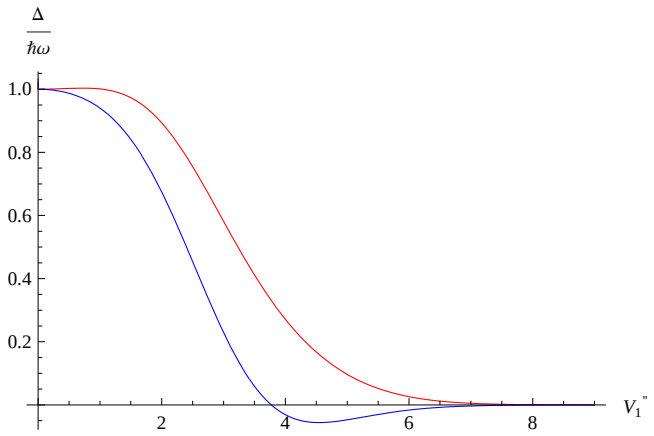

Figure 7.5: Tunnelling splittings between the A (Δ_1) and G (Δ_2) symmetry-adapted states and the H state (zero energy) as a function of the dimensionless linear coupling constant $V_1^{''}$.

The expressions for the well states in terms of the SASs are found to be:

$$
\begin{aligned}
|a\rangle &= \frac{|A_a\rangle}{\sqrt{10}N_A} - \frac{|H_4\rangle + |H_5\rangle + |H_6\rangle}{\sqrt{6}N_H} - \frac{3|G_a\rangle}{2\sqrt{15}N_G} + \frac{|G_x\rangle + |G_y\rangle + |G_z\rangle}{2\sqrt{3}N_G},\\
|b\rangle &= \frac{|A_a\rangle}{\sqrt{10}N_A} - \frac{|H_4\rangle - |H_5\rangle - |H_6\rangle}{\sqrt{6}N_H} - \frac{3|G_a\rangle}{2\sqrt{15}N_G} + \frac{|G_x\rangle - |G_y\rangle - |G_z\rangle}{2\sqrt{3}N_G},\\
|c\rangle &= \frac{|A_a\rangle}{\sqrt{10}N_A} - \frac{|H_4\rangle - |H_5\rangle + |H_6\rangle}{\sqrt{6}N_H} - \frac{3|G_a\rangle}{2\sqrt{15}N_G} + \frac{|G_x\rangle - |G_y\rangle + |G_z\rangle}{2\sqrt{3}N_G},\\
|d\rangle &= \frac{|A_a\rangle}{\sqrt{10}N_A} + \frac{|H_4\rangle + |H_5\rangle - |H_6\rangle}{\sqrt{6}N_H} + -\frac{3|G_a\rangle}{2\sqrt{15}N_G} - \frac{|G_x\rangle + |G_y\rangle - |G_z\rangle}{2\sqrt{3}N_G},\\
|e\rangle &= \frac{|A_a\rangle}{\sqrt{10}N_A} - \frac{|H_\theta\rangle}{2\sqrt{3}N_H} + \frac{|H_\epsilon\rangle}{\sqrt{3}N_H} - \frac{|H_4\rangle}{\sqrt{6}N_H} + \frac{|G_a\rangle}{\sqrt{15}N_G} - \frac{|G_x\rangle}{\sqrt{3}N_G},\\
|f\rangle &= \frac{|A_a\rangle}{\sqrt{10}N_A} - \frac{|H_\theta\rangle}{2\sqrt{3}N_H} + \frac{|H_\epsilon\rangle}{2N_H} - \frac{|H_4\rangle}{\sqrt{6}N_H} + \frac{|G_a\rangle}{\sqrt{15}N_G} + \frac{|G_x\rangle}{\sqrt{3}N_G},\\
|g\rangle &= \frac{|A_a\rangle}{\sqrt{10}N_A} - \frac{|H_\theta\rangle}{2\sqrt{3}N_H} - \frac{|H_\epsilon\rangle}{2N_H} - \frac{|H_5\rangle}{\sqrt{6}N_H} + \frac{|G_a\rangle}{\sqrt{15}N_G} - \frac{|G_y\rangle}{\sqrt{3}N_G},\\
|h\rangle &= \frac{|A_a\rangle}{\sqrt{10}N_A} - \frac{|H_\theta\rangle}{2\sqrt{3}N_H} - \frac{|H_\epsilon\rangle}{2N_H} + \frac{|H_5\rangle}{\sqrt{6}N_H} + \frac{|G_a\rangle}{\sqrt{15}N_G} + \frac{|G_y\rangle}{\sqrt{3}N_G},\\
|i\rangle &= \frac{|A_a\rangle}{\sqrt{10}N_A} + \frac{|H_\theta\rangle}{\sqrt{3}N_H} + \frac{|H_6\rangle}{\sqrt{6}N_H} + \frac{|G_a\rangle}{\sqrt{15}N_G} + \frac{|G_z\rangle}{\sqrt{3}N_G},\\
|j\rangle &= \frac{|A_a\rangle}{\sqrt{10}N_A} + \frac{|H_\theta\rangle}{\sqrt{3}N_H} - \frac{|H_6\rangle}{\sqrt{6}N_H} + \frac{|G_a\rangle}{\sqrt{15}N_G} - \frac{|G_z\rangle}{\sqrt{3}N_G},
\end{aligned}
\tag{7.1.15}
$$

These states are normalised after multiplying them by the normalisation constant

$$N = \frac{\sqrt{15}}{\sqrt{15 + 2S_t - 2S_t^2}}. \tag{7.1.16}$$

Using Eq. (3.2.9) implies that the probabilities of finding the system in wells a, b

or e at time t are, respectively,

$$\begin{aligned}
P_{aa}(t) &= 1 - 15F_1 \sin^2\left(\frac{\Delta_1 t}{2\hbar}\right) - 20F_2 \sin^2\left(\frac{\Delta_2 t}{2\hbar}\right) - 12F_3 \sin^2\left(\frac{(\Delta_2 - \Delta_1)t}{2\hbar}\right) \\
P_{ab}(t) &= \frac{1}{9}F_4 + 5F_1 \sin^2\left(\frac{\Delta_1 t}{2\hbar}\right) + \frac{10}{9}F_2 \sin^2\left(\frac{\Delta_2 t}{2\hbar}\right) - 2F_3 \sin^2\left(\frac{(\Delta_2 - \Delta_1)t}{2\hbar}\right) \\
P_{ae}(t) &= \frac{1}{9}F_5 - 5F_1 \sin^2\left(\frac{\Delta_1 t}{2\hbar}\right) + \frac{40}{9}F_2 \sin^2\left(\frac{\Delta_2 t}{2\hbar}\right) + 8F_3 \sin^2\left(\frac{(\Delta_2 - \Delta_1)t}{2\hbar}\right)
\end{aligned} \tag{7.1.17}$$

where the F_n are functions of S_t and given by:

$$\begin{aligned}
F_1 &= (1 - S_t)(1 + 2S_t)(3 + S_t + 2S_t^2)(15 + 2S_t - 2S_t^2)^{-2} \\
F_2 &= (1 - S_t)(3 + 2S_t)(3 + S_t + 2S_t^2)(15 + 2S_t - 2S_t^2)^{-2} \\
F_3 &= (1 - S_t)^2(1 + 2S_t)(3 + 2S_t)(15 + 2S_t - 2S_t^2)^{-2} \\
F_4 &= S_t^2(1 - 16S_t)^2(15 + 2S_t - 2S_t^2)^{-2} \\
F_5 &= S_t^2(11 + 4S_t)^2(15 + 2S_t - 2S_t^2)^{-2}.
\end{aligned} \tag{7.1.18}$$

Once again the probabilities of finding the system in wells $\{c, d, f, h, i\}$ and wells $\{g, j\}$ are equal to P_{ab} and P_{ae} respectively. The sum of the probabilities of being in any of the ten well states at time t is

$$\sum_{x=a}^{j} P_{ax}(t) = 1 + \frac{2}{3}F_4 + \frac{1}{3}F_5. \tag{7.1.19}$$

The probability sum is time independent and tend to unity in the infinite coupling as expected and as discussed earlier.

As in the $p^2 \otimes h$ system, the system here in the D_{3d} case shows a similar complicated inter-well dynamics. This is again because it can migrate to two different sets of equivalent wells.

The temporal evolution of the system is plotted in Fig. 7.6 for three particular values of the phonon overlap corresponding to values of the coupling constant between that for the crossover. In the first diagram, $S_t = 2S_t^X$ ($V_1'' \approx 3.09$) and the system is more weakly coupled than at the $H - A$ crossover (see Ref. [94]). Pseudorotation here is clearly fairly rapid with five reoccurrences of the initial localisation occurring within the time period shown. In between the reoccurrences, the probability of finding the system in well a becomes quite small and the system is delocalised over the other wells. The situation is complicated with regard to the

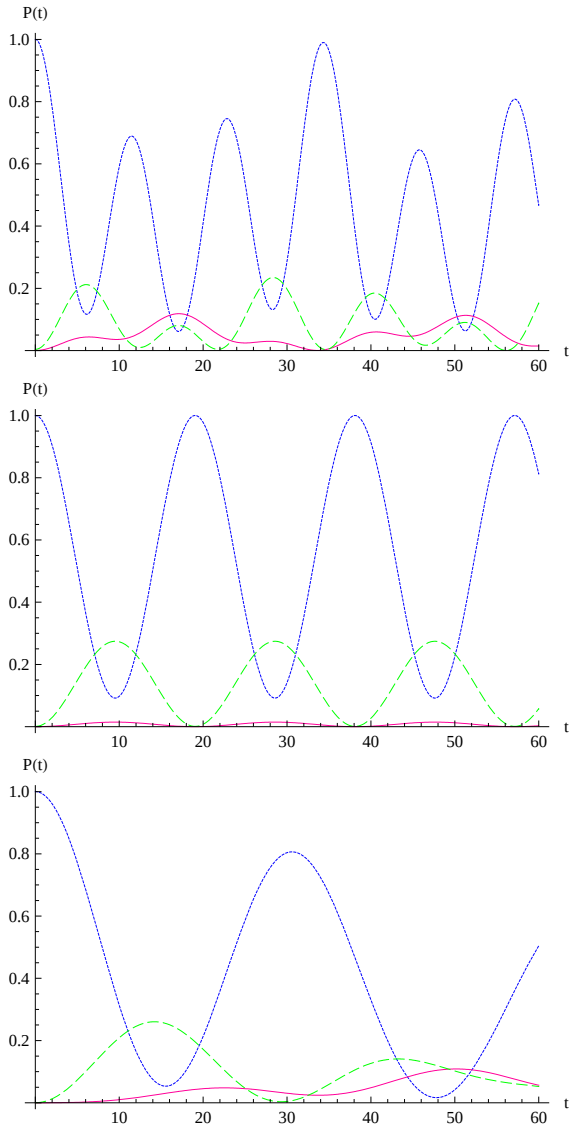

Figure 7.6: Inter-well dynamics for a trigonal system initially localised in well a. The variation for three different values of the phonon overlap are illustrated, where S_t^X is the phonon overlap between adjacent wells at the H-A cross-over.

pseudorotational period but it does seem sensible to continue to use the definition used for the pentagonal case. That is we define the pseudorotational period between trigonal wells T_t to be the time at which the first reoccurrence occurs. From the first figure, this occurs when $T_t \approx 11.5$. Prior to the first reoccurrence, the system becomes predominately localised in the nearest-neighbour wells $\{e, g, j\}$ and then, afterwards, in the next-nearest-neighbour wells $\{b, c, d, f, h, i\}$.

For coupling corresponding to the crossover point, $V_1'' \approx 3.77$, the situation is as shown in the second diagram in Fig. 7.6. Clearly, the dynamics is much more regular now and perfect reoccurrences of the initial state are observed. Pseudorotation is slower than before and only three reoccurrences occur in the period shown. The pseudorotational period in this instance will be given exactly by $T_t^X = 2\pi\hbar\omega/\Delta_2 \approx 19.05$ (when $S_t^X = 0.121$). It is clear from this figure that, for this unique value of the linear coupling constant, the times taken for the system to pseudorotate to wells $\{e, g, j\}$ and $\{b, c, d, f, h, i\}$ are identical and are given by $T_t^X/2$.

Finally, the third diagram in Fig. 7.6 shows the dynamics for the case when $S_t = S_t^X/2$ and the vibronic coupling constant $V_1'' \approx 4.35$ exceeds that at the crossover. The rate of pseudorotation has again decreased and only one reoccurrence is visible in the plot. At the minima in P_{aa}, the system is delocalised over the other wells to degrees that vary with the minimum considered.

7.2 Discussion

In this chapter, the quantum mechanical time evolution operator has been used to study the evolution of the C_{60}^{+} cation modelled as a $H \otimes h_g$ JT system. Due to the JT coupling, the molecule shows a lowering of the symmetry into two different species of symmetries D_{5d} and D_{3d}. These symmetries have 6 and 10 wells in their APESs respectively. The probabilities of finding the system evolving into another well when is initially prepared in one particular well at a later time t has been found for each of these cases, using the SASs that describe the tunnelling state of the JT system in the dynamic motion. These resulting expressions are plotted versus the time to show the pseudorotation dynamics of the system. In each symmetry, the system has shown different pseudorotation regimes due to the differences in the separations between the wells. At the D_{5d} distortion, a regular

pattern of pseudorotation between the wells has been observed and no unexpected situation arises. For the D_{3d} case, the expressions for the probabilities has been plotted for different values of the coupling constants including that where the crossover between the H and A states occur. The system shows different patterns of pseudorotation for each value with a decreasing of the rate of pseudorotation as the coupling increases.

If we accept the dominance of the $h_g(1)$ mode with $\hbar\omega = 261\text{cm}^{-1}$ and make use of the linear coupling constant $V_1^{'} = 1.52$ which has been computed using density functional theory (DFT) [7] we can estimate the rate at which pseudorotation will occur between pentagonal wells. Using Eq. (7.1.4) the phonon overlap is $S_p = 0.33$ together with $T_p = \frac{2\pi\hbar}{\Delta}$ and Eq. (7.1.5), thus the estimated period for the system to complete one pseudorotation circuit is $T_p = 208$ fs. Thus, we can expect that in order to detect pseudorotation between the D_{5d} wells in C_{60}^{+}, experiments must be performed on a femtosecond time scale. In addition, the inter-well dynamics are expected to be quite simple and follow the trends shown in Fig. 7.3.

This work has been published in Ref. [95]

Chapter 8

The $(h^+)^2 \otimes h$ JT system: A model for C_{60}^{2+}

In this Chapter, the time evolution of the $(h_u^+)^2 \otimes h_g$ JT system is investigated by applying the same method as those described in previous chapters. Before studying the evolution of the system, it is useful to summarise firstly some of the main features of this system.

As mentioned previously, when electrons are removed from the H_u the HOMO of the neutral C_{60} molecule, a number of holes is generated. The removal of two electrons from this orbit produces two positive holes and therefore the dication C_{60}^{2+} is produced. The modes of vibrations allowed to couple in order to form JT coupling in this molecule are the same as that for the C_{60}^{+} cation. Therefore, JT interactions for this system is the coupling of the two holes of H_u symmetry to the a_g, g_g or h_g normal modes of vibrations. Again, the coupling between the holes and the a_g and g_g vibrational modes will not be considered here, because it has been shown that these modes do not result in any significant distortions [7]. Therefore, we will only concentrate on the coupling involving the two holes of H_u symmetry and the h_g normal mode and the problem will be denoted as $(h_u^+)^2 \otimes h_g$.

As in Chapter 7, the interaction Hamiltonian consists of two different Hamiltonians due to the two sets of CG coefficients. One of them is represented by $\mathcal{H}_a$ and the coupling parameters are taken from the first column of CG coefficients for $H \otimes H$ table in Rf.[27]. The second coupling represented by $\mathcal{H}_b$ is derived using the second column in the same table.

The geometry of the distorted ion can be deduced from the study the structure of

the APES and finding the number of the minima and the corresponding positions. As before, the pseudorotation of the system between these minima is studied using the time evolution operator and is applied to one of the wells as will be seen in the following section.

8.1 The $(h^+)^2 \otimes h$ JT system

The total Hamiltonian for this system takes the form

$$\mathcal{H}_{tot} = \mathcal{H}_{vib} + \mathcal{H}_{TS} + \mathcal{H}_{JT}, \tag{8.1.1}$$

The interaction Hamiltonian has been derived previously in Ref. [96]. This Hamiltonian involves coupling between the spin and the orbital angular momentum of the two holes. Coupling of the spin angular momentum of the two holes gives either singlet spin states ($S = 0$) or triplet spin states ($S = 1$). The coupling of the orbital states can be predicted from the Kronecker product of the H_u orbital by itself $H \otimes H = [A \oplus G \oplus 2H]_S \oplus \{T_1 \oplus T_2 \oplus G\}_A$. The symmetric part of the Kronecker product couples to the singlet spin states to give rise to low-spin terms and the anti-symmetric part couples to the triplet spin state to generate the high-spin terms. Thus, the allowed terms are ${}^1A, {}^1G, {}^1H_a, {}^1H_b, {}^3T_1, {}^3T_2, {}^3G$, where the superscript represents the spin multiplicity $(2S + 1)$. The calculations by Nikolaev *et al.* [78] indicate that the high-spin terms are lower in energy than the low-spin terms satisfying Hund's rule. As there is no coupling between the terms which have different spins, only the high-spin terms $\{{}^3T_1, {}^3T_2, {}^3G\}$ will be considered here. These terms are of different energies due to Coulomb interaction between the two holes. In this thesis we will treat these terms as degenerate to make our analysis generally applicable.

The interaction Hamiltonian can be written in terms of the CG coefficients as [97]

$$\mathcal{H}_{int} = V_{Hh_a}\mathcal{H}_a + V_{Hh_b}\mathcal{H}_b, \tag{8.1.2}$$

where V_{Hh_a} and V_{Hh_b} are the coupling constants defined in polar form by

$$V_{Hh_a} = V \sin\beta; \quad V_{Hh_b} = V \cos\beta, \tag{8.1.3}$$

where V is a measure of the combined coupling strength and β represents a mixing angle of the two sets of CG coefficients. The matrix representation of each of the

interaction Hamiltonians $(\mathcal{H}_a, \mathcal{H}_b)$ can be written in a basis derived using the wavefunctions associated with the high-spin term. This corresponding matrix is of the order 10×10 and it has been investigated in Ref. [98].

Applying the minimisation procedures to this Hamiltonian produces minima in the APES of either D_{5d}, D_{3d}, D_{2h} or C_{2h} symmetry as β varies (see Fig.2 in Ref. [97]). A study by Manini *et al.* [7] shows that the C_{60}^{2+} ion is favoured to be localised in a D_{2h} well. This result has been confirmed again by Hands *et al.* [99]. Therefore, only the D_{2h} distortion will be considered here in the investigation of the pseudorotation motion.

The APES has been found to have a D_{2h} minima in the range where $1.35 \leqslant \beta \leqslant 1.79$ [98]. There are 15 equivalent wells represented by$\{A, B, C, D, \ldots\}$ in Fig. 8.1. These wells are located in the centres of the C-C double bonds which is the mid point of two joined hexagons in real space. The corresponding positions of these wells and the associated electronic states in the Q-space are given in Table 8.1 [98, 97].

From the results shown in Table 8.1, it should be noted that the separations between the wells in the Q-space divides them into two sets such that each well has 8 nearest-neighbours and 6 next-nearest neighbours. For example, well $\{A\}$ has $\{B, C, D, E, J, K, L, M\}$ as the nearest-neighbour wells and $\{F, G, H, I, N, O\}$ as the next-nearest neighbours. This situation should not be necessary consistent with that appearing in Fig. 8.1. The figure shows a 4 nearest-neighbour wells, 8 next-nearest and 2 furthest-neighbour wells for each well. This inconsistency is simply due to the differences between the real space and the Q space.

8.2 Pseudorotation in D_{2h}

When the system is pseudorotating, the 15-fold degeneracy of the ground states split and produce SASs of T_{1g}, T_{2g}, G_g and H_g symmetry. These states have been obtained in Ref.[98] and are given in Appendix A for completeness. They are inverted so that a state for each well is obtained as a linear combination of the SASs as in Eq. (3.2.2). The matrix which represents the $a_j^{(i)}$ coefficients in Eq. (3.2.2) is a 15×15 matrix which is

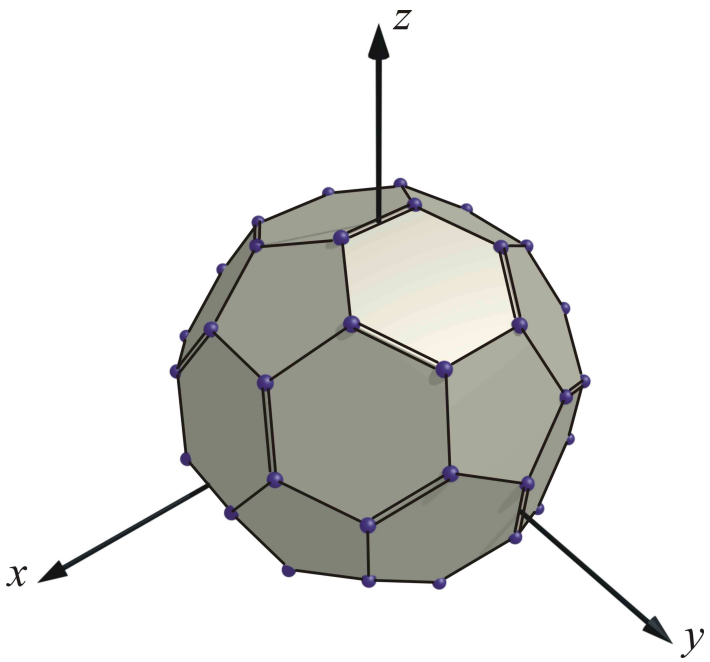

(a)

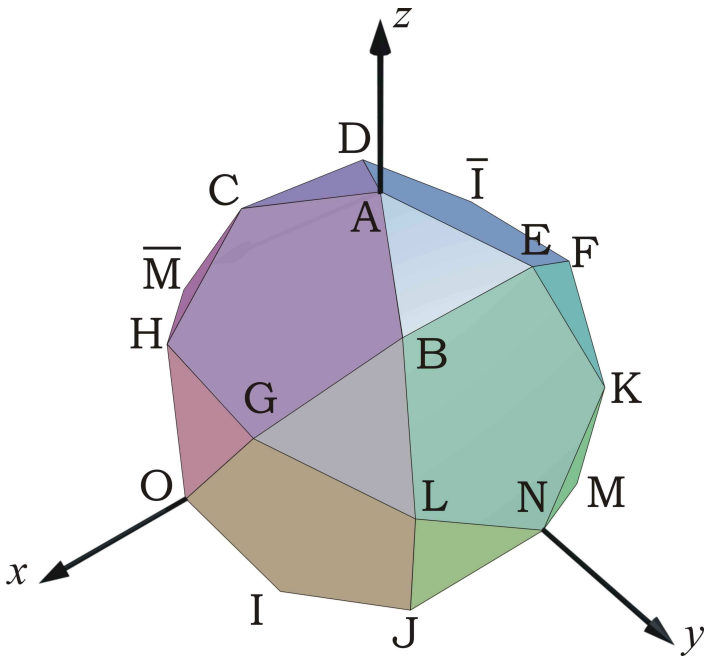

(b)

Figure 8.1: (a) The location of the C-C double bonds in the fullerene C_{60}. (b) An icosidodecahedron formed by connecting the mid points on the double bonds. The vertices are labelled as $A, B, C, \ldots, O$ as presented in Table 8.1.

Table 8.1: Well positions and the associated electronic states of the 15 minima of the D_{2h} symmetry grouped according to their equivalence with respect to the minimum A when the term splitting set to zero (see Ref. [97]).

Label	position	electronic state
A	$\frac{-3}{4}(0,\sqrt{2},0,0,0)$	$\sqrt{\frac{3}{10}}(0,0,1,0,0,1,0,0,0,\frac{2}{\sqrt{3}})$
B	$\frac{-3}{16}(-\sqrt{6},\sqrt{2},-2\sqrt{3},0,-2\sqrt{3})$	$\frac{1}{2}\sqrt{\frac{3}{10}}(\frac{1}{\phi},1,\phi,-\phi,1,\frac{-1}{\phi},-\sqrt{\frac{5}{3}},\frac{-1}{\sqrt{3}},-\sqrt{3},\frac{1}{\sqrt{3}})$
C	$\frac{-3}{16}(-\sqrt{6},\sqrt{2},2\sqrt{3},0,2\sqrt{3})$	$\frac{1}{2}\sqrt{\frac{3}{10}}(\frac{1}{\phi},-1,\phi,-\phi,-1,\frac{-1}{\phi},\sqrt{\frac{5}{3}},\frac{-1}{\sqrt{3}},\sqrt{3},\frac{1}{\sqrt{3}})$
D	$\frac{-3}{16}(-\sqrt{6},\sqrt{2},2\sqrt{3},0,-2\sqrt{3})$	$\frac{1}{2}\sqrt{\frac{3}{10}}(\frac{-1}{\phi},-1,\phi,\phi,-1,\frac{-1}{\phi},-\sqrt{\frac{5}{3}},\frac{1}{\sqrt{3}},\sqrt{3},\frac{1}{\sqrt{3}})$
E	$\frac{-3}{16}(-\sqrt{6},\sqrt{2},-2\sqrt{3},0,-2\sqrt{3})$	$\frac{1}{2}\sqrt{\frac{3}{10}}(\frac{-1}{\phi},1,\phi,\phi,1,\frac{-1}{\phi},\sqrt{\frac{5}{3}},\frac{1}{\sqrt{3}},\sqrt{3},\frac{1}{\sqrt{3}})$
J	$\frac{-3}{16}(\sqrt{6},\sqrt{2},0,2\sqrt{3},-2\sqrt{3})$	$\frac{1}{2}\sqrt{\frac{3}{10}}(1,\phi,\frac{-1}{\phi},1,\frac{-1}{\phi},\phi,\sqrt{\frac{5}{3}},-\sqrt{3},\frac{-1}{\sqrt{3}},\frac{1}{\sqrt{3}})$
K	$\frac{-3}{16}(\sqrt{6},\sqrt{2},0,2\sqrt{3},2\sqrt{3})$	$\frac{1}{2}\sqrt{\frac{3}{10}}(1,-\phi,\frac{-1}{\phi},1,\frac{1}{\phi},\phi,-\sqrt{\frac{5}{3}},-\sqrt{3},\frac{-1}{\sqrt{3}},\frac{1}{\sqrt{3}})$
L	$\frac{-3}{16}(\sqrt{6},\sqrt{2},0,-2\sqrt{3},-2\sqrt{3})$	$\frac{1}{2}\sqrt{\frac{3}{10}}(-1,-\phi,\frac{-1}{\phi},-1,\frac{1}{\phi},\phi,\sqrt{\frac{5}{3}},\sqrt{3},\frac{-1}{\sqrt{3}},\frac{1}{\sqrt{3}})$
M	$\frac{-3}{16}(\sqrt{6},\sqrt{2},0,-2\sqrt{3},2\sqrt{3})$	$\frac{1}{2}\sqrt{\frac{3}{10}}(-1,\phi,\frac{-1}{\phi},-1,\frac{-1}{\phi},\phi,-\sqrt{\frac{5}{3}},\sqrt{3},\frac{1}{\sqrt{3}},\frac{1}{\sqrt{3}})$
F	$\frac{-3}{8}(0,-\sqrt{2},-\sqrt{3},\sqrt{3},0)$	$\frac{1}{2}\sqrt{\frac{3}{10}}(\phi,\frac{-1}{\phi},-1,\frac{-1}{\phi},\phi,-1,-\sqrt{\frac{5}{3}},\frac{1}{\sqrt{3}},\frac{1}{\sqrt{3}},\sqrt{3})$
G	$\frac{-3}{8}(0,-\sqrt{2},-\sqrt{3},-\sqrt{3},0)$	$\frac{1}{2}\sqrt{\frac{3}{10}}(\phi,\frac{-1}{\phi},-1,\frac{-1}{\phi},\phi,-1,-\sqrt{\frac{5}{3}},\frac{1}{\sqrt{3}},\frac{1}{\sqrt{3}},\sqrt{3})$
H	$\frac{-3}{8}(0,-\sqrt{2},\sqrt{3},-\sqrt{3},0)$	$\frac{1}{2}\sqrt{\frac{3}{10}}(-\phi,\frac{1}{\phi},-1,\frac{1}{\phi},-\phi,-1,\sqrt{\frac{5}{3}},\frac{1}{\sqrt{3}},\frac{-1}{\sqrt{3}},\sqrt{3})$
I	$\frac{-3}{8}(0,-\sqrt{2},\sqrt{3},\sqrt{3},0)$	$\frac{1}{2}\sqrt{\frac{3}{10}}(\phi,\frac{1}{\phi},-1,\frac{-1}{\phi},-\phi,-1,\sqrt{\frac{5}{3}},\frac{1}{\sqrt{3}},\frac{-1}{\sqrt{3}},\sqrt{3})$
N	$\frac{-3}{8}(\sqrt{6},-\sqrt{2},0,0,0)$	$\sqrt{\frac{3}{10}}(0,1,0,0,1,0,0,0,\frac{2}{\sqrt{3}},0)$
O	$\frac{-3}{8}(-\sqrt{6},-\sqrt{2},0,0,0)$	$\sqrt{\frac{3}{10}}(1,0,0,1,0,0,0,\frac{2}{\sqrt{3}},0,0)$

$$M = \begin{bmatrix}
0 & 2 & 0 & \phi & -\phi & \phi & -\phi & \frac{1}{\phi} & \frac{-1}{\phi} & \frac{-1}{\phi} & \frac{1}{\phi} & 1 & 1 & -1 & -1 \\
0 & 0 & 2 & \frac{1}{\phi} & \frac{1}{\phi} & \frac{-1}{\phi} & \frac{-1}{\phi} & -1 & -1 & 1 & 1 & -\phi & \phi & \phi & -\phi \\
2 & 0 & 0 & -1 & -1 & -1 & -1 & \phi & \phi & \phi & \phi & \frac{-1}{\phi} & \frac{-1}{\phi} & \frac{-1}{\phi} & \frac{-1}{\phi} \\
0 & 2 & 0 & \frac{-1}{\phi} & \frac{1}{\phi} & \frac{-1}{\phi} & \frac{1}{\phi} & -\phi & \phi & \phi & -\phi & 1 & 1 & -1 & -1 \\
0 & 0 & 2 & -\phi & -\phi & \phi & \phi & -1 & -1 & 1 & 1 & \frac{1}{\phi} & \frac{-1}{\phi} & \frac{-1}{\phi} & \frac{1}{\phi} \\
2 & 0 & 0 & -1 & -1 & -1 & -1 & \frac{-1}{\phi} & \frac{-1}{\phi} & \frac{-1}{\phi} & \frac{-1}{\phi} & \phi & \phi & \phi & \phi \\
0 & 0 & 0 & 1 & -1 & -1 & 1 & 1 & -1 & 1 & -1 & -1 & 1 & -1 & 1 \\
0 & 4 & 0 & 1 & -1 & 1 & -1 & -1 & 1 & 1 & -1 & -3 & -3 & 3 & 3 \\
0 & 0 & 4 & -1 & -1 & 1 & 1 & 3 & 3 & -3 & -3 & -1 & 1 & 1 & -1 \\
4 & 0 & 0 & 3 & 3 & 3 & 3 & 1 & 1 & 1 & 1 & 1 & 1 & 1 & 1 \\
0 & 0 & 0 & 2 & -2 & -2 & 2 & -1 & 1 & -1 & 1 & 1 & -1 & 1 & -1 \\
0 & 0 & 0 & 0 & 0 & 0 & 0 & -1 & 1 & -1 & 1 & -1 & 1 & -1 & 1 \\
0 & 2 & 0 & -1 & 1 & -1 & 1 & 1 & -1 & -1 & 1 & 0 & 0 & 0 & 0 \\
0 & 0 & 2 & 1 & 1 & -1 & -1 & 0 & 0 & 0 & 0 & 1 & -1 & -1 & 1 \\
2 & 0 & 0 & 0 & 0 & 0 & 0 & -1 & -1 & -1 & -1 & -1 & -1 & -1 & -1
\end{bmatrix}.$$

Taking the inverse of this matrix and multiplying it by the column matrix containing the SASs produces 15 normalised well states:.

The first set of nearest-neighbour wells are:

$$
\begin{aligned}
|A';0\rangle &= \frac{\sqrt{3}(|T_{1z}\rangle + |T_{2z}\rangle) + 2|G_z\rangle}{\sqrt{15}N_1} + \frac{|H_6\rangle}{\sqrt{3}N_2}, \\
|B';0\rangle &= \frac{(\phi-1)(|T_{1x}\rangle - |T_{2z}\rangle) + (|T_{1y}\rangle + |T_{2y}\rangle) + \phi(|T_{1z}\rangle - |T_{2x}\rangle)}{2\sqrt{5}N_1} \\
&- \frac{\sqrt{5}|G_a\rangle + |G_x\rangle + 3|G_y\rangle - |G_z\rangle}{2\sqrt{15}N_1} + \frac{|H_\theta\rangle + \sqrt{3}|H_\epsilon\rangle + \sqrt{2}(|H_4\rangle - |H_6\rangle)}{2\sqrt{6}N_2}, \\
|C';0\rangle &= \frac{(\phi-1)(|T_{1x}\rangle - |T_{2z}\rangle) - (|T_{1y}\rangle + |T_{2y}\rangle) + \phi(|T_{1z}\rangle - |T_{2x}\rangle)}{2\sqrt{5}N_1} \\
&+ \frac{\sqrt{5}|G_a\rangle - |G_x\rangle + 3|G_y\rangle + |G_z\rangle}{2\sqrt{15}N_1} - \frac{|H_\theta\rangle + \sqrt{3}|H_\epsilon\rangle - \sqrt{2}(|H_4\rangle - |H_6\rangle)}{2\sqrt{6}N_2}, \\
|D';0\rangle &= -\frac{(\phi-1)(|T_{1x}\rangle + |T_{2z}\rangle) + (|T_{1y}\rangle + |T_{2y}\rangle) - \phi(|T_{1z}\rangle + |T_{2x}\rangle)}{2\sqrt{5}N_1} \\
&- \frac{\sqrt{5}|G_a\rangle - |G_x\rangle - 3|G_y\rangle - |G_z\rangle}{2\sqrt{15}N_1} + \frac{|H_\theta\rangle + \sqrt{3}|H_\epsilon\rangle - \sqrt{2}(|H_4\rangle + |H_6\rangle)}{2\sqrt{6}N_2}, \\
|E';0\rangle &= -\frac{(\phi-1)(|T_{1x}\rangle + |T_{2z}\rangle) - (|T_{1y}\rangle + |T_{2y}\rangle) - \phi(|T_{1z}\rangle + |T_{2x}\rangle)}{2\sqrt{5}N_1} \\
&+ \frac{\sqrt{5}|G_a\rangle + |G_x\rangle - 3|G_y\rangle + |G_z\rangle}{2\sqrt{15}N_1} - \frac{|H_\theta\rangle + \sqrt{3}|H_\epsilon\rangle + \sqrt{2}(|H_4\rangle + |H_6\rangle)}{2\sqrt{6}N_2}, \\
|J';0\rangle &= \frac{(|T_{1x}\rangle + |T_{2x}\rangle) + \phi(|T_{1y}\rangle + |T_{2z}\rangle) - \phi^{-1}(|T_{1z}\rangle + |T_{2y}\rangle)}{2\sqrt{5}N_1} \\
&+ \frac{\sqrt{5}|G_a\rangle - 3|G_x\rangle + |G_y\rangle + |G_z\rangle}{2\sqrt{15}N_1} - \frac{|H_\theta\rangle - \sqrt{3}|H_\epsilon\rangle + \sqrt{2}(|H_5\rangle + |H_6\rangle)}{2\sqrt{6}N_2}, \\
|K';0\rangle &= \frac{(|T_{1x}\rangle + |T_{2x}\rangle) - \phi(|T_{1y}\rangle - |T_{2z}\rangle) - \phi^{-1}(|T_{1z}\rangle) - |T_{2y}\rangle}{2\sqrt{5}N_1} \\
&- \frac{\sqrt{5}|G_a\rangle + 3|G_x\rangle + |G_y\rangle - |G_z\rangle}{2\sqrt{15}N_1} + \frac{|H_\theta\rangle - \sqrt{3}|H_\epsilon\rangle + \sqrt{2}(|H_5\rangle - |H_6\rangle)}{2\sqrt{6}N_2}, \\
|L';0\rangle &= \frac{-(|T_{1x}\rangle + |T_{2x}\rangle) - \phi(|T_{1y}\rangle - |T_{2z}\rangle) - \phi^{-1}(|T_{1z}\rangle - |T_{2y}\rangle)}{2\sqrt{5}N_1} \\
&+ \frac{\sqrt{5}|G_a\rangle + 3|G_x\rangle - |G_y\rangle + |G_z\rangle}{2\sqrt{15}N_1} - \frac{|H_\theta\rangle - \sqrt{3}|H_\epsilon\rangle - \sqrt{2}(|H_5\rangle - |H_6\rangle)}{2\sqrt{6}N_2}, \\
|M';0\rangle &= \frac{-(|T_{1x}\rangle + |T_{2x}\rangle) + \phi(|T_{1y}\rangle + |T_{2z}\rangle) - \phi^{-1}(|T_{1z}\rangle + |T_{2y}\rangle)}{2\sqrt{5}N_1} \\
&- \frac{\sqrt{5}|G_a\rangle - 3|G_x\rangle - |G_y\rangle - |G_z\rangle}{2\sqrt{15}N_1} + \frac{|H_\theta\rangle - \sqrt{3}|H_\epsilon\rangle - \sqrt{2}(|H_5\rangle + |H_6\rangle)}{2\sqrt{6}N_2}.
\end{aligned}
$$

The second set of the next-nearest neighbour wells are:

$$
\begin{aligned}
|F';0\rangle &= \frac{(\phi+2)(|T_{1x}\rangle+|T_{2y}\rangle)+(\phi^{-1}-2)(|T_{1y}\rangle+|T_{2x}\rangle)-\sqrt{5}(|T_{1z}\rangle+|T_{2z}\rangle)}{10N_1} \\
&- \frac{\sqrt{5}|G_a\rangle-|G_x\rangle-|G_y\rangle-3|G_z\rangle}{2\sqrt{15}N_1}-\frac{\sqrt{2}|H_\theta\rangle+|H_4\rangle+|H_5\rangle}{2\sqrt{3}N_2}, \\
|G';0\rangle &= \frac{-(\phi+2)(|T_{1x}\rangle-|T_{2y}\rangle)+(\phi^{-1}-2)(|T_{1y}\rangle-|T_{2x}\rangle)-\sqrt{5}(|T_{1z}\rangle+|T_{2z}\rangle)}{10N_1} \\
&+ \frac{\sqrt{5}|G_a\rangle-|G_x\rangle+|G_y\rangle+3|G_z\rangle}{2\sqrt{15}N_1}+\frac{\sqrt{2}|H_\theta\rangle+|H_4\rangle-|H_5\rangle}{2\sqrt{3}N_2}, \qquad (8.2.1) \\
|H';0\rangle &= -\frac{(\phi+2)(|T_{1x}\rangle+|T_{2y}\rangle)+(\phi^{-1}-2)(|T_{1y}\rangle+|T_{2x}\rangle)+\sqrt{5}(|T_{1z}\rangle+|T_{2z}\rangle)}{10N_1} \\
&- \frac{\sqrt{5}|G_a\rangle+|G_x\rangle+|G_y\rangle-3|G_z\rangle}{2\sqrt{15}N_1}-\frac{\sqrt{2}|H_\theta\rangle-|H_4\rangle-|H_5\rangle}{2\sqrt{3}N_2}, \\
|I';0\rangle &= \frac{(\phi+2)(|T_{1x}\rangle-|T_{2y}\rangle)-(\phi^{-1}-2)(|T_{1y}\rangle-|T_{2x}\rangle)-\sqrt{5}(|T_{1z}\rangle+|T_{2z}\rangle)}{10N_1} \\
&+ \frac{\sqrt{5}|G_a\rangle+|G_x\rangle-|G_y\rangle+3|G_z\rangle}{2\sqrt{15}N_1}+\frac{\sqrt{2}|H_\theta\rangle-|H_4\rangle+|H_5\rangle}{2\sqrt{3}N_2}, \\
|N';0\rangle &= \frac{\sqrt{3}(|T_{1y}\rangle+|T_{2y}\rangle)+2|G_y\rangle}{\sqrt{15}N_1}+\frac{|H_5\rangle}{\sqrt{3}N_2}, \\
|O';0\rangle &= \frac{\sqrt{3}(|T_{1x}\rangle+|T_{2x}\rangle)+2|G_x\rangle}{\sqrt{15}N_1}+\frac{|H_4\rangle}{\sqrt{3}N_2}.
\end{aligned}
$$

where

$$N_1 = \frac{1}{\sqrt{(1+\frac{S_{AC}}{2})}}, \qquad (8.2.2)$$

and

$$N_2 = \frac{1}{\sqrt{1-S_{AC}}}. \qquad (8.2.3)$$

S_{AC} is the phonon overlap between the adjacent wells such as A and C and given by [97]

$$S_{AC} = \exp[-\frac{27}{64}(V')^2]. \qquad (8.2.4)$$

The straightforward calculations of the probabilities of finding the system in a particular well at time t using Eq. (3.2.9), are

$$
\begin{aligned}
P_{AA}(t) &= 1-\frac{4}{9}((2-S_{AC}-S_{AC}^2)\sin^2[\frac{\Delta t}{2\hbar}]), \\
P_{AC}(t) &= \frac{1}{144}(9S_{AC}^2+8(2-S_{AC}-S_{AC}^2)\sin^2[\frac{\Delta t}{2\hbar}]), \\
P_{AO}(t) &= 0. \qquad (8.2.5)
\end{aligned}
$$

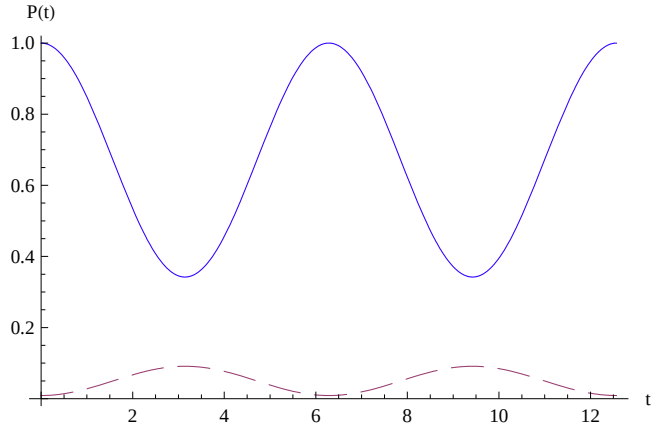

Figure 8.2: Diagram showing the dynamics in the D_{2h} symmetry when the system is initially localised in well A

where $P_{AC}(t)$ and $P_{AO}(t)$ are the probabilities that a system initially localised in well A migrates to well C or well O respectively. For completeness, the phonon overlap between non-adjacent wells such as wells A and O for example, is calculated and given by

$$S_{AO} = \exp[-\frac{27}{32}(V')^2]. \tag{8.2.6}$$

The energy difference Δ between the SASs T_1, T_2, G and H is evaluated to be

$$\Delta = -\frac{3S_{AC}\ln S_{AC}}{(1-S_{AC})(2+S_{AC})}\hbar\omega. \tag{8.2.7}$$

The results from Eq. (8.2.5) are plotted in Fig. 8.2. The D_{2h} case shows similarity with the D_{3d} distortions, since there are two sets of wells associated with the differences in their separations the Q-space. The system in this case is pseudorotating freely between the wells in the first set when it is initially prepared in well A. However, pseudorotation to the other wells in the other set is forbidden. This is due to the orthogonality between the electronic states associated with those wells. In the D_{3d} case, the system was free to pseudorotate to both sets with no zero electronic overlap. This means that, in the D_{2h} case when the system starts off from well A, it never visits any of the wells $\{F, G, H, I, N, O\}$ during its journey and the pseudorotation trend follows the plotted curve of Eq. (8.2.5) as shown in Fig. 8.2. From the figure, it is very obvious that the system is completing one period of pseudorotation when $T_p = \frac{2\pi\hbar}{\Delta}$. The pseudorotation rate is the inverse of the period T_p and is shown in Fig. 8.3 as a function of the linear coupling constant

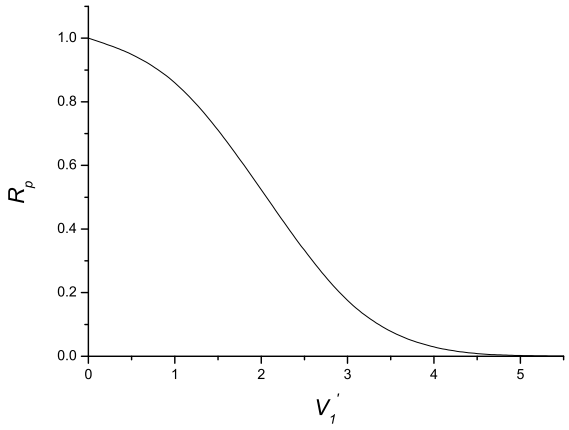

Figure 8.3: Plot of the pseudorotation rate R_p for the D_{2h} distortion as a function of the linear coupling constant.

V'. The figure shows that, as the value of the linear coupling constant increases, the rate of the pseudorotation decreases. This situation is expected and agrees with the basic idea of the JT interaction which shows that in strong coupling limit when the barrier height between the wells is large, the system will be confined in one of the wells and no pseudorotation dynamics will occur. This situation can also be inferred from the sum of the probabilities written as:

$$\sum_{X=A}^{O} P_{AX} = 1 + 2S_{AC}^2, \tag{8.2.8}$$

this expression tends to one as $V' \longrightarrow \infty$. This means that the system must be found localised into one of the wells as expected.

8.3 Summary

In this chapter, the pseudorotaton dynamics for the $(h_u^+)^2 \otimes h_g$ JT system when distorted to D_{2h} symmetry has been studied using the method outlined in Chapter 3. The probabilities of finding the system migrating to another well has been plotted in order to follow the progress of the trend.

The results showed that, when the system is localised in one of the D_{2h} wells then it can pseudorotate only to the nearest-neighbours since the pseudorotation between the other wells is forbidden due to the orthogonality between well states.

The effect of the term splitting has been neglected throughout this calculation. If this term is included then a different picture of the well separations than that used in this problem will appear and therefore a different situation of pseudorotation dynamics will occur. The inclusion of this term will complicate the problem which is already complicated due to its high dimension. This problem will be an interesting point to be studied in the future work.

Chapter 9

Conclusions

The main purpose of this thesis has been to study the dynamical nature of some JT systems involving different ions. The investigation has been accomplished through studying the pseudorotation between equivalent minima in the APES under the assumption that the JT interaction overwhelms the other interactions within the molecule. The pseudorotation phenomenon is a characteristic feature of JT systems and the method that has been used in this thesis to study this internal rotation can be applied to any real system undergoing dynamical JT interaction.

The thesis began with a brief introduction representing the motivation of this study and outlined the subjects contained in each chapter in the thesis. Chapter 2 began with a historical review of the origin of the JT effect and the research studies related to this subject. Also there are a description of the approximations that led to the construction of the interaction Hamiltonian which describes the electron-phonon coupling. The chapter provided the mathmatical tools that are essential in order to produce a simple expression for the vibronic Hamiltonian under consideration. This Hamiltonian has been simplified in order to find a solution using the shift transformation technique and the method of Öpik and Pryce [4] which is used to find the location of the distinct minima on the APES. A general idea of the icosahedral point group to which our systems belong and the method of how to specify the electronic orbital and the vibrational modes that involved in the interaction was also discussed in the same chapter.

The theory of the time evolution operator was introduced in the following chapter. This method used the quantum mechanical concept of the time evolution operator to study the progress of a system at a time t in the strong JT coupling

limit where the minima are considered to be sufficiently deep with high barriers between them. The method has been applied to different systems having different distortion symmetries.

In Chapter 4, the pseudorotation in the $T \otimes (e \oplus t_2)$ JT system has been studied using the method discussed in Chapter 3. This system shows three different examples of coupling depending on the coupling strength of the T electronic state to the e and t_2 vibrational modes. The first case involving the $T \otimes e$ coupling showed no tunnelling performed by the system since the well states in that system are mutually orthogonal. The second case was the $T \otimes t_2$ coupling distorted to a D_{3d} symmetry. This system showed equal transitions between the four wells. The last case was for D_{2h} symmetry when the coupling to the e and t_2 modes is involved. Here, the system was allowed to tunnel only between the non-orthogonal electronic states localised in the wells with strictly forbidden tunnelling between the orthogonal ones. Studying the pseudorotation of this system has been used as an introduction to study the pseudorotation of different but more sophisticated icosahedral JT systems.

In Chapter 5 a model for the C_{60}^{2-} anion has been developed when the quadratic coupling term is included in the problem. This problem was treated using all the techniques that have been outlined in Chapter 2. The Hamiltonian of the problem also has been written as a function of the mixing angle β which represents a mixing of the two different sets of CG coefficients. The APES obtained showed two kinds of minima having D_{5d} and D_{3d} symmetry depending on the value of the mixing angle. Both systems have been investigated in the static and dynamic regimes by finding the positions of the minimum points on the APES and the corresponding states. The inter-molecular motion of the system has been determined using the method outlined in Chapter 3. The system showed equal transitions between the D_{5d} wells as the separations between them are equal. The D_{3d} revealed more complicated pseudorotation since the system has the opportunity to migrate to two distinct types of wells leading to two different tunnelling splittings.

A further investigation of this model was continued when the Coulomb interaction between the electrons is taken into account in Chapter 6. The inclusion of this term complicates the analytical expressions of both the states and the corresponding energies.

Chapter 7 dealt with the $H \otimes h_g$ JT system for the C_{60}^{+} cation. The probabilities

of the system while is pseudorotating was plotted for both cases of D_{5d} and the D_{3d} symmetries. The system showed a regular pseudorotation between wells of the D_{5d} case similar to that in the $p^2 \otimes h$ system. In the D_{3d} distortion, the system again showed a complicated situation due to the two different separation distances between wells. The probabilities for this case have been plotted for different values of the coupling constants when the $H - A$ crossover between the two SASa occurs. The system showed tunnelling behaviour of similar regime as that appeared in the C_{60}^{2-}.

The study of inter-well dynamics of the $(h_u^+)^2 \otimes h$ system was the subject of Chapter 8. This system involves wells of D_{2h} symmetry which consist of two equivalent sets of wells in the APES similar to that in D_{3d} symmetry. The system showed here that pseudorotation is only allowed between the nearest-neighbour wells. The orthogonality between the other wells (next-nearest neighbour) made the electronic overlap between them tends to zero and therefore no migration for the system to those wells occurs.

Although the theory presented in this thesis for studying the internal motion depends on many approximations, such as ignoring the presence of exited vibronic states, nevertheless the theory still can be accepted as a first approximation to a description of the dynamics that occur in JT systems undergoing pseudorotation.

In this study, the term splitting which appeared as a result of Coulomb interaction in both C_{60}^{2-} and C_{60}^{2+} systems has been neglected and the calculations were achieved by regarding the JT interaction as overwhelming the other interactions in the problem. Neglecting the term splitting led to have a degenerate ground state in both system. If this term is included, then a shift in the energy between the SASs occurs and the degeneracy of the ground state will be removed. This could lead to have a more accurate picture of the APES and therefore a clearer view of the sets of wells between which the system is allowed to pseudorotate will appear. This indeed will lead to have a very complicated system to be studied since the C_{60}^{2+} system for example has more than one tunnelling splitting term. Investigation of such problems needs an advanced computer programs to solve the problem numerically rather than analytically which could be an interesting problem to focus on for the future work.

Pseudorotation can be observed experimentally in NMR spectra, isotopic substitution experiments, central-atom nuclear quadrupole resonance spectra and

other spectroscopic measurements [48]. The distorted geometry of the molecule whilst pseudorotating could be viewed if measurements on a very short time scale are made. This time scale is estimated from electron paramagnetic resonance (EPR) [100] data and it appears to be of the order of picoseconds, while from the strength of the vibronic coupling [101] it is estimated to be of the order of femtoseconds. A multiple-pulse technique or the "pumb-probe" which produces pulses on the femtosecond time-scale to freeze the nuclear dynamics in real time (see for example [102]), has already been used in measuring how quickly the rotation of the C_{60} and C_{70} molecules in various solutions. As the pseudorotation involves movement of the nuclei in JT systems, the nuclear dynamics should be then observable using such ultrafast techniques. An idea of such experiments that capable of measuring pseudorotation in the fullerene ions has been discussed in Chapter 3 using what is called transient grating techniques.

To our knowledge, pseudorotation motion of some molecules such as the Na_3 has already been detected using the two-photon ionisation (TPI) experiment [103] and showed a fairly rapid pseudorotation. The period of this pseudorotation was found to be of the order of 3 ps. However, experiments have been conducted to try to measure the rate of pseudorotation in C_{60}^{-}, C_{60}^{2-} and C_{60}^{3-}. As always, experimental realisation of a theoretically simple process was found to be difficult. Some preliminary results have been presented in a recent PhD thesis [104] with subsequent publication to follow. One of the conclusions from the work is that the experiments seem to point to reorientational dynamics faster than 2 ps duration (and faster, depending on the technique used). This is interesting if confirmed because Rubtsov *et al.* [1, 55] found that the C_{60} in decalin has a reorentational relaxation time of 3.5 ps, which, they point out, is close to the rotation rate associated with free gaseous C_{60} (other rotation rates were much slower). A relaxation of 2 ps, therefore, could be a strong indicator that pseudorotation is occurring. A better estimate of the actual time is called for, however, if this rate is to be useful. Nevertheless, if a time can be measured that can reasonably be assigned to pseudorotation, then it could be equated with the time taken for a C_{60}^{-} to 'hop' from one well to another. Hence, the expermental time could provide vital evidence for the likely magnitudes of V_1, V_2 and V_3. However, temperature dependent studies may be required if a true attempt is to be made to isolate V_2/V_3 from V_1.

Appendix A

The SASs arising from the D_{2h} wells in the C_{60}^{2+} cation

$$
\begin{aligned}
|T_1x\rangle &= \frac{N_1}{2\sqrt{5}}[2\ |b';0\rangle + \phi|d';0\rangle - \phi|e';0\rangle + \phi|f';0\rangle - \phi|g';0\rangle + \phi^{-1}|h';0\rangle \\
&- \phi^{-1}|i';0\rangle - \phi^{-1}|j';0\rangle + \phi^{-1}|k';0\rangle + |l';0\rangle + |m';0\rangle - |n';0\rangle - |o';0\rangle], \\
|T_1y\rangle &= \frac{N_1}{2\sqrt{5}}[2\ |c';0\rangle + \phi^{-1}|d';0\rangle + \phi^{-1}|e';0\rangle - \phi^{-1}|f';0\rangle - \phi^{-1}|g';0\rangle - |h';0\rangle \\
&- |i';0\rangle + |j';0\rangle + |k';0\rangle - \phi|l';0\rangle + \phi|m';0\rangle + \phi|n';0\rangle - \phi|o';0\rangle], \\
|T_1z\rangle &= \frac{N}{2\sqrt{5}}[2\ |a';0\rangle - |d';0\rangle - |e';0\rangle - |f';0\rangle - |g';0\rangle + \phi|h';0\rangle + \phi|i';0\rangle \\
&+ \phi|j';0\rangle + \phi|k';0\rangle - \phi^{-1}|l';0\rangle - \phi^{-1}|m';0\rangle - \phi^{-1}|n';0\rangle - \phi^{-1}|o';0\rangle],
\end{aligned}
\tag{A.0.1}
$$

$$
\begin{aligned}
|T_2x\rangle &= \frac{N_1}{2\sqrt{5}}[2\ |b';0\rangle - \phi^{-1}|d';0\rangle + \phi^{-1}|e';0\rangle - \phi^{-1}|f';0\rangle + \phi^{-1}|g';0\rangle - \phi|h';0\rangle \\
&+ \phi|i';0\rangle + \phi|j';0\rangle - \phi|k';0\rangle + |l';0\rangle + |m';0\rangle - |n';0\rangle - |o';0\rangle], \\
|T_2y\rangle &= \frac{N_1}{2\sqrt{5}}[2\ |c';0\rangle - \phi|d';0\rangle - \phi|e';0\rangle + \phi|f';0\rangle + \phi|g';0\rangle - |h';0\rangle - |i';0\rangle \\
&+ |j';0\rangle + |k';0\rangle + \phi^{-1}|l';0\rangle - \phi^{-1}|m';0\rangle - \phi^{-1}|n';0\rangle + \phi^{-1}|o';0\rangle], \\
|T_2z\rangle &= \frac{N_1}{2\sqrt{5}}[2\ |a';0\rangle - |d';0\rangle - |e';0\rangle - |f';0\rangle - |g';0\rangle - \phi^{-1}|h';0\rangle - \phi^{-1}|i';0\rangle \\
&- \phi^{-1}|j';0\rangle - \phi^{-1}|k';0\rangle + \phi|l';0\rangle + \phi|m';0\rangle + \phi|n';0\rangle + \phi|o';0\rangle],
\end{aligned}
\tag{A.0.2}
$$

$$
\begin{aligned}
|Ga\rangle &= \frac{N_1}{\sqrt{12}}[\ |d';0\rangle - |e';0\rangle - |f';0\rangle + |g';0\rangle + |h';0\rangle - |i';0\rangle \\
&+ |j';0\rangle - |k';0\rangle - |l';0\rangle + |m';0\rangle - |n';0\rangle + |o';0\rangle], \\
|Gx\rangle &= \frac{N_1}{2\sqrt{15}}[4\ |b';0\rangle + |d';0\rangle - |e';0\rangle + |f';0\rangle - |g';0\rangle - |h';0\rangle + |i';0\rangle \\
&+ |j';0\rangle - |k';0\rangle - 3|l';0\rangle - 3|m';0\rangle + 3|n';0\rangle + 3|o';0\rangle], \\
|Gy\rangle &= \frac{N_1}{2\sqrt{15}}[4\ |c';0\rangle - |d';0\rangle - |e';0\rangle + |f';0\rangle + |g';0\rangle + 3|h';0\rangle + 3|i';0\rangle \\
&- 3|j';0\rangle - 3|k';0\rangle - |l';0\rangle + |m';0\rangle + |n';0\rangle - |o';0\rangle], \\
|Gz\rangle &= \frac{N}{2\sqrt{15}}[4\ |a';0\rangle + 3|d';0\rangle + 3|e';0\rangle + 3|f';0\rangle + 3|g';0\rangle + |h';0\rangle + |i';0\rangle \\
&+ |j';0\rangle + |k';0\rangle + |l';0\rangle + |m';0\rangle + |n';0\rangle + |o';0\rangle], \qquad \text{(A.0.3)}
\end{aligned}
$$

$$
\begin{aligned}
|H\theta\rangle &= \frac{N_2}{2\sqrt{6}}[2\ |d';0\rangle - 2|e';0\rangle - 2|f';0\rangle + 2|g';0\rangle - |h';0\rangle + |i';0\rangle \\
&- |j';0\rangle + |k';0\rangle + |l';0\rangle - |m';0\rangle + |n';0\rangle - |o';0\rangle], \\
|H\epsilon\rangle &= \frac{N_2}{2\sqrt{2}}[-|h';0\rangle + |i';0\rangle - |j';0\rangle + |k';0\rangle - |l';0\rangle + |m';0\rangle - |n';0\rangle + |o';0\rangle], \\
|Hx\rangle &= \frac{N_2}{2\sqrt{3}}[2\ |b';0\rangle - |d';0\rangle + |e';0\rangle - |f';0\rangle + |g';0\rangle + |h';0\rangle - |i';0\rangle \\
&- |j';0\rangle + |k';0\rangle, \\
|Hy\rangle &= \frac{N_2}{2\sqrt{3}}[2\ |c';0\rangle + |d';0\rangle + |e';0\rangle - |f';0\rangle - |g';0\rangle + |l';0\rangle - |m';0\rangle \\
&- |n';0\rangle + |o';0\rangle], \\
|Hz\rangle &= \frac{N_2}{2\sqrt{3}}[2\ |a';0\rangle - |h';0\rangle - |i';0\rangle - |j';0\rangle - |k';0\rangle - |l';0\rangle - |m';0\rangle \\
&- |n';0\rangle - |o';0\rangle].
\end{aligned}
$$

Bibliography

[1] I. V. Rubtsov, D. V. Khudiakov, V. A. Nadtochenko, A. S. Lobach, and A. P. Moravskii, Chem. Phys. Lett. **229**, 517 (1994).

[2] I. D. Hands, J. L. Dunn, and C. A. Bates, Phys. Rev. B **73**, 235425 (2006).

[3] C. A. Bates, J. L. Dunn, and E. Sigmund, J. Phys. C **20**, 1965 (1987).

[4] U. Öpik and M. H. L. Pryce, Proc. Roy. Soc. London, Ser. A **238**, 425 (1957).

[5] I. B. Bersuker and V. Z. Polinger, *Vibronic Interactions in Molecules and Crystals*, Springer-Verlag, Berlin, Heidelberg, New York, 1989.

[6] M. C. M. O'Brien, Phys. Rev. **187**, 407 (1969).

[7] N. Manini, A. Dal Corso, M. Fabrizio, and E. Tosatti, Philos. Mag. B **81**, 793 (2001).

[8] H. A. Jahn and E. Teller, Proc. Roy. Soc. London, Ser. A **161**, 220 (1937).

[9] J. H. Van Vleck, J. Chem. Phys. **7**, 61 (1939).

[10] W. Low, *Paramagnetic resonance in solids*, Academic Press, 1960.

[11] A. Abragam and M. H. L. Pryce, Proc. Roy. Soc. London, Ser. A **63**, 409 (1950).

[12] W. Moffit and W. Thorson, Phys.Rev. **108**, 1251 (1957).

[13] H. C. Longuet-Higgins, U. Öpik, M. H. L. Pryce, and R. A. Sack, Proc. Roy. Soc. Lond. A. **244**, 1 (1958).

[14] A. D. Liehr and C. J. Ballhausen, Ann. Phys. (N.Y.) **3**, 304 (1958).

[15] I. B. Bersuker, Opt. Spectrosc. **11**, 319 (1961).

[16] M. C. M. O'Brien, Proc. Roy. Soc. A **281**, 323 (1964).

[17] F. S. Ham, Phys. Rev. A **138**, 1727 (1965).

[18] R. Englman, *The Jahn-Teller Effects In Molecules and Crystals*, London, Wiley-Interscience, 1972.

[19] V. P. Khlopin, V. Z. Polinger, and I. B. Bersuker., Theor. Chim. Acta **48**, 87 (1978).

[20] D. R. Pooler, J. Phys. C: Solid State Phys. **13**, 1029 (1980).

[21] H. W. Kroto, J. R. Heath, S. C. O'Brien, R. F. Curl, and R. E. Smalley, Nature **318**, 162 (1985).

[22] J. L. Dunn and C. A. Bates, Phys. Rev. B **52**, 5996 (1995).

[23] M. Born and K. Huang, *Dynamical Theory of Crystal Lattices*, Oxford University Press, 1954.

[24] M. Born and R. Oppenheimer, Ann. Phys. **84**, 457 (1927).

[25] J. S. Griffith, *The Irreducible Tensor Method for Molecular Symmetry Groups*, Prentice-Hall, Englewood Cliffs, N. J., 1962.

[26] S. L. Altmann and P. Herzig, *Point Group Theory Tables*, Clarendon Press, Oxford, 1994.

[27] P. W. Fowler and A. Ceulemans, Mol. Phys. **54**, 767 (1985).

[28] R. M. Golding, Mol. Phys. **26**, 661 (1973).

[29] J. P. Cullerne, M. N. Angelova, and M. C. M. O'Brien, J. Phys.: Condens. Matter **7**, 3247 (1995).

[30] A. Ceulemans and P. W. Fowler, J. Chem. Phys. **93**, 1221 (1990).

[31] B. R. Judd and E. E. Vogel, Phys. Rev. B **11**, 2427 (1975).

[32] M. J. Shultz and R. Silbey, J. Phys. C: Solid State Phys. **7**, L325 (1974).

[33] J. L. Dunn, J. Phys. C: Solid State Phys. **21**, 383 (1988).

[34] C. J. Bradley and A. P. Cracknell, *The Mathematical Theory of Symmetry in Solids*, Clarendon Press, Oxford, 1972.

[35] F. A. Cotton, *Applications of Group Theory*, Wiley-Interscience, 3 edition, 1989.

[36] J. L. Dunn, J. Phys: Condens. Matter **1**, 7861 (1989).

[37] A. G. McLellan, J. Chem. Phys. **34**, 1350 (1961).

[38] P. W. Fowler and J. Woolrich, Chem. Phys. Lett. **127**, 78 (1986).

[39] R. C. Haddon, L. E. Brus, and K. Raghavachari, Chem. Phys. Lett. **125**, 459 (1986).

[40] M. S. Dresselhaus, G. Dresselhaus, and P. C. Eklund, *Science of Fullerenes and Carbon Nanotubes*, Acadamic Press, 1995.

[41] Y. Deng and C. N. Yang, Phys. Lett. **170**, 116 (1992).

[42] N. Laouini, O. K. Andersen, and O. Gunnarsson, Phys. Rev. B **51**, 17446 (1995).

[43] W. H. Green, S. M. Gorun, G. Fitzgerald, P. W. Fowler, A. Ceulemans, and B. C. Titeca, J. Phys. Chem. **100**, 14892 (1996).

[44] I. D. Hands, J. L. Dunn, and C. A. Bates, Adv. Quant. Chem. **44**, 335 (2003).

[45] R. L. Carter, *Molecular Symmetry and Group Theory*, John Wiley and Sons, 1998.

[46] G. Herzberg, *Molecular Structure III Electronic Spectra and Electronic Structure of Polyatomic Molecules*, Van Nostrand, Princeton, N. J., 1966.

[47] M. C. M. O'Brien, Phys. Rev. B **53**, 3775 (1996).

[48] I. B. Bersuker, *The Jahn-Teller Effect*, Cambridge University Press, 2006.

[49] R. S. Berry, J. Chem. Phys. **32**, 933 (1960).

[50] J. L. Dunn, I. D. Hands, and C. A. Bates, J. Mol. Struct. **838**, 60 (2007).

[51] I. D. Hands, J. L. Dunn, and C. A. Bates, Phys. Rev. B **73**, 014303 (2006).

[52] I. D. Hands, J. L. Dunn, and C. A. Bates, Fullerenes, Nanotubes, and Carbon Nanostructures **14**, 551 (2006).

[53] N. Zettili, *Quantum Mechanics: Concepts and Applications*, John Wiley and Sons, 2001.

[54] J. J. Sakurai, *Modern Quantum Mechanics*, Addison-Wesley, 1994.

[55] I. V. Rubtsov, D. V. Khudiakov, A. P. Moravskii, and V. A. Nadtochenko, Chem. Phys. Lett. **249**, 101 (1996).

[56] I. B. Bersuker and V. Polinger, Sov. Phys. JETP **39**, 1023 (1974).

[57] P. J. Kirk, C. A. Bates, and J. L. Dunn, J. Phys.: Condens. Matter. **6**, 5465 (1994).

[58] V. Z. Polinger, C. A. Bates, and J. L. Dunn, J. Phys.: Condens. Matter **10**, 1293 (1998).

[59] H. Li, V. Z. Polinger, J. L. Dunn, and C. A. Bates, Adv. Quantum Chem. **44**, 89 (2003).

[60] J. L. Dunn and C. A. Bates, J. Phys. C: Solid State Phys. **21**, 2495 (1988).

[61] H. Li, *Vibronic States of Cubic and Icosahedral Jahn-Teller Systems*, PhD thesis, University of Nottingham, 2004.

[62] L. D. Landau and E. M. Lifshitz, *Mechanics and Electrodynamics (Shorter Course of Theoretical Physics, Vol 1)*, Pergamon, Oxford, 1972, Chapter 3, Section 10.

[63] M. Poliakoff and A. Ceulemans, J. Am. Chem. Soc. **106**, 50 (1984).

[64] M. Poliakoff and J. Turner, Angew. Chem. Int. **40**, 2809 (2001).

[65] B. Davies, A. McNeish, M. Poliakoff, and J. Turner, J. Am. Chem. Soc. **99:23**, 7573 (1977).

[66] A. Ceulemans and E. Lijnen, Chem. Soc. Jpn. **80**, 1229 (2007).

[67] H. J. ´Worner, R. V. der Veen, and F. Merkt, Phys. Rev. Lett. **97**, 173003 (2006).

[68] A. F. Hebard, M. J. Rosseinsky, R. C. Haddon, D. W. Murphy, S. H. Glarum, T. T. M. Palstra, A. P. Ramirez, and A. R. Kortan, Nature **350**, 600 (1991).

[69] T. T. M. Palstra, O. Zhou, Y. Iwasa, P. E. Sulewski, R. M. Fleming, and B. R. Zegarski, Solid State Commun. **93**, 327 (1995).

[70] G. Klupp, P. Matus, D. Quintavalle, L. F. Kiss, É. Kováts, N. M. Nemes, K. Kamarás, S. Pekker, and A. Jánossy, Phys. Rev. B **74**, 195402 (2006).

[71] S. C. Erwin, *Buckminsterfullerenes*, chapter 9, pp. 217–256, VCH, New York, 1993.

[72] S. C. Erwin and C. Bruder, Physica B **199-200**, 600 (1994).

[73] J. E. Han, E. Koch, and O. Gunnarsson, Phys. Rev. Lett. **84**, 1276 (2000).

[74] M. Fabrizio and E. Tosatti, Phys. Rev. B **55**, 13465 (1997).

[75] M. Lüders, N. Manini, P. Gattari, and E. Tosatti, Eur. Phys. J. B **35**, 57 (2003).

[76] C. A. Reed and R. D. Bolskar, Chem. Rev. **100**, 1075 (2000).

[77] M. Wierzbowska, M. Luders, and E. Tosatti, J. Phys. B-At. Mol. Opt. Phys. **37**, 2685 (2004).

[78] A. V. Nikolaev and K. H. Michel, J. Chem. Phys. **117**, 4761 (2002).

[79] G. Klupp, K. Kamarás, N. M. Nemes, and C. M. Brown, Phys. Rev. B **73**, 085415 (2006).

[80] O. Gunnarsson, S. C. Erwin, E. Koch, and R. M. Martin, Phys. Rev. B **57**, 2159 (1998).

[81] S. Sookhun, *Jahn-Teller Effects in C_{60} anions*, PhD thesis, University of Nottingham, 2003.

[82] C. C. Chancey and M. C. M. O'Brien, *The Jahn-Teller Effect in C_{60} and other Icosahedral Complexes*, Princeton UP, 1997.

[83] S. Sookhun, J. L. Dunn, and C. A. Bates, Phys. Rev. B **68**, 235403 (2003).

[84] L. Hallam, C. A. Bates, and J. L. Dunn, J. Phys.: Condens. Matter **4**, 6775 (1992).

[85] O. Gunnarsson, H. Handschuh, P. S. Bechthold, B. Kessler, G. Ganteför, and W. Eberhardt, Phys. Rev. Lett. **74**, 1875 (1995).

[86] L. M. Sindi, I. D. Hands, J. L. Dunn, and C. A. Bates, J. Mol. Struct. **838**, 78 (2007).

[87] V. Brouet, H. Alloul, T. Le, S. Garaj, and L. Forró, Phys. Rev. Lett. **86**, 4680 (2001).

[88] M. Granath and S. Östlund, Phys. Rev. B **66**, 180501 (2002).

[89] A. M. Panich, I. Felner, A. I. Shames, S. Goren, P. K. Ummat, and W. R. Datars, Solid State Commun. **129**, 81 (2004).

[90] V. P. Antropov, O. Gunnarsson, and A. I. Liechtenstein, Phys. Rev. B **48**, 7651 (1993).

[91] M. Saito, Phys. Rev. B **65**, 220508 (2002).

[92] C. P. Moate, *Vibronic Coupling In Icosahedral Molecules*, PhD thesis, University of Nottingham, 1998.

[93] C. P. Moate, J. L. Dunn, C. A. Bates, and Y. M. Liu, J. Phys.: Condens. Matter **9**, 6049 (1997).

[94] C. P. Moate, M. C. M. O'Brien, J. L. Dunn, C. A. Bates, Y. M. Liu, and V. Z. Polinger, Phys. Rev. Lett. **77**, 4362 (1996).

[95] I. D. Hands, L. M. Sindi, J. L. Dunn, and C. A. Bates, Phys. Rev. B **74**, 115410 (2006).

[96] W. A. Diery, J. L. Dunn, and C. A. Bates, Fullerenes. Nanot. and Carb. Nanostructurs **14**, 573 (2006).

[97] I. D. Hands, W. A. Diery, J. L. Dunn, and C. A. Bates, J. Mol. Struct. **838**, 66 (2007).

[98] W. A. Diery, *Jahn-Teller Effects in Fullerene Molecules*, PhD thesis, University of Nottingham, 2005.

[99] I. D. Hands, J. L. Dunn, W. A. Diery, and C. A. Bates, Phys. Rev. B **73**, 115435 (2006).

[100] W. Z. Wang, C. L. Wang, A. R. Bishop, L. Yu, and Z. B. Su, Synth. Met. **86**, 2365 (1997).

[101] C. M. Varma, J. Zaanen, and K. Raghavachari., Science **254**, 989 (1991).

[102] L. Khundkar and A. H. Zewail, Ann. Rev. Phys. Chem. **41**, 15 (1990).

[103] J. Gaus, K. Kobe, V. Bonačić-Koutecký, H. Kühling, J. Manz, B. Reischl, S. Rutz, E. Schreiber, and L. Wöste, J. Phys. Chem. **97**, 12509 (1993).

[104] M. J. Hope, *Spectroelectrochemistry and Ultrafast Polarisation Spectroscopy of Buckminsterfullerene Anions*, PhD thesis, University of East Anglia, 2008.